Ultra wideband gigabit powerline communication

Chen, Shuxian

Ultra Wideband Gigabit Powerline Communication

Shuxian Chen

School of Electronic Engineering and Computer Science
Queen Mary University of London
London E1 4NS, United Kingdom

A Thesis Submitted to the faculty of the University of London in partial fulfillment of the requirements of the degree of Doctor of Philosophy

September 2009

I hereby declare that the work presented in this thesis is my own work.

To my family ...

Abstract

Powerline Communication (PLC) has long been established for low data rate applications by the electric supply companies. Since 1991, the European CENELEC standard EN 50065 has ruled the use of 3 - 148.5KHz frequency range for narrow band PLC applications. Similar standard has been established by the IEEE in the US, where a frequency range of 50 - 450KHz is available.

The fast growth of Internet since the 1990s accelerated the demands for digital communication services. Furthermore, with the development of in-home networking, there is a need to establish high speed data links between multiple household devices. This makes PLC systems march rapidly into the high frequency range above 1MHz. Existing broadband PLC system in the 1.6 - 30MHz frequency range only provides data rates smaller than 200Mbps. With the growing demand of multimedia services such as High Definition (HD) video streaming, much faster transmission speed up to Gigabits per second is required and this can be achieved by increasing the operating frequencies.

Ultra Wideband (UWB) transmission in free space provides extremely broad bandwidth for short-range, high data rate applications. If UWB signals could be transmitted over the powerline channels in the high frequency range above 30MHz, data rates up to gigabits per second could be achieved.

In this thesis, the possibility of implementing ultra wideband transmission over the low voltage indoor powerline is investigated. The starting point is to understand the signal propagation characteristics over powerline cables, in the UWB frequency range. Experimental results indicate that the signal degrades at an acceptable rate over the

mains cable in a scaled down UWB frequency band (50MHz - 1GHz), which provides a potential operation band for UWB over PLC applications. Key component for the PLC system, a broadband Radio Frequency (RF) coupler is designed and developed, to introduce UWB signals to the transmission channel. With the channel properties and coupling unit, extensive experimental investigations are carried out to analyse the powerline network environment, including channel loss, noise and radiated emission. Furthermore, theoretical channel capacity and link budget are derived from measured parameters. It is shown that the indoor powerline is a suitable media for data transmission in the high frequency range from 50 to 550MHz in the home environment. Finally, system level performance is analysed by modelling the Physical Layer (PHY) data transmission. The Multiband-OFDM UWB proposal for IEEE 802.15.3a standard is used to predict the transmission performance under different propagation paths and data rates. The research work conducted in this project has proven that UWB over PLC is highly feasible for future in-home applications. With the global promotion of smart grid applications, UWB over PLC will play an important role in providing high speed data transmission over the power networks.

Acknowledgements

First of all, I would like to express my gratitude to supervisor Professor Xiaodong Chen for his guidance and support throughout my study. I have benefited from his extraordinary motivation, great intuition and technical insight, without which I would not be able to accomplish the work that has been done. I would also like to express my sincere thanks to Professor Clive G. Parini and Dr. Rob Donnan for their suggestions and encouragement during my study.

My special thanks to Mr John Dupuy for his guidance and assistance during my measurement work conducted in the Antenna Measurement Laboratory at Queen Mary, University of London. Many thanks to Mr Fraser Robertson for his help in the measurements carried out in the Open University, Milton Keynes.

Many thanks to all my colleagues and friends for all their help, advices and valuable contributions. I am especially obliged to Dr. Choo C. Chiau, Dr. Yue Gao, Dr. Yasir Alfadhl, Dr Zhao Wang, Dr. Marianna Setta, Dr. Sheng Wang, Dr. Daohui Li, Mr. Lu Guo and Mr. Shihua Wang.

I would like to give my special thanks to my parents, grand parents, relatives and Mr Zhijia Huang for their support, patience and love. Without their encouragement, motivation and understanding it would be impossible for me to complete this work.

The financial support from the DTI and EPSRC is thankfully acknowledged.

Contents

List of Figures

List of Tables

Abbreviations

AC	Alternating Current
ADS	Advanced Design System
ADSL	Asymmetric DSL
ANSI	American Standards Institute
AWGN	Additive White Gaussian Noise
BPL	Broadband Powerline Communication
BPM	Bi-Phase Modulation
BPSK	Binary Phase Shift Key
CDF	Cumulative Probability Distribution
CDMA	Code Division Multiple Access
CEN	European Standardisation Committee
CENELEC	European Committee for Electrotechnical Standardisation
CEPT	European Conference of Postal and Telecommunications Administrations
CIR	Channel Impulse Response
CISPR	Information Special Committee on Radio Interference
DAB	Digital Audio Broadcasting
DC	Direct Current
DS	Direct Sequence
DSL	Digital Subscriber Lines
DSP	Digital Signal Processing
DS-UWB	Direct Sequence - UWB
DVB-T	Terrestrial Digital Video Broadcasting
EC	European Commission
ECC	European Communications Council
EMC	Electromagnetic Compatibility
EMI	Electromagnetic Interference
ETSI	European Telecommunications Standards Institute
EUT	Equipment Under Test

FCC	Federal Communications Commission
FEC	Forward Error Correction
FFT	Fast Fourier Transform
GSM	Global System for Mobile Communications
HD	High Definition
HD-PLC	High Definition Powerline Communications
HDTV	High Definition TV
HF	High Frequency
HPAV	Homeplug AV
IEC	International Electrotechnical Commission
IFFT	Inverse Fast Fourier Transform
ISI	Inter Symbol Interference
ITE	Information Technology Equipment
ITU	International Telecommunication Union
JWG	Joint Working Group
LDPC	Low Density Parity Check
LoS	Line of Sight
MB-OFDM	Multiband - OFDM
OFDM	Orthogonal Frequency Division Multiplexing
PCB	Printed Circuit Board
PHY	Physical Layer
PLC	Powerline Communication
PPM	Pulse Position Modulation
PSD	Power Spectral Density
PVC	Polyvinyl Chloride
QAM	Quadrature Amplitude Modulation
QPSK	Quadrature Phase Shift Key
RF	Radio Frequency
SMA	SubMiniature version A
SNR	Signal to Noise Ratio
TDR	Time Domain Reflectometry
TX/RX	Transmiter/Receiver
UWB	Ultra Wideband
VLSI	Very Large Scale Integration
VNA	Vector Network Analyser
VoIP	Voice over IP
WiMax	Worldwide Interoperability for Microwave Access
WLAN	Wireless Local Area Network
WPAN	Wireless Personal Area Network

Publications

Research Journals and Conference Papers

1. **S. Chen**, M. Magani, X. Chen and C. Parini,"Exploit Adaptive Modulation in UWB Powerline Communication for Improved BER Performance", submitted to the IEEE International Symposium on Powerline Communications and its Applications, 2010.

2. **S. Chen**, X. Chen and C. Parini, "UWB Communication over Powerline Channel above 30MHz: Channel Characterisation and Simulation", submitted to the IEEE Transactions on Power Delivery.

3. **S. Chen**, M. Setta, X. Chen, C. Parini, "Ultra Wideband Powerline Communication (PLC) above 30MHz", IET Communications, vol 3, no. 10, pp. 1587 - 1596, October 2009.

4. **S. Chen**, X. Chen, C. Parini, "Measurement and Simulation of Powerline Channel using OFDM for UWB Communication", IEEE International Symposium on Powerline Communications and its Applications, Dresden, Germany, 29 March - 1 April 2009, pp. 79 - 84.

5. **S. Chen**, M. Setta, X. Chen, C. Parini, "Indoor Broadband Powerline Communication above 30MHz", Workshop on Applications for Powerline Communications, Thessaloniki, Greece, 2 - 3 October 2008.

6. **S. Chen**, M. Setta, X. Chen, "Experimental study of UWB transmission over powerline channel", International Symposium on Antennas and Propagation, Taipei, Taiwan, 27 - 30 October 2008.

7. **S. Chen**, X. Chen, C. Parini, "Characterisation of Powerline for UWB Communication", IET Seminar on Wideband and Ultrawideband Systems and Technologies, London, United Kingdom, 6 November 2008.

8. **S. Chen**, C. Chiau, X. Chen, C. Parini, "Characterisation of Powerline for indoor-home network in very high frequency band", Workshop on Network Design and Protocol Engineering for Powerline Communications, Dresden, Germany, 6 - 7 September 2007.

9. **S. Chen**, C. Chiau, X. Chen, C. Parini, "Characteristics of UWB pulses over Powerline Communication", Loughborough Antennas and Propagation Conference, Loughborough, United Kingdom, 2 - 3 April 2007.

10. J. Yu, Y. Cen, **S. Chen**, S. Wang, X. Chen, S. Liu, M. Zhou, Y. Gao, "Design of EMC Testing Equipment for Mobile Phones", submitted to the International Conference on Microwave Technology & Computational Electromagnetics, Beijing, China, 3 - 6 November 2009.

11. M. Hadef, M., J.D. Reiss, C. Almeida, **S. Chen**, X. Chen, "New Chaotic Spreading Codes for Galileo", 3rd ESA Workshop on Satellite Navigation User Equipment Technologies NAVITEC, 2006.

Project Report/Proposal

1. **S. Chen**, X. Chen, C. Parini, "Exploiting Gigabit Powerline Communications", EPSRC Follow-On-Fund Project Proposal, 26 February 2009 (Project Grant Awarded)

2. **S. Chen**, X. Chen, C. Parini, "Gigabit Powerline Communications - Final Report Summary", EPSRC Project Final Report, 31 October 2008

Chapter 1

Introduction

1.1 Powerline Communication, Advantages and Challenges

The powerlines were originally devised to transmit electricity from power stations through power grids to the vast number of users throughout the country [11]. Due to their wide coverage, power supply companies also exploit their networks for data transmission, in order to better manage, control and monitor the power plant and distribution system [1].

The idea of remote electricity supply metering was proposed as long ago as 1838 and the introduction of Powerline Communication (PLC) can be dated back to the 1920s [11, 12]. Initial PLC applications were mainly for power grid control signaling and fault protection facilities, therefore, reliability and robustness were more important than transmission data rate and bandwidth. In Europe the CENELEC band (3 - 148.5KHz, EN 50065 Standard) is allocated to these classical narrow band PLC applications. Similar standard has been established by the IEEE in US, where a frequency range of 50 - 450KHz is available [13].

In the mean time, the growth of the Internet and the advancements in Very Large Scale Integration (VLSI) and Digital Signal Processing (DSP) stimulate the demands for digital communication services. Powerline Communication has entered rapidly into a new development phase, researches have focused on the behavior of power networks above 1MHz [14]. Power companies are trying to

utilise their networks to provide value added services such as smart metering, Internet access, Voice over IP (VoIP) and home entertainment for the so-called "home network". The home network has drawn a lot of interests these years, due to the increasing demand for multimedia services, such as High Definition (HD) video streaming, Internet Protocol Television (IPTV) and online gaming, all of which require data rates much higher than before. A number of solutions are being developed to target this market, i.e. Wireless Local Area Network (WLAN) IEEE 802.11a, b, g, IEEE 802.3 Ethernet and Cable [15]. However, all these technologies require pre-installation and configuration, or even new cable wiring before implementation, whilst customers are more appealed to the "plug and play" technology. This is where PLC comes in, the wide availability of powerlines at home makes it an ideal medium for in-door applications. New wiring installation can be eliminated by reusing the powerline infrastructure. Moreover, it is not challenged by walls and other obstacles because the signals mainly run along the wires. Virtually, any device plugged into a power socket can become a member of this home network, such as PC, TV, DVD player and printer, as illustrated in Figure 1.1.

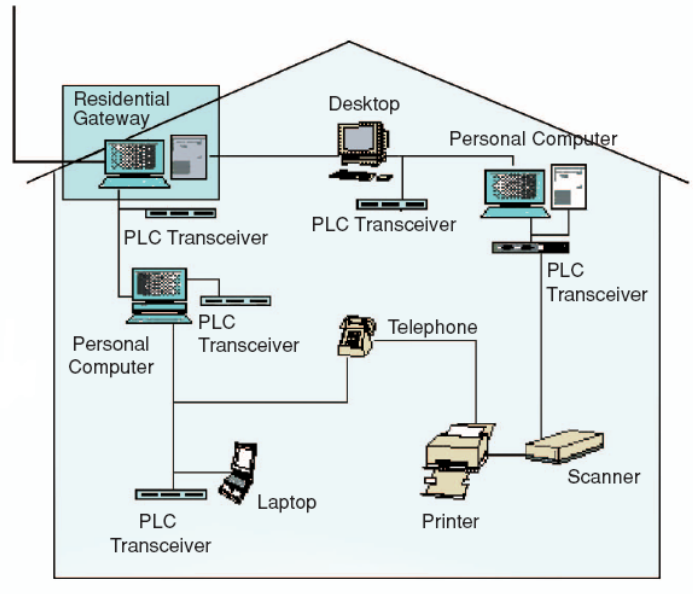

Figure 1.1: Powerline Communication: In-home networking [1].

Although widely available, there is an issue in PLC that needs to be addressed, namely the transmission rate. So far, the majority of studies on PLC only cover the frequency band of 1.6 - 30MHz. The development of HomePlug AV (HPAV) has largely increased the transmission rate of indoor PLC systems, from 14Mbps in HomePlug 1.0 to 189Mbps maximum in HPAV [16, 17]. This is achieved by using more OFDM sub-carriers and higher order constellation maps. There are only 84 sub-carriers in HomePlug 1.0, while this number has been increased to 1155 in HPAV [18]. The number of bits per sub-carrier has also been increased from 2 bits to a maximum of 10 bits. However, there is little space for HPAV to upgrade the system data rate, since very high order modulation scheme has already been used. In order to support future applications mentioned earlier, there is a growing demand to exploit higher operating frequencies to increase the transmission data rate.

Recently, Ultra Wideband (UWB) radio communication has gained widespread interest in wireless applications. It has a number of advantages in terms of simple base band implementation, low interference to co-existing systems, robustness against severe multi-path channel propagation, and more importantly, the potential achievable data rate can be very high, i.e. gigabits per second [19]. Although wireless UWB can achieve very high data rates, it is not suitable for home networking, due to the limited transmission distance (up to 10m maximum [20]) and the high frequency signal is unable to propagate through concrete walls or different floors [21]. These problems could be solved by using the powerline as a transmission channel. The advantages of sending UWB signals over powerlines are: increasing the limited data rate of existing PLC systems and expanding the transmission range limited by wireless UWB systems. However, UWB over powerline technology has not attracted much research interest yet. The channel characteristics of powerline have not been explored above 100MHz, the noise and emission properties in such a high frequency range are unknown, and there is not any coupling unit available to couple wideband signals into the powerline channel. Therefore, the possibility of UWB transmission over the powerline channel is not clear, and the frequency range that could be utilised for such technology has not been defined either.

Although being considered as a good alternative for broadband PLC, much work needs to be done to fully understand the science base of this technology.

1.2 Aims and Objectives

In order to achieve a high speed home network that delivers in-demand multimedia services, PLC network needs to provide high data rate transmissions between different nodes and PLC modems. One of the major tasks in developing such a system is to determine and understand the communication channel characteristics. Although PLC has been widely studied below 30MHz, the channel characteristics above this frequency are rarely known and, therefore, the potential of using low-voltage powerline for data transmission above this threshold is not clear and deserves an in-depth study.

The aim of the research work presented in this thesis is to investigate the feasibility of UWB communication over mains cables in the high frequency range (above 30MHz). A range of technical challenges are required to be tackled, in order to develop and validate models. The research undertaken contains the following steps:

1. Examination of UWB signal transmission over powerline cables above 30MHz. Understand the signal propagation characteristics and select the suitable frequency band for coupler design.

2. Development of a broadband powerline communication coupler that can operate in the desired frequency band for UWB over PLC applications.

3. Investigation of powerline network performance with respect to channel attenuation, transmission distance, noise and potential radiated emission. Analyse the link budget and channel capacity for UWB over PLC systems and define the operating frequency range for potential applications.

4. System level modelling of data transmission over the measured powerline channels based on the existing UWB Physical Layer (PHY) standard proposal. Evaluate the system performance under different propagation channels (i.e. different transmission distances) and data rates.

1.3 Organisation of the Thesis

The thesis is organised in six additional chapters as follows:

Chapter 2 introduces the background of PLC and UWB technologies and highlights the main technologies considered in this study for potential broadband PLC. Existing standards related to both PLC and UWB applications are also discussed.

Chapter 3 investigates the signal transmission characteristics over mains cables in the high frequency range above 30MHz. It provides a comprehensive study on the frequency response of powerline cable, the effect of coupling modes and signal attenuation rate. A suitable frequency band has been selected for further studies on broadband PLC.

Based on the results in Chapter 3, an RF coupler has been developed for UWB over PLC systems in **Chapter 4**, in the frequency band of interest. The design process of the coupler is addressed. The transmission performance of powerline is examined using the coupler in both frequency and time domain.

In **Chapter 5**, a powerline laboratory test bed simulating the UK indoor wiring environment is built and tested. A comprehensive measurement campaign in time and frequency domain is conducted, together with examinations on the powerline system's noise level. This chapter also measures the emission signal from a single ring main powerline circuit. The measured field strength is compared with regulatory standards to see if high level of disturbance will be introduced to existing radio systems.

After theoretical analysis of system parameters such as link budget and channel capacity, **Chapter 6** carries out a system level modelling of data transmission over the measured powerline channels, by using the UWB PHY proposal submitted to the IEEE 802.15.3a standard group. This model is further modified to model other transmission rates over the powerline channels. The usefulness of this model in UWB over PLC system design is evaluated and possible ways of improvement are proposed.

Chapter 7 concludes the main contributions and findings of the research work. Suggestions for future work are also given in this chapter.

Chapter 2

Broadband Powerline Communication and Ultra Wideband

2.1 Introduction

This chapter reviews the background of Broadband Powerline Communication and Ultra Wideband technology. It provides an over view of the existing PLC applications and their technical challenges, together with an introduction to the UWB radio concept and its advantages. The standardisation progress of both technologies and existing studies on UWB over PLC are also summarised. Base on the limitations of existing studies, it is noted that there is a need to understand the transmission characteristics of the powerline channel in the high frequency range above 30MHz.

2.2 Broadband Powerline Communication

2.2.1 Powerline Carrier Communication Applications

Since its introduction to the market, PLC has been exploited in different applications, providing both low data rate and high data rate transmission to customers, as listed in Table 2.1. Power companies use the powerline to control, maintain

	Frequency	Data Rate	Powerline Category	Applications
Narrow band	Europe: 3KHz to 148.5KHz; US: 50KHz to 450KHz	A few hundred $Kbps$	Medium to high voltage powerline, low voltage powerline	Power Grid Control and Monitor, Remote Meter Reading, Smart Grid, Smart Home, in vehicle use.
Broad band	Europe: 1.6 to 30MHz; US: 1.6 to 100MHz	Up to $200Mbps$	Medium and low voltage powerline	In-home Networking, Broadband Internet Access

Table 2.1: Existing applications of powerline communication.

their systems and provide customers with value added services, such as home automation and remote meter reading [22]. Electricity usage is automatically collected and transmitted to the data/billing centre using low and medium voltage powerlines, this can save costs and guarantee data accuracy [23]. Such services require a long transmission distance, i.e. a few hundred meters. Therefore, the data rate is very low and it is called narrow band PLC. PLC is also used in energy saving projects, known as the Smart Grid [24]. The Smart Grid delivers electricity from suppliers to consumers using digital technology to save energy, reduce cost and increase reliability and transparency. It will take pressure off the overloaded grid infrastructure and turn the current electricity grid into an interactive service network, which provides consumers with the ability to monitor and repair their network in real time [25].

Also shown in Table 2.1, broadband powerline communication (BPL) operating in the 1.6 - 30MHz range provides much higher data rate up to 200Mbps. BPL can be deployed in the "last mile" access network and the home network. Access to the Internet can be achieved from homes to the local distribution centre, by using the low voltage network within a residential area. Existing solutions include cable modem, Digital Subscriber Lines (DSL) and Asymmetric DSL (ADSL). The major attraction with BPL is its existing infrastructure, making it a cost effective

way of broadband provision to rural area where other alternatives are not available. Moreover, PLC has also become an important player in the home network market, where there is a need to provide high speed links between household devices, i.e. computers, TV sets and DVD players [26]. All the electrical devices can be linked together simply by plugging into the wall socket, forming a high speed data network environment, where people can enjoy fast speed multimedia services anywhere in the home.

Additionally, powerline is widely used as a data transmission medium in large transportation vehicles (i.e. automobiles, trains and cargo ships) and in-building CCTV surveillance services where other solutions are too expensive to employ [27, 28, 29]. Globally, PLC has been promoted by industrial organisations and governments. In UK, British Telecommunications plc (BT) has announced to use PLC technology to enable the delivery of its digital content and next-generation digital TV services, BT Vision [30]. In Germany and US, BPL has been used as the alternative to DSL for internet access. Smart metering is also widely used in countries such as Italy, Spain and China [31]. In summary, many applications and services can be provided by the PLC system, with its existing infrastructure and wide availability, that make the laying of expensive new cables redundant.

2.2.2 Powerline Channel as A Transmission Path

Despite its ubiquity, the powerline channel is a harsh environment for fast speed communication at high frequencies, being not specifically designed for data transmission. Varying impedance, considerable noise that is not white in nature, frequency dependent attenuation and branching topology, as well as potential electromagnetic disturbance, present technical challenges for system implementation [32].

In the frequency range up to tens of megahertz, the powerline can be regarded as a transmission line, and its impedance varies with frequency [33]. Generally speaking, the average impedance of an indoor mains cable varies between 100 - 150Ω in DC - 30MHz [34]. The situation becomes more complex when determining the impedance from a wall socket. The net input impedance is strongly influenced by the network topology and the connected loads [35, 36]. So the low

voltage mains do not have a fixed characteristic impedance since various loads that are being switched on and off randomly introduce a change in impedance. This makes it extremely difficult to design a suitable coupler that can input the data signal into a powerline communication system [37].

Noise is another crucial parameter of the channel characteristics. Powerline channels rarely have noise properties similar to that of the Additive White Gaussian Noise (AWGN). The noise in powerlines can be separated into 5 classes: coloured background noise, narrow-band noise, periodic impulsive noise that is synchronous or asynchronous to the mains frequency and asynchronous aperiodic impulsive noise [1][2].

Figure 2.1 presents an overview of the noise scenario in a PLC channel. Interference $n(t)$ is added to the transmitted signal before arriving at the receiver. The properties of the first three types of noise usually remain stable over periods of seconds or minutes or even hours and can be summarised as background noise. However, asynchronous impulsive noise, generally caused by switching transients, contains considerable energy that can seriously affect high speed communication, by causing burst errors in the data transmission. Asynchronous impulsive noise can cause strong interference to the powerline system. Analysis and modelling of this type of noise are still the subject of active research [38, 39, 40, 41].

Signal attenuation in powerline is frequency dependent as it exhibits a frequency selective fading characteristic similar to that of a multi-path channel. The presence of branches and impedance mismatch cause multiple signal reflections in a powerline network. Just like a wireless channel, signal propagation takes place between the transmitter (Tx) and receiver (Rx) not only along a line-of-sight (LoS) path, but also other non LoS paths. As a result, frequency selective fading can be observed. A lot of efforts have been devoted to model the powerline channel below 30MHz, among them the multi-path model proposed by Philipps [42] and Zimmermann and Dostert [43] is widely used. In the multi-path model, powerline channels are regarded as the propagation of a number of multi-path signals:

$$H(f) = \sum_{i=1}^{N} g_i e^{-\alpha_i d_i} \cdot e^{-j2\pi f d_i / v_p}, \tag{2.1}$$

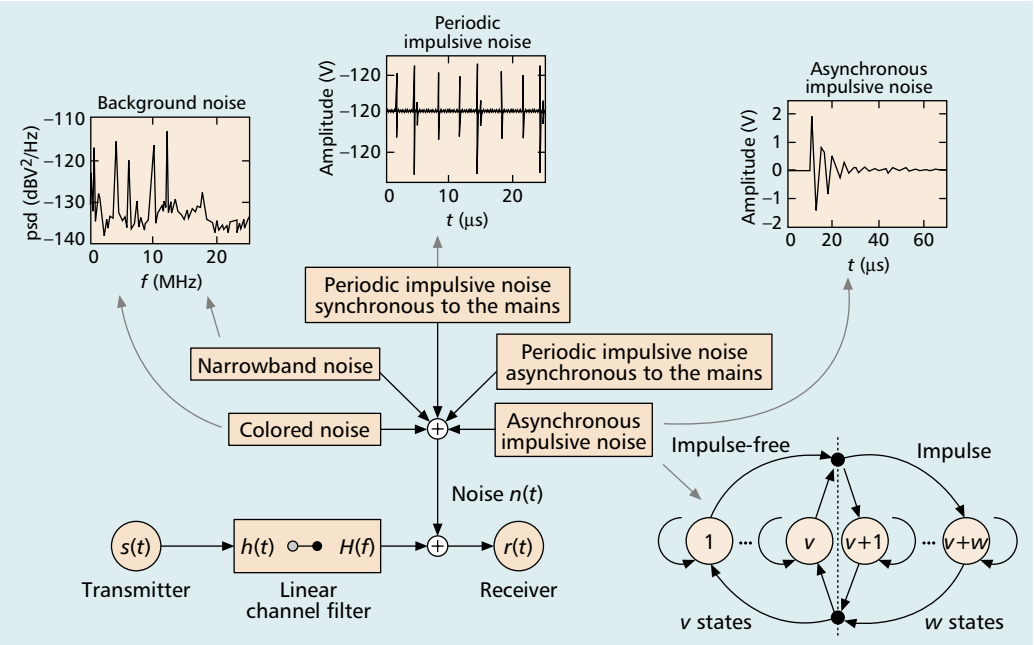

Figure 2.1: Noise scenario on powerlines [2].

where g_i is the weighing factor for each multi-path signal, α_i and d_i are the attenuation coefficient and delay of the ith signal. v_p represents the signal propagation speed. This model is only used in frequency range below 30MHz, and the channel parameters are based on statistical analysis of the measured channel response [44]. When the operating frequency increases, this model can be very complicated, the number of multi-path signals increases dramatically because more frequency components are included.

Another channel model is proposed by Galli and Benwell [45, 46]. The powerline channel is regarded as the cascade of a series of two port networks. This model can be used before actual measurements of the powerline channel. However, it requires knowledge of the channel's propagation constant and characteristic impedance, which are frequency dependent. The estimation of different loads' impedance and socket interface can also be very complicated in high frequency range. Until now, the modelling of broadband powerline channel is still a challenge. Practical measurement of the channel remains a valid approach to understand the variable characteristics of the channel.

Furthermore, it has been observed that PLC devices and the powerline cables have the potential to act as unintentional radiators[1] [47, 48]. The amount of radiation depends on the symmetry of the network and the frequency[49]. Powerlines have poor symmetry (bad impedance matching) and therefore will cause common mode current transmission, where in-phase current with equal amplitude flowing on all the conductors. As illustrated in Figure 2.2, common mode current will produce more radiation in the environment than differential mode current, which is described as antipodal current (currents with equal amplitude but different directions) on both conductors [3]. Moreover, as frequency increases, the transmitted signal will change from being dominantly conducted transmission to having an additional path through radiation. High Frequency (HF) radio services may be affected by the unwanted radiation from the new broadband PLC systems [50]. In order to protect existing systems, PLC system should operate below the emission limits introduced by regulatory bodies.

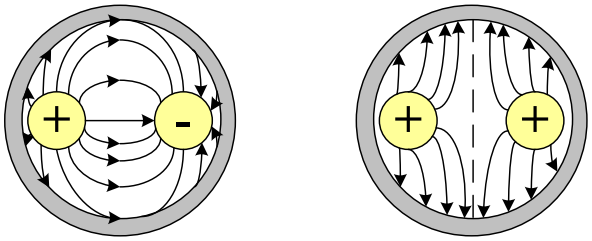

Figure 2.2: Electrical field distribution of differential mode and common mode current in a two conductor powerline.

Although being a very harsh environment for data transmission (e.g. poor impedance matching, strong noise that is not AWGN and frequency selective fading), powerlines still exhibit a high potential in establishing the high speed home network, especially with the advancements in VLSI and DSP systems. Many industrial organisations are exploiting the powerline channel to provide high data rate services, the aim is to increase the transmission speed up to 1Gbps to support HD multimedia contents around the home.

[1]Devices that are not designed to produce radio waves, but do anyway, such as computers.

2.2.3 Modulation Schemes for Powerline Communication

As the properties of powerline channel differ from other well known channels, special care is needed to select a modulation scheme that can exploit the channel as much as possible, and minimise the deteriorating effects. An adequate modulation scheme should be able to overcome the following problems in a powerline channel [51]:

- The frequency selective fading of the powerline channel.
- The interference scenario, especially the narrow band interference and strong impulsive noise causing a relatively low Signal to Noise Ratio (SNR).
- Regulatory constraints regarding to Electromagnetic Compatibility (EMC) that limit the transmitted Power Spectral Density (PSD).

There are three classes of modulation schemes proposed for PLC: Single-carrier Modulation, Spread Spectrum Modulation such as Code Division Multiple Access (CDMA) and Multi-carrier Modulation Orthogonal Frequency Division Multiplexing (OFDM) [38]. Considering the above requirements, it has been proven that OFDM-based multi-carrier signalling is most promising. OFDM is a well proven technique in applications such as Digital Audio Broadcasting (DAB), Terrestrial Digital Video Broadcasting (DVB-T), ADSL and Worldwide Interoperability for Microwave Access (Wi-Max). It is also a possible scheme for Multiband UWB and PLC. Serial data of information is transmitted in parallel on N orthogonal narrow band sub-carriers whose frequencies are $f_0, f_1, \cdots, f_{N-1}$. Thus, each sub-carrier transmits $1/N$ of the original data, so the symbol duration of the sub-carrier increases N times. Hence, a frequency selective channel becomes equivalent to a set of multiple flat-fading sub-channels [52].

Another significant advantage of OFDM is known as adaptive bit loading. That is, variable bits of information are allocated to different sub-carriers according to the SNR. For example, sub-carriers with higher SNR are made to carry more information and are modulated to a higher level constellation (Figure 2.3). Moreover, it can switch off a sub-carrier when the SNR drops below a certain threshold level, or when that frequency band is already occupied by local radio

systems. This is the so called "frequency notching" technique, which has been widely adopted by existing PLC standards [53, 54]. Lastly, OFDM solves the Inter-Symbol-Interference (ISI) problem resulted from multi-path transmission, by adding guard interval and cyclic prefix (a part of the end of a symbol is appended at its beginning) to an OFDM symbol [52]. Thus, OFDM is regarded as the most suitable candidate for high speed PLC. A PHY layer standard using OFDM has already been developed for commercial use in HomePlug 1.0 and HPAV standard [18].

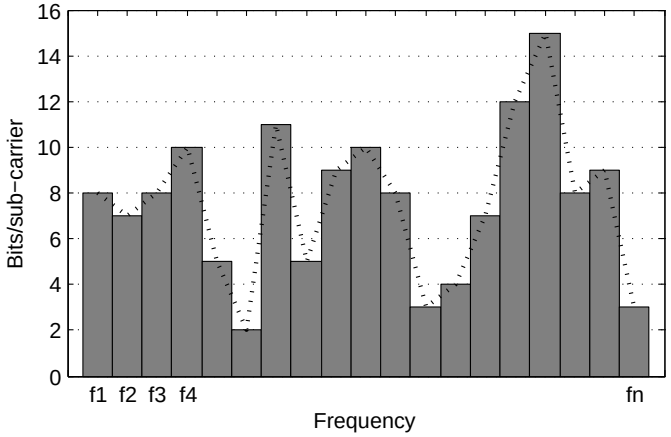

Figure 2.3: Concept of bit loading: more bits are transmitted in sub-carriers with higher SNR.

2.2.4 PLC Standards and Regulations

2.2.4.1 PLC Standards

Just as other communication technologies, broadband PLC needs a national or international standard for its use in the industry and chip set design. Currently, there are four competing powerline home networking standards - the HomePlug AV standard, the High Definition Power Line Communications (HD-PLC) standard, the IEEE P1901 standard, and the new International Telecommunication Union (ITU) G.9960 standard, also known as G.hn [55].

HPAV, proposed by the HomePlug Powerline Alliance, is designed for transmitting HDTV and VoIP around the home. HPAV supports raw data rates up to 150Mbps, it employs adaptive fast Fourier transform (FFT) OFDM over a bandwidth from 1.8 to 30MHz, with possible modulation range from Binary Phase Shift Key (BPSK) to 1024 Quadrature Amplitude Modulation (QAM) [16, 56]. HD-PLC is a competing standard proposed by $Panasonic^{TM}$. Instead of using traditional OFDM, it uses Wavelet-OFDM modulation method. The theoretical maximum data transmission rate is up to 210Mbps in 2 - 28MHz range [57]. The IEEE P1901 working group was formed to develop a standard for high speed (>100Mbps at the PHY) communication devices via alternating current (AC) power lines. The standard will use transmission frequencies below 100MHz [58]. IEEE P1901 will also enable the incompatible HPAV and HD-PLD standards to coexist in a home network without interference.

G.hn is the next generation home network technology standard being developed by the ITU-T and promoted by the HomeGrid Forum. Unlike other specifications that only support one type of wire (powerlines only, or coaxial cable only), G.hn specifies a unified PHY and Data Link Layer that can operate over multiple wire types, i.e. powerlines, phone lines and coaxial cables [59, 60]. G.hn specifies a single PHY based on FFT OFDM modulation and Low-Density Parity-Check (LDPC) forward error correction (FEC) code [54]. G.hn includes the capability to notch specific frequency bands to avoid interference with amateur radio bands and other licensed radio services. Moreover, G.hn aims at higher transmission rates to support services such as IPTV. The promise is a 400Mbps rate with aggregated of 250Mbps throughput, with a 1Gbps rate on the road map.

Above all, there will be mainly two standards for PLC, namely the IEEE P1901 and G.hn [53], the standard frequency range and transmission rate is getting higher also. Furthermore, the two standards are considering coexistence, so that G.hn and IEEE 1901 devices can coexist over a powerline.

2.2.4.2 Regulatory Standards

The full deployment of PLC also needs the support from regulating bodies. Regulations allocate the frequency spectrum that can be used for PLC and impose

emission limits on PLC devices and systems, to protect existing HF radio services. Worldwide, there are a number of projects being conducted to ensure the safe and adequate use of PLC systems.

- **Existing Standards**

  According to the EMC Directive 2004/108/EC, equipment must be designed and manufactured to ensure that the electromagnetic disturbance generated does not exceed the level above which radio and telecommunications equipment or other equipment can not operate as intended. The ITU-T has published Recommendation K60 "Emission levels and test methods for wire-line telecommunication network in case of complaint", which established radiated limits that all wire-line systems including PLC must comply with in case of interference complaints. The ITU-T proposed peak emission limits measured at 3m distance are [61]:

  - 1 - 30MHz: $52 - 28.8log(f_{MHz}/10) dB\mu V/m$
  - 30 - 220MHz: $40 dB\mu V/m$

  Additionally, the International Electrotechnical Commission (IEC) is another regulatory body that seeks to establish and promulgate international standards and good practice in all aspects of electrical, electronic and associated technologies. Among the EMC standards in IEC, the most applicable is CISPR 22 (Information Special Committee on Radio Interference), it's European counter part is EN 55022 [62]. CISPR22 deals with "Information Technology Equipment (ITE) - Radio disturbance characteristics - Limits and methods of measurement". ITE is subdivided into two categories denoted as Class A and Class B. Class B ITE is intended for use in the domestic environment and has to satisfy more stringent limits. Class A is a category for all other ITE equipment with a less strict emission limit. PLC systems are in the Class B category and the ITE limits below 30MHz are [63]:

  (a) Conducted disturbance at the mains ports (disturbance voltage): $56 dB\mu V/m$ quasi-peak in 0.5 - 5 MHz and $60 dB\mu V/m$ quasi-peak in 5 - 30MHz.

(b) Conducted common mode (asymmetric mode) current at the telecommunications ports (quasi-peak values): 84 to $74dB\mu V/m$ in 0.15 - 0.5MHz and $74dB\mu V/m$ in 0.5 - 30MHz.

- **The European Union**

  In Europe, deployment of PLC systems is subject only to a general authorisation pursuant to Directive 2002/20/EC of the European Parliament and of the Council on the authorisation of the electronic communication networks and services. In 2001, the European Commission (EC) called for a draft harmonised European standards for wireline networks. It mandated a Joint Working Group (JWG)(Mandate 313) consisting members from CEN (European Standardisation Committee), CENELEC (European Committee for Electrotechnical Standardiation) and ETSI (European Telecommunications Standards Institute) to prepare standards for the new broadband wireline telecommunication network.

  As of April 2005, the EC again recommended promotion of PLC by its member states, considering that PLC system fall within the scope of the EMC Directive. "In case of radio interference, the national authorities should perform in situ measurements considering that only a common mode current limit is prescribed in the High Frequency range." The limit for common mode emission is $30dB\mu A$ (measured at 3m to the line using 9KHz bandwidth), corresponding to a peak electrical field strength level of $59.5dB\mu V/m$, which is identical to the standards in CISPR 22 Class B ITE [3].

  In terms of complaints, national regulatory authorities are allowed to take special measurements at a specific site in order to overcome the problem. In June 2005, the European Conference of Postal and Telecommunications Administrations (CEPT) adopted the ECC (European Communications Council) Recommendation (05)04 about the assessment of complaints caused by telecommunications networks [64]. Permanent, dynamic and programmable frequency notching will be used at different frequencies.

- **FCC Standard**

  In the USA, the general EMC requirements are set by the Federal Communications Commission (FCC). FCC Part 15 Rules cover equipment capable of (not deliberately) emitting RF energy in the range of 9kHz - 200GHz. FCC Report and Order adopts new requirements and measurement guidelines for Access BPL in 1.705 - 80MHz. The FCC advocates BPL and considers it offers a number of benefits, including: 1) increasing the availability of broadband services to homes and business; 2) improving the competitiveness of broadband services market; 3) improving the quality and reliability of electric power delivery and 4) advancing homeland security [65].

  Compared to European limits, FCC limit is less stringent. According to FCC, carrier current devices, including BPL equipment, are subject to the Commission's existing Part 15 rules for low power, unlicensed equipment that operates on a non-interference basis. FCC Part 15 Section §15.209 specifies the intentional emission limit below 30MHz, at $29.5dB\mu V/m$ measured at 30m, or $73.5dB\mu V/m$ (peak) when converted to 3m distance. For BPL equipment operating above 30MHz, Section §15.109 limits should be applied. The peak field strength of radiated emission limits measured at 3m are $44dB\mu V/m$ in 30 - 88MHz, $47.5dB\mu V/m$ in 88 - 216MHz and $50dB\mu V/m$ in 216 - 960MHz [66].

  FCC also requires adaptive interference mitigation techniques. "BPL equipments should remotely reduce power and adjust operating frequencies, in order to avoid site specific, local use of the same spectrum by licensed users. These techniques may include adaptive or notch filtering, or complete avoidance of frequencies locally used by licensed radio operations" [65].

Figure 2.4 illustrates the field strength limits proposed to broadband wireline telecommunication networks, in the frequency range from 1MHz to 1GHz. The field strength should be measured in 3m distance to the powerline, using a measurement bandwidth of 9KHz below 30MHz and 120KHz above 30MHz.

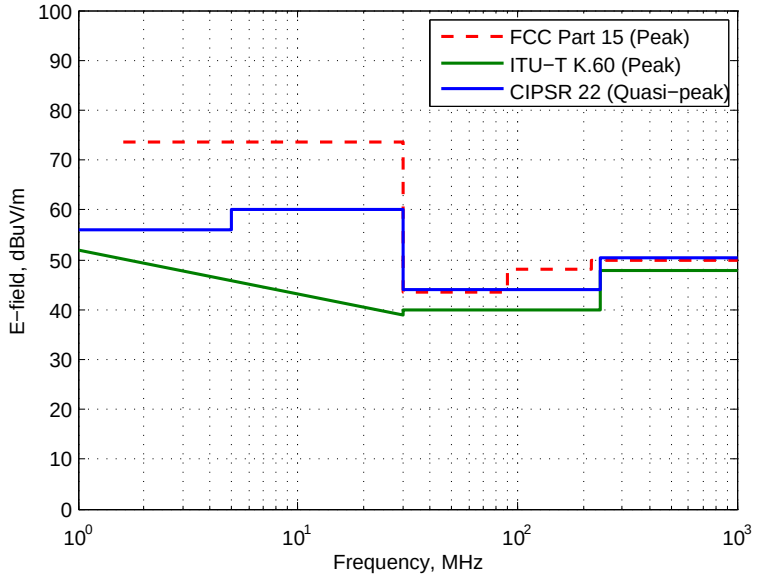

Figure 2.4: Field strength limits proposed to broadband wire-line telecommunication networks. All limits extrapolated to 3m measurement distance (Reproduced from [3]).

2.3 Ultra Wideband Technologies

With broadband PLC gaining widespread interest these years, a number of research projects have been carried out to exploit the channel in the high frequency range, aiming to increase the transmission data rate. Among them, UWB over powerline is an attractive topic of research.

Ultra Wideband is a novel technology that can provide much higher data rate than existing communication systems. While most studies on UWB are related to short range wireless communication, wire-line communications using UWB technology also starts to attract interests recently.

2.3.1 UWB Definition

UWB radio communication is known as a "carrier-free", "baseband" or "impulse" technology. The basic concept is to convey information by mapping an information symbol stream into a sequence of short-duration pulses, with the resulting waveforms extremely broadband in frequency. A unique characteristic of UWB is that it usually employs carrier-less, short duration pulses for information transmission and reception. A second derivative Gaussian pulse, or Gaussian Doublet is often used as a UWB signal. It has the very interesting property that its spectrum does not occupy the low frequencies where the level of man made background noise is high [67]. The waveform of the pulse can be defined as:

$$s(t) = (1 - 2\frac{(t - T_0)^2}{\tau^2})e^{-((t-T_0)/\tau)^2} \tag{2.2}$$

where t is the time, τ and T_0 are the time-scaling factor and pulse delay respectively. Figure 2.5 illustrates an example of a $0.4ns$ Gaussian doublet, it has very wide frequency band from 3GHz to 10GHz.

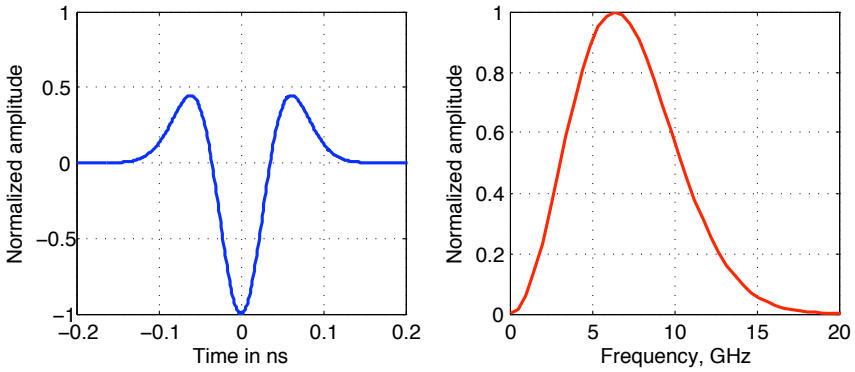

Figure 2.5: Second derivative Gaussian pulse: (a) pulse shape (b) power spectrum.

To distinguish UWB signals from other narrowband systems, any signal that occupies bandwidth equal to or greater than 500MHz or whose fractional bandwidth is equal to or greater than 0.2 is recognised as an ultra wideband signal. The fractional bandwidth is defined as:

$$B_f = 2\frac{f_H - f_L}{f_H + f_L} \tag{2.3}$$

where f_H and f_L are the higher and lower bounds that are 10dB below the maximum radiated emission. The FCC has approved the use of 3.1 - 10.6GHz frequency band for UWB devices and has provided the radiation limit for UWB devices in indoor and outdoor environment, as illustrated in Figure 2.6 [19].

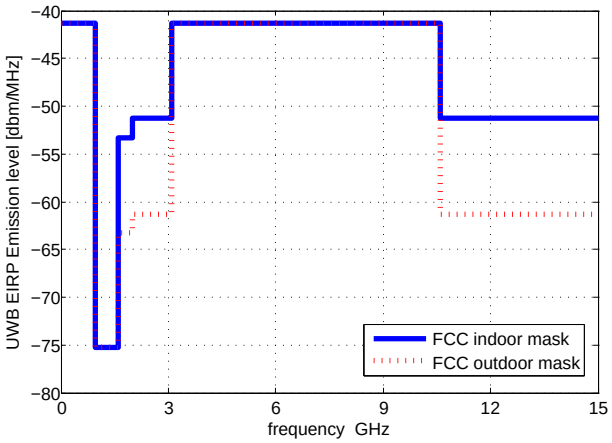

Figure 2.6: FCC defined radiation emission mask for UWB communications.

2.3.2 UWB Standards

The standardisation of UWB PHY used to be looked after by the IEEE 802.15.3a task group. IEEE 802.15.3a was an attempt to provide a higher speed UWB PHY enhancement amendment to IEEE 802.15.3 Wireless Personal Area Network (WPAN), for applications involving imaging and multimedia. Currently there are two proposals to the UWB standard: Multiband OFDM (MB-OFDM) supported by WiMedia and Direct Sequence UWB (DS-UWB) supported by UWB forum.

DS-UWB is often referred to as a pulse based technology. It operates by sending low power Gaussian shaped pulses which are coherently received at the Rx. DS-UWB can use two formes of modulation, namely the Pulse Position Modulation (PPM) and Bi-Phase Modulation (BPM) (Figure 2.7) [68]. PPM encodes the information by modifying the time interval and hence the position of the pulse. BPM on the other hand, is to reverse the phase of the pulse to signify the information data. The main advantage with DS-UWB is the simple

Tx design. However, the pulse based system makes it difficult to collect significant multi-path energy using a single RF chain, and the switching time requirement is very stringent, usually less than $100ps$. The Rx signal processing is also very sensitive to group delay variations of the system [69].

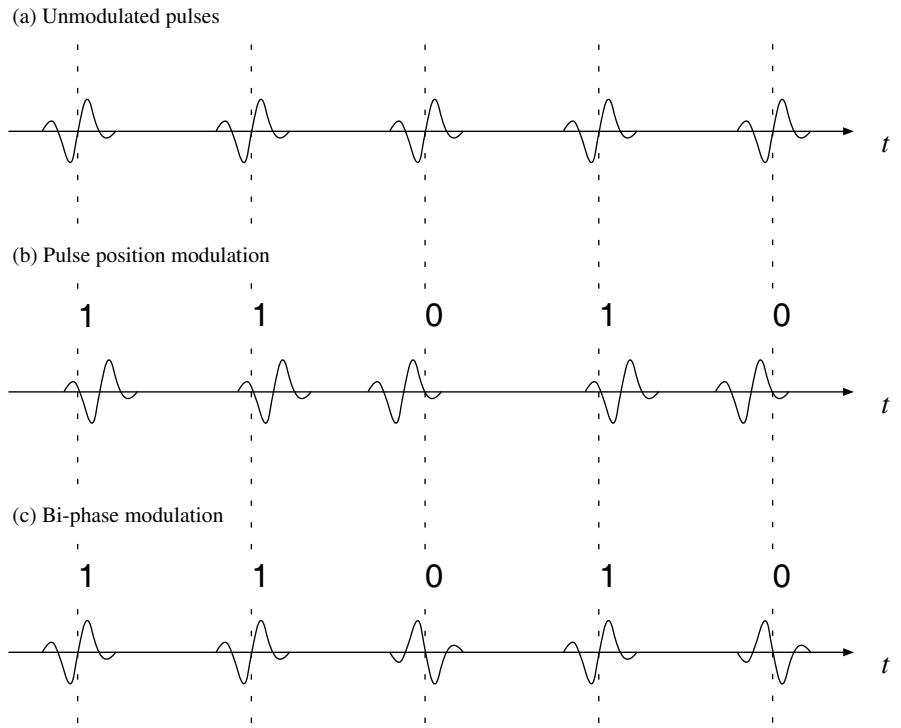

Figure 2.7: Comparison of PPM and BPM methods for UWB communications [4].

Industrial organisations tend to support the MB-OFDM system proposed by WiMedia, due to its ability to address performance requirements such as data throughput and range, while maintaining low cost, low complexity and reduced power consumption. According to the FCC requirements that UWB signals have to be at least 500MHz, MB-OFDM UWB divides the spectrum into 5 band groups consisting of 14 bands, each band being 528MHz wide (Figure 2.8). Each 528MHz band is further divided into 128×4.125MHz sub-carriers which are orthogonal to each other. User data and other control information are mapped into individual

sub-carriers in the frequency domain. Such information will pass through the Inverse Fast Fourier Transform (IFFT) block and generate the OFDM symbol in the time domain. "Multibanding" refers to the time-interleaving or hopping of OFDM symbols across bands in any particular band group [70]. For initial system development, only Band Group 1(3.168 - 4.752GHz) is used.

MB-OFDM has a number of advantages, including high spectral efficiency, resilience to RF interference, robustness to multi-path and narrowband interference [69]. The only draw back of this type of system is that the Tx is more complex compared to DS-UWB, because it requires an IFFT operation. Nevertheless, this can be handled by using advance DSP techniques and chip sets. Given its ability to overcome multi-path environment and its similarity to conventional OFDM system, it is possible to employ the MB-OFDM PHY specification in the powerline channel.

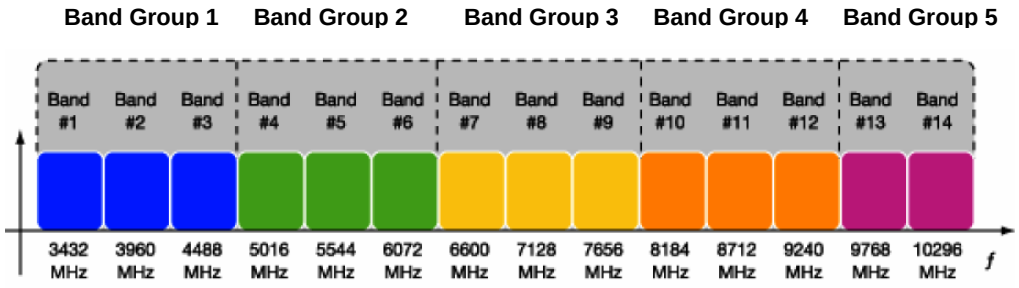

Figure 2.8: The MB-OFDM UWB frequency band plan (Reproduced from [5]).

2.3.3 Advantages of UWB

One of the most significant advantages of UWB over existing wireless alternatives is the extremely high transmission data rate. According to Shannon's Shannon-Nyquist criterion [71, 72], the upper bound on the maximum achievable data rate for an ideal band-limted AWGN channel is:

$$C = B \times log_2(1 + S/N), \tag{2.4}$$

where B is the system bandwidth, S is the signal power and N represents the noise power. Channel capacity C increases linearly with the operating bandwidth

B, thus UWB can provide much higher data rate compared with narrowband applications such as Wi-Fi IEEE 802.11g. IEEE 802.11g operates at 2.4GHz, it provides a maximum data rate of 54Mbps for indoor transmission [73]. While WiMedia UWB can achieve short range (less than 10m) multimedia file transfer with data rate up to 480Mbps [74]. Further, industrial organisations such as Pulse∼Link^{TM} is working on in-door UWB communication to increase data rates up to gigabits per second [75].

UWB also has low power consumption. WiMedia UWB systems have been designed for this purpose, currently at 1.5 to 2mW/Mbps. While the state-of-the-art IEEE 802.11g radio typically consumes 15 to 20mW/Mbps, 10 times higher than UWB appliances [74]. This makes UWB practical for today's consumer electronic devices, when only limited power can be transmitted.

Finally, due to the low emission rate of UWB, it will not cause significant interference to existing radio systems. Meanwhile, UWB signal occupies a very wide frequency band, making it more immune to narrowband interference from other communication systems, such as IEEE 802.11a, which is operating in 5.4GHz frequency band.

2.4 UWB over Powerline - State of the Art

Although mainly used in wireless applications, wired UWB transmission has started to attract interests. UWB transmission over the low voltage powerline can link up devices in a house, as signals mainly propagate along the powerline conductors, while UWB radio only covers a room, in ranges up to 10m maximum. UWB radio is more suitable for short-range, high-speed communications, such as large file transfer between nearby devices, including digital cameras, PCs and MP3 players. It is very difficult for UWB radio signals to penetrate through walls or concretes, because of the high operating frequency [21]. Hence, transmitting UWB signals over powerline cables can potentially solve the limitations in UWB radio, as well as the slow data rate issue in PLC.

A number of research projects are carried out on UWB over powerline in order to increase the channel capacity. Encouraging results on UWB pulse transmission over powerline has been shown in the 100MHz frequency range [76]. Wideband

impulse modulation for powerline below 50MHz has been extensively studied in the European Union "WireNet" project - "Powerline data exchange for domestic and industrial automation based on the UWB approachapplication", with promising results shown in [67, 77]. The main achievements have been to investigate, in a specialised laboratory set-up, the fundamental aspects of the wide-band impulse modulated solution, prototype and test specialised hardware components, develop a physical layer, a MAC and a link layer, demonstrate the exploitation potential of the technology by means of a demonstrator that is focused on a low-cost system for home and industrial applications [78]. Other applications of UWB over in-door coaxial cables have also been reported as successful [79].

A fabless semiconductor company developing advanced UWB technologies, Artimi^{TM}, also indicated that it is possible to transmit UWB pulses along mains cable [80]. So far Artimi^{TM} has demonstrated the transmission of video digital content under simple laboratory conditions. The configuration and key components of their demonstration system are shown in Figure 2.9 [81].

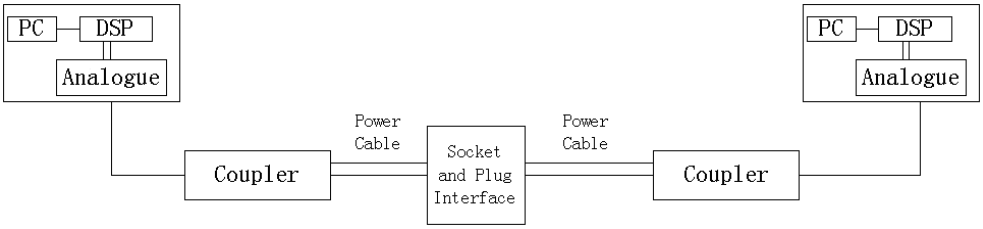

Figure 2.9: Artimi's UWB pulse over powerline demo system (10m mains cable, one plug and socket).

The system consists of a pair of Tx/Rx, two RF over mains cable couplers, a plug and socket interface and a 10m mains cable. Artimi et al have reported that they have transmitted UWB pulses that are fully compatible with the FCC defined spectrum mask over powerline. Their experiment results are shown in Figure 2.10.

However, the preliminary study conducted by Artimi^{TM} is far from exhaustive, and only base-band pulse transmission is considered. As mentioned earlier, pulse based transmission has a number of limitations and is not preferred in practice.

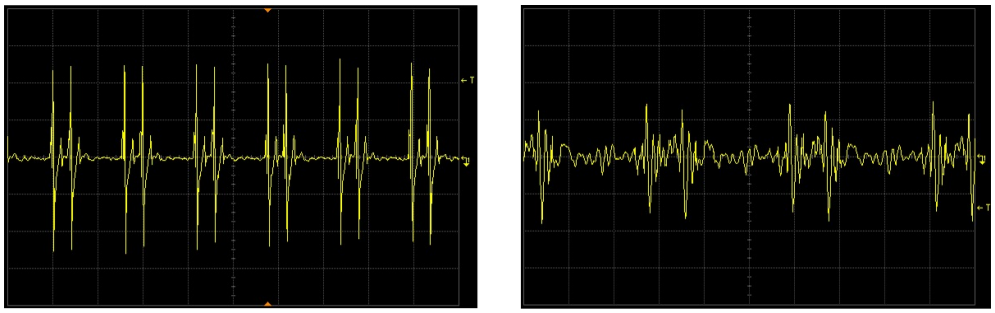

Figure 2.10: UWB pulses used in Artimi's demo: transmitted pulse (left) and received pulse(right) (The scale of the diagram is not given).

Moreover, existing studies have not examined the channel properties thoroughly, especially above 30MHz. The powerline channel characteristics in the UWB band and the signal attenuation rate are unknown (as noted from Figure 2.10), and the possible data rate is not given either. Further investigation are required to understand the signal transmission characteristics over powerline channels in a much higher frequency band.

2.5 Summary

The technological background of PLC and UWB have been introduced in this chapter. A review of the various applications provided by PLC showed that it is a promising technology in energy saving and communications market. Broadband PLC is promoted globally by regulatory bodies, such as the EC and FCC, both of which believe that PLC is the cheapest way to bring high data rate internet connection to the home. Developing PLC standards are aiming to increase the operating frequency band and transmission rate over the powerline channel. However, the powerline as a transmission medium is mainly studied under 30MHz range, channel characteristics in high frequency range are still not very well understood.

UWB over powerline has been considered as a viable solution to the limited transmission rate of PLC and the short range problem in wireless UWB. UWB radio has advantages in terms of high potential data rate and low PSD as the

energy is spread in a wide frequency range. A few preliminary studies have been done on UWB over PLC, but none of them have fully studied the broadband channel characteristics, nor have they addressed other technical issues such as the coupler design. Therefore, further investigations need to be conducted to fully characterise and analyse such technique to maximise its potential benefits.

Chapter 3

Powerline Channel Characteristics in UWB Frequency Band

3.1 Introduction

It is noted in Chapter 2 that the transmission environment of the powerline channel plays an important role in the feasibility of UWB over PLC technology. In this chapter, the signal transmission properties and attenuation characteristics over the powerline channel will be examined in a very wide frequency range. Following the analyses, a frequency range for UWB over PLC will be defined for coupler design and system development.

3.2 Powerline Cables

There are many types of mains cables for indoor, outdoor, industrial and residential use. Different applications often use powerlines that have different cross sectional structures. Powerlines used for single-phase indoor wiring are often comprised of three or four conductors. All are confined by an outer jacket to maintain close conductor spacing, some even have a metallic sheath to reduce radiation. Experimental studies show that the mean impedance of in-home powerline is

between 100Ω and 150Ω [49, 82].

In the UK, there are two predominant types of cables for indoor wiring: the three-core flexible and the 2.5mm flat twin and earth cable.

The three-core flexible cable (Figure 3.1) is often used to connect an electrical appliance to a power outlet. It is soft and usually has a length of several meters. It consists of three conductors: the brown "live", blue "neutral" and green/yellow stripped "earth" wires. Each conductor consists of 40 stranded copper wires, covered and separated by a Polyvinyl Chloride (PVC) insulated sheath.

Another type of powerline is the 2.5mm flat twin and earth cable. It is not directly visible in a home environment because it is laid inside the walls, connecting power outlets and the customer premises. This is the main cable used for in-home wiring. It can be decades of meters long depending on the size of the house or the room. As illustrated in Figure 3.2, a 2.5mm flat twin and earth cable consists of three conductors, "live" (red or brown), "neutral" (blue or black) and "earth" (a single conductor without plastic sheath). Different from the three-core flexible cable, the conductor of 2.5mm flat twin and earth cable is a single copper wire, with "earth" relatively smaller than "live" and "neutral".

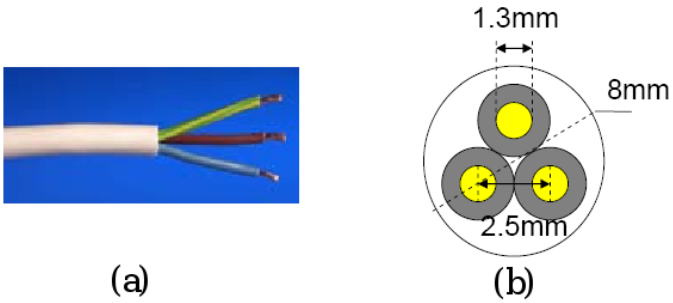

Figure 3.1: Three-core flexible cable: (a) side view (b) cross sectional view.

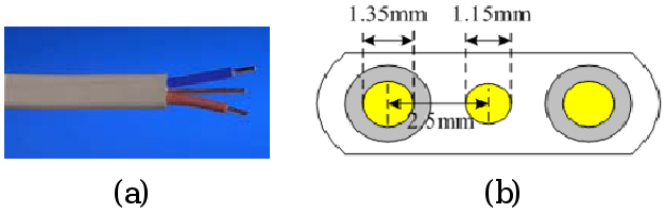

Figure 3.2: 2.5mm flat twin and earth cable: (a) side view (b) cross sectional view.

3.3 Powerline Channel in FCC Defined UWB Band

In order to achieve UWB communication over powerline, it is important to understand the high frequency signal transmission characteristics of the channel. The FCC defined UWB frequency band as 3.1 - 10.6GHz, so firstly, the powerline channel is examined in the frequency range up to 10GHz. The twin and earth cable has been studied using software modelling and measurement.

3.3.1 Modelling of Powerline Channel

Firstly, CST Microwave Studio^{TM} [83] is used to model the time domain signal transmission in the powerline, namely the 2.5mm flat twin and earth cable. The simulation model is shown Figure 3.3, a 1m cable is terminated by a 50Ω coaxial connector[1] at both ends. A short duration impulse will be transmitted and the received and reflected signal will be simulated.

3.3.1.1 Signal Coupling Modes

Due to the multi-conductor structure of the powerline, there are many ways to connect the conductors to the coaxial connector. In order to find the best coupling mode, two kinds of transmission mode have been simulated, i.e. common mode and differential mode. In common mode excitation, all three conductors are

[1]The 50Ω coaxial connector is chosen to match the output impedance of the network analyser, which is 50Ω.

connected to the coaxial feed, while in differential mode, "live" is connected to the coaxial feed, "neutral" to the coaxial ground and "earth" is not connected.

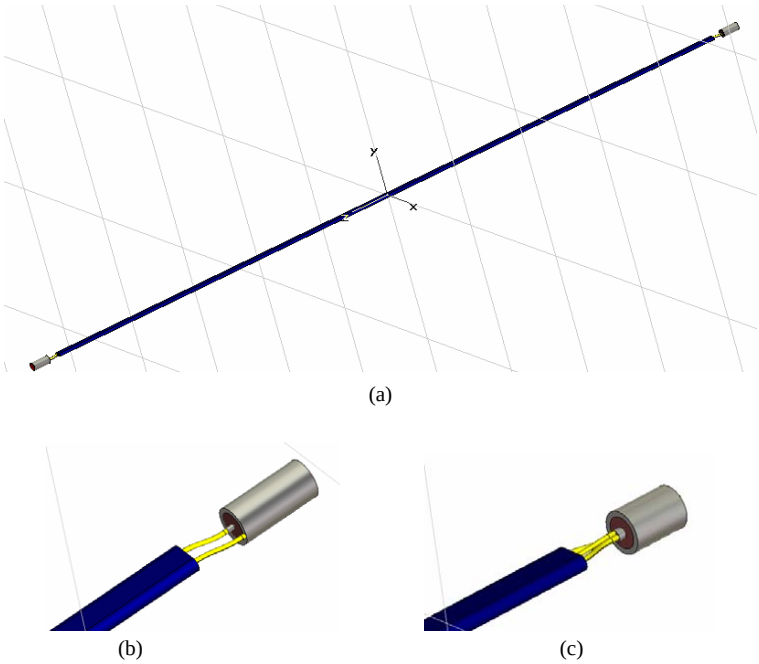

Figure 3.3: CST powerline simulation model (a) 1m flat twin and earth cable (b) differential mode coupling (c) common mode coupling.

In the CST Microwave Studio^{TM} time domain solver, a $5th$ derivative Gaussian pulse is transmitted. As illustrated in Figure 3.4, the transmitted pulse have $0.5ns$ duration and it meets the FCC indoor mask in 3.1 - 10.6GHz. The received and reflected signals are shown in Figure 3.5. It can be seen that in common mode transmission, only a single ringing pulse is received at $4.8ns$. While in differential mode, two signals with different velocities are received when only one pulse is transmitted, a fast travelling ringing pulse and the main transmitted signal. Compared with common mode transmission, it can be proved that the early arriving ringing pulse is the common mode signal excited by the unbalanced current distribution between the two conductors. Such asymmetry will give rise to an unwanted common mode signal, which is described as in-phase current with equal amplitude on all the conductors [84]. Common mode signal will cause

strong far field radiation due to its current distribution and is usually regarded as noise in a transmission system.

Moreover, we can observe that the common mode signal travels faster. This is because the powerline provides an inhomogeneous dielectric environment, which supports slightly different propagation velocities for the two modes [85, 86]. In differential mode, the electromagnetic (EM) field is mainly inside the powerline cable and propagates along the dielectric material of the powerline, therefore $v_{diff} = c_0/\sqrt{\varepsilon_r}$, where c_0 is the free space velocity and ε_r is the powerline's dielectric permittivity. While for common mode transmission, most of the EM field will be outside the cable, making the common mode signal travel at a higher velocity between c_0 and v_{diff}.

In summary, the time domain simulation has shown that common mode is not suitable for transmitting signal and should be avoided by using a proper RF coupler.

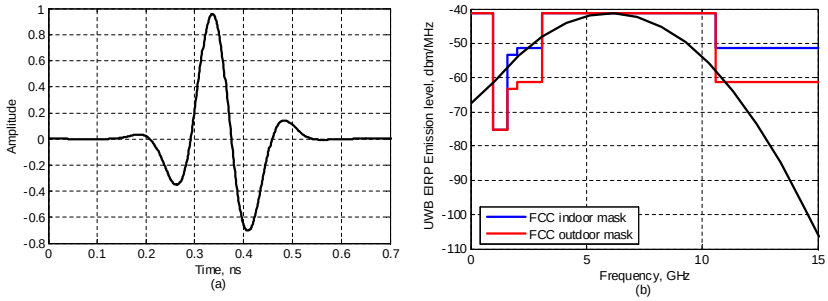

Figure 3.4: The 5th derivative Gaussian Pulse and its PSD.

3.3.1.2 Signal Radiation

In CST Microwave Studio^{TM}, the electrical field distribution near the conductor can be observed to see the field variations at different frequencies. This is very useful in studying the radiation characteristics in high frequency band. Figure 3.6 shows the electrical field distribution of power cables when fed differentially, at three different frequencies, 1GHz, 5GHz and 10GHz. At 1GHz, most of the electrical field is bounded around the conductor, only little is radiated in the

air. At 5GHz, more energy is radiated. However, at 10GHz, it is clearly noticed that most of the field energy has been radiated into the air, only little has been transmitted over the powerline.

Usually, powerlines can be regarded as long antennas that radiate energy in high frequency bands [49]. Although differential mode will cause much less far field radiation compared to common mode, radiation may still arise from the asymmetrical current distribution in powerline conductors. Further, radiation in the near field also contributes to energy loss. As from Figure 3.6, signal transmission above 1GHz can cause most of the energy to be radiated and thus not suitable for PLC applications.

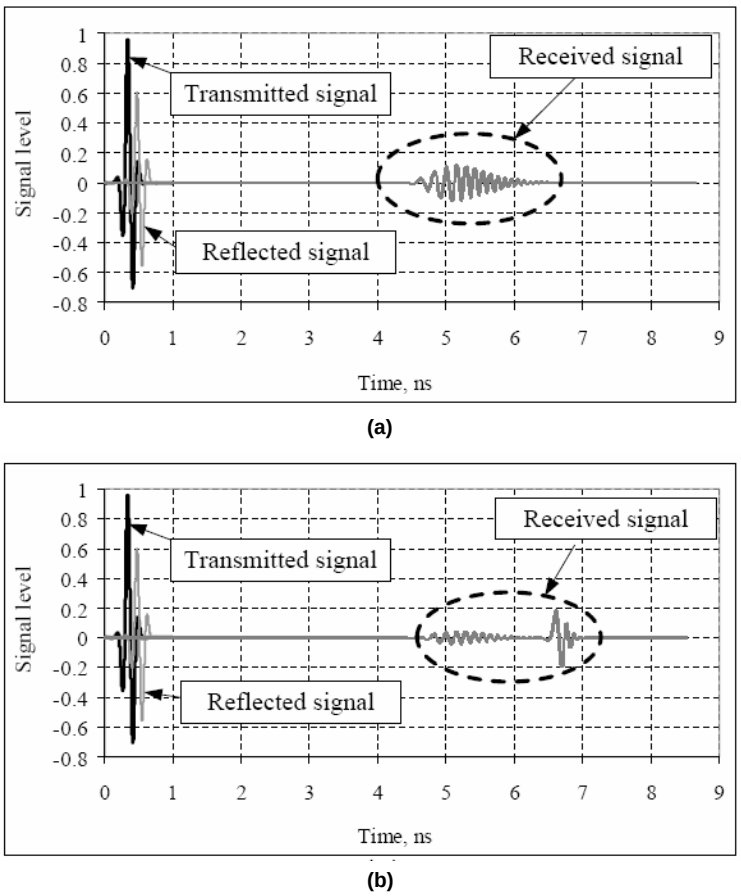

Figure 3.5: Simulated result of received pulse (a) common mode (b) differential mode.

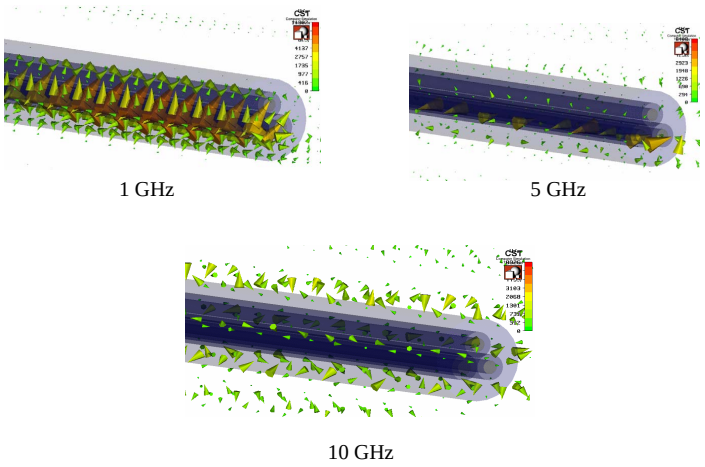

Figure 3.6: Electric field distribution over powerline at different frequencies.

3.3.1.3 Powerline Impedance

In addition to the above results, CST^{TM} simulation tool can also obtain the analytical line impedance of a multi-conductor transmission line [83]. By examining the pulse transmission, time domain refractometry (TDR) can be used to calculate the powerline impedance. TDR was initially developed for locating faults on long electrical systems, i.e. twisted wire pairs and coaxial cables [87]. TDR transmits a short rise-time signal and measures the reflections that result from the signal travelling through the cable [88]. It is also used to determine the impedance of the cable, by using the reflection coefficient ρ, which is the ratio of the reflected pulse amplitude to the incident pulse amplitude, as shown in Equation (3.1):

$$\rho = \frac{V_{Reflected}}{V_{Incident}} = \frac{Z_L - Z_0}{Z_L + Z_0}, \tag{3.1}$$

where Z_0 is the transmission line impedance and Z_L is the load impedance. With the load impedance available, the line impedance can be calculated.

$$Z_0 = Z_L \times \frac{1-\rho}{1+\rho}. \tag{3.2}$$

Figure 3.7 illustrates the simulated differential mode line impedance of the cable. There is strong impedance mismatch before $1ns$, when the pulse is injected

from the coaxial connector to the cable. Afterwards, the signal is transmitted without reflection and the line impedance becomes stable at around 115Ω.

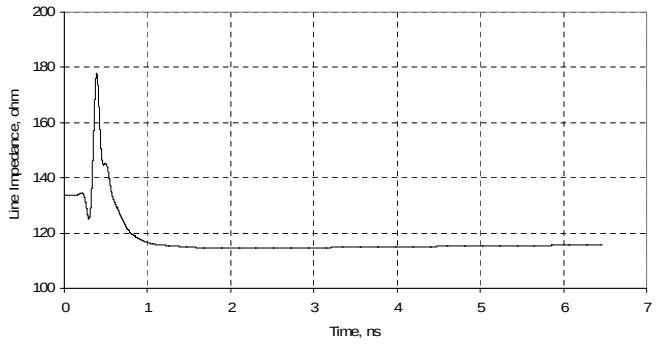

Figure 3.7: TDR simulation of the line impedance of differential mode.

3.3.2 Frequency Domain Characterisation

After numerical simulation of pulse transmission over powerline, its transfer function is examined experimentally in the frequency domain. As mentioned earlier, differential mode transmission is preferred in PLC. So all the signals are injected differentially to the powerline via a 50Ω coaxial connector, where antipodal current flows on "live" and "neutral" (Figure 3.8).

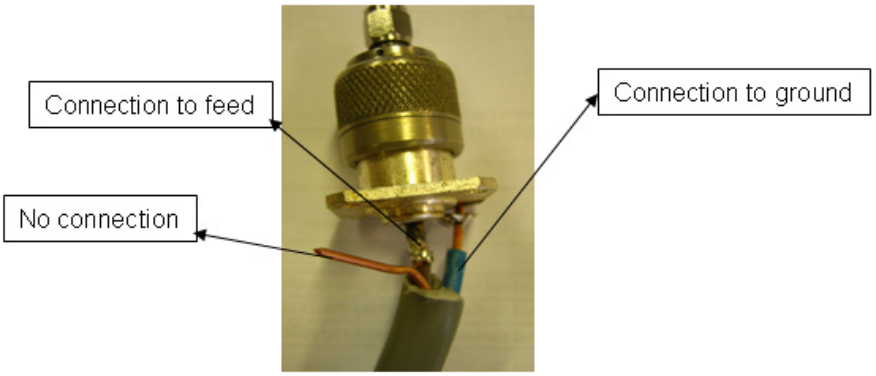

Figure 3.8: Differential mode connection to the coaxial connector.

A Vector Network Analyser (VNA) HP8720ES is used to record the transfer functions (S_{21}). Both types of the powerlines have been measured in different environments, i.e. on the ground and in the air. Figures 3.9 and 3.10 illustrate the transfer functions of both types of cables in 1m and 2m.

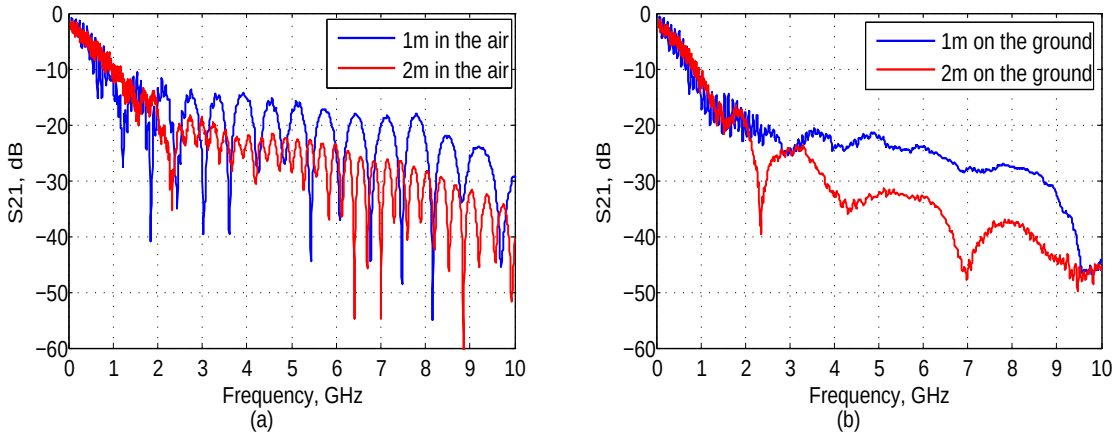

Figure 3.9: Measured S_{21} of 2.5mm flat twin and earth cable (a) in the air (b) on the ground.

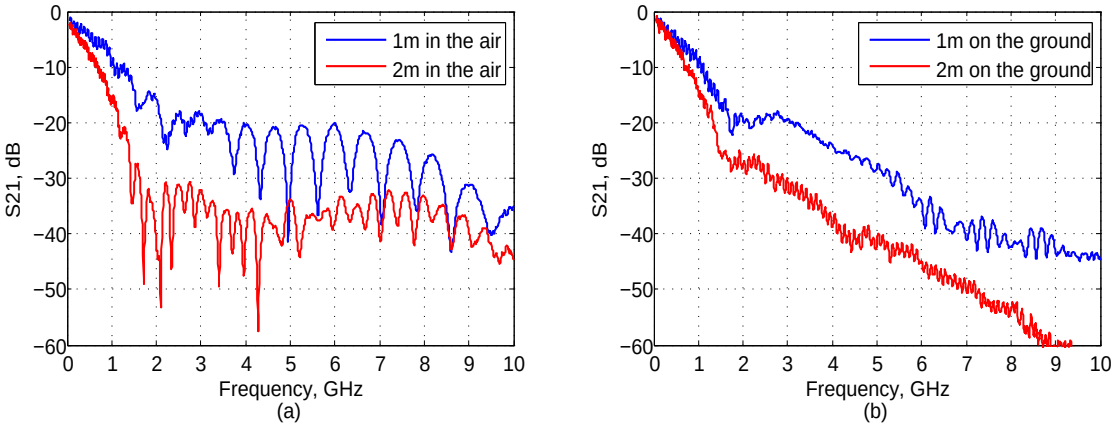

Figure 3.10: Measured S_{21} of three-core flexible cable (a) in the air (b) on the ground.

It is noticed that signal attenuation in powerline is very similar below 1GHz

in both scenarios, whereas at high frequencies above 1GHz, the S_{21} curves are quite different. Higher attenuation is experienced by cables laid on the ground, despite the S_{21} curves being much flatter than those measured in the air. When the cables are measured in the air, big cycles of notches can be observed.

The frequency intervals of notches are dependent on the cable length. Figure 3.11 illustrates the points of notches in 5 - 8GHz frequency band. The average frequency interval between deep notches for 1m and 2m twin and earth cables are 0.68GHz and 0.3GHz respectively, which are inversely proportional to the cable length. Such cycles of transmission nulls are caused by the resonance of the powerline, because in high frequency bands, the communication signals are radiated rather than being transmitted [89].

Thus, when the cable is held in the air, it begins acting an like antenna that radiates an EM field in the environment. Radiated emissions will not only cause strong attenuation to the transmitted signal, but also give rise to potential interference to other radio systems.

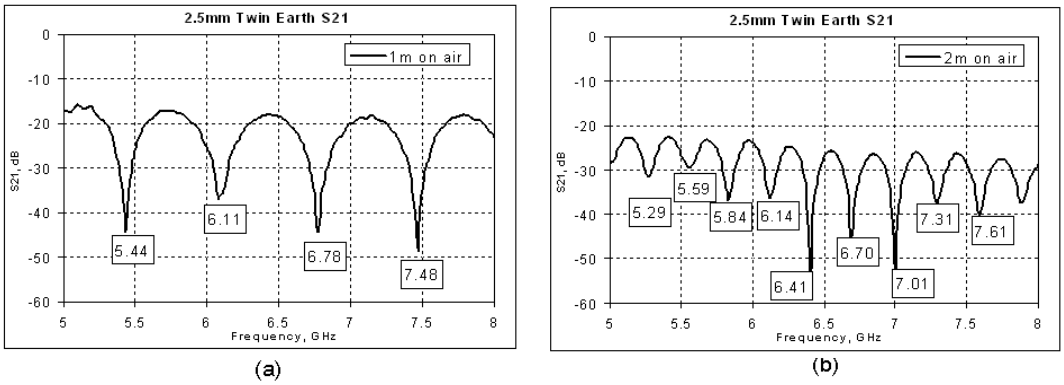

Figure 3.11: Frequency points of deep notches of S_{21}, in the air (a) 1m (b) 2m.

When measured on the ground, a smoother curve is observed and deep notches disappear. The radiated high frequency energy has been absorbed by the earth ground, hence the radiation resonance is damped. Measurements of longer cables has been carried out, as shown in Figure 3.12. Still, the channel loss is too high above 1GHz. At 10m, S_{21} varies between 30dB and 90dB in 1 - 10GHz frequency

band and the average attenuation reaches 54.7dB in 5 - 10GHz range, making the powerline a very hostile environment for data transmission.

Despite the strong channel losses, it is noted that attenuation within the 50MHz - 1GHz frequency band is much smaller and the channel transfer functions do not exhibit deep frequency selective fading effect. This provides a potential frequency window for the intended UWB over PLC application. Therefore further channel characteristics analysis is conducted below 1GHz in the following section.

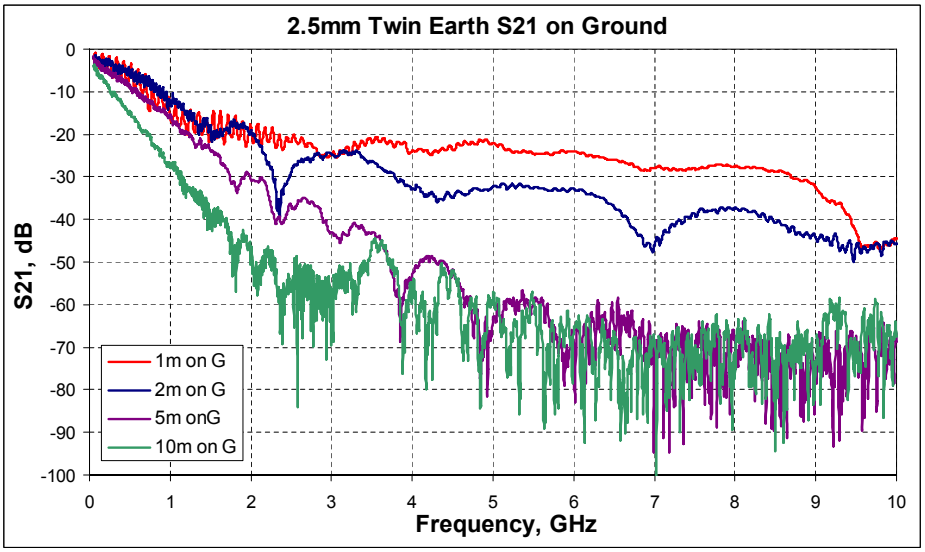

Figure 3.12: Frequency response of twin and earth cable measured on the ground.

3.4 Powerline Channel Characteristics below 1GHz

In this section, signal transmission over the powerline is further examined in the 50MHz - 1GHz frequency band, in order to verify that the channel provides a possible path for UWB signal transmission. A VNA is used to measure the S_{21} parameters, 1601 frequency points are collected at a sweep time of 3.21 seconds. Since there is not much difference between the in-the-air and on-the-ground cases (Figure 3.13), all the measurements are carried out with mains cables lying on

the ground. Figure 3.14 shows the measured transfer functions of both cable types, from 50MHz to 1GHz. A number of characteristics can be observed from the measurement results.

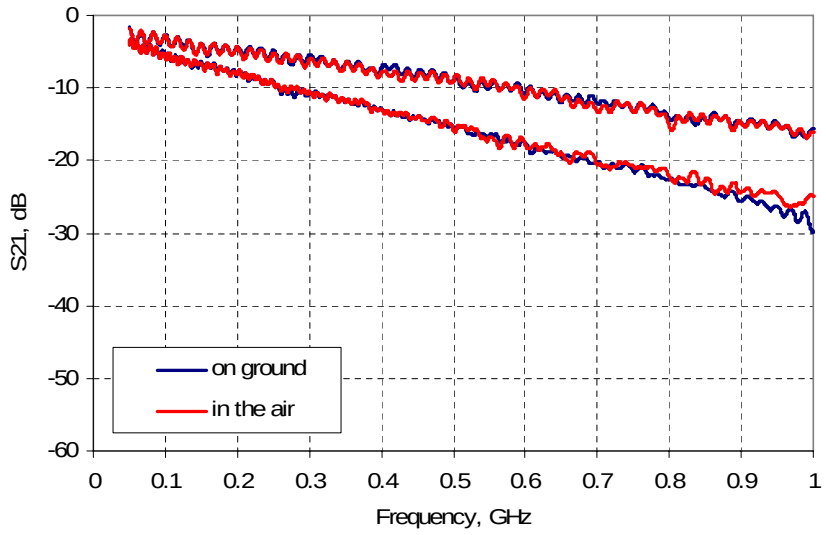

Figure 3.13: Comparison between frequency responses of twin and earth cable measured on the ground and in the air (upper curves - 1m, lower curves - 2m).

3.4.1 The Effect of Different Cable Types

It is observed from Figure 3.14 that 2.5mm flat twin and earth cable has much better performance than the three-core flexible cable. At the same transmission distance, i.e. 10 metre, the three-core flexible cable attenuates at 4dB/100MHz while the twin and earth cable only degrades at 2.4dB/100MHz. At 500MHz, the same signal will experience 10dB more losses when transmitted on a three-core flexible cable. Such difference can be explained by the configuration of the mains cable itself. In the high frequency range, "skin effect" causes current to flow on the surface of a good conductor, the power transmitted through this surface is dissipated as heat [9]. When the conductor surface increases, the total current floating on the surface increases and more energy is dissipated. A three-core flexible conductor consists of 40 stranded copper wires, whereas the twin

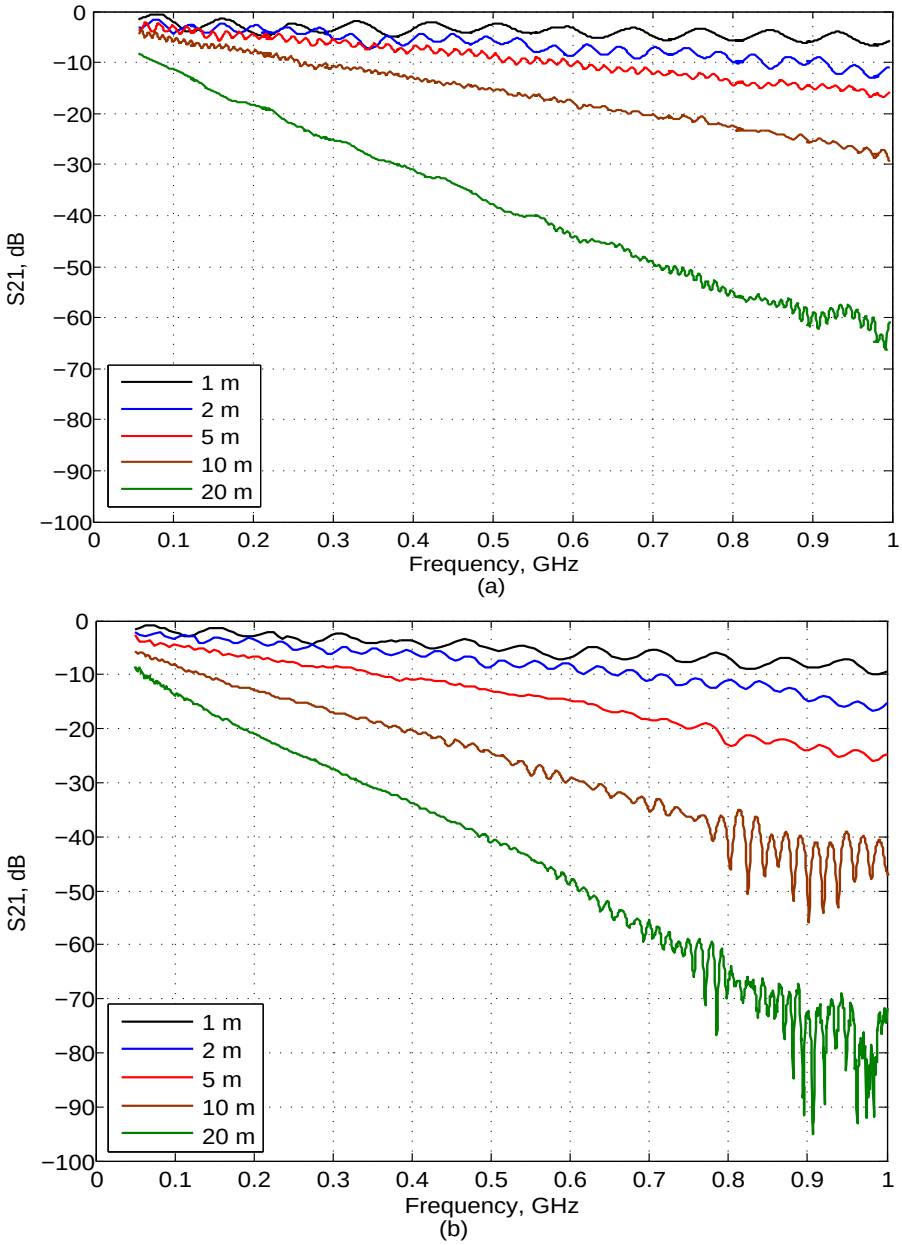

Figure 3.14: Frequency response of (a) twin earth and (b) three-core flexible cable in 50MHz - 1GHz.

and earth conductor is a solid core. So the total surface current on the three-core conductor is larger. As a result, higher attenuation can be observed on the three-core flexible powerline.

Such difference illustrates that good quality powerlines (e.g. new cables or cables with solid conductors) will provide a better channel for signal transmission. In this case, the flat twin and earth cable has better performance and is used for further testing.

3.4.2 The Effect of Impedance Mismatch

Multiples of small ripples are observed in the S_{21} curves (Figure 3.14) and their number increases with cable length. This is mainly due to the mismatch between the powerline characteristic impedance and that of the coaxial connector. The signal will be reflected where there is a disconnection, causing multi-path transmission. A multi-path channel with two transmission paths can be represented as shown in Figure 3.15, where $f(t)$ is the transmitted signal, V_0 is a constant. $V_0 f(t-t_0)$ and $V_0 f(t-t_0-\tau)$ represent the received signals after passing through the channel. t_0 and τ are the fixed delay and relative time delay between the two paths.

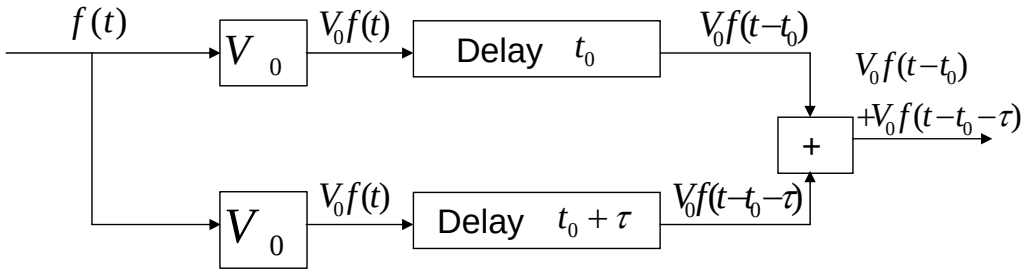

Figure 3.15: Transmission model of two path transmission.

Using the fourier transform which relates the time domain and frequency domain signal, the two received signals can be represented in the frequency domain:

$$\begin{aligned} V_0 f(t-t_0) &\Leftrightarrow V_0 F(\omega) e^{-j\omega t_0} \\ V_0 f(t-t_0-\tau) &\Leftrightarrow V_0 F(\omega) e^{-j\omega(t_0-\tau)} \end{aligned} \tag{3.3}$$

where $F(\omega)$ is the fourier transform of the transmitted signal $f(t)$.

The two offset signals will be added at the Rx, so the transfer function $H(\omega)$ of this multi-path model is:

$$H(\omega) = \frac{V_0 F(\omega) e^{-j\omega t_0}(1 + e^{-j\omega\tau})}{F(\omega)} = V_0 e^{-j\omega t_0}(1 + e^{-j\omega\tau}) \tag{3.4}$$

It can be seen that the transfer function is dependent on the relative time delay τ and frequency. Figure 3.16 illustrates the magnitude of the transfer function of a two path channel model, where the frequency interval between nulls is:

$$\Delta f = \frac{1}{\tau}. \tag{3.5}$$

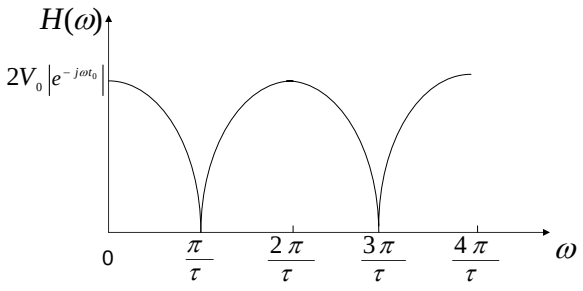

Figure 3.16: Magnitude of the two path transmission model

The measured frequency interval between adjacent ripples (1m flat twin and earth cable) is approximately 85MHz (Figure 3.17) and the time delay between the first received and reflected signal is:

$$\tau = \frac{2l}{v_p} = 2l \times \frac{\sqrt{\varepsilon_r}}{c_0}. \tag{3.6}$$

Where l is the length of powerline, $v_p = c_0/\sqrt{\varepsilon_r}$ is the phase velocity and c_0, ε_r are the speed of light in free space and the dielectric permittivity of the medium respectively. The reflected signal travels twice the length of the powerline. Actually the transmitted signal will be traveling back and forth along the powerline, however, only the first reflected signal is considered. Due to high attenuation, the energy of later signals are considered to be negligible. As in [90], dielectric

permittivity of the powerline is $\varepsilon_r = 3.1$, so the relative time delay is $\tau \approx 11.74ns$ and the frequency interval is:

$$\Delta f = \frac{1}{11.74 \times 10^{-9}} = 85.2MHz. \tag{3.7}$$

The same relation can be found in other transmission distances and it can be seen from (3.5) and (3.6) that frequency interval decreases as cable length grows. Further, we should differentiate these small ripples from the big cycles of resonance observed previously. The intervals between the resonating frequencies are much wider and are mainly observed above 1GHz, they are caused by the radiation of the transmitted signal. While the small ripples are due to multiple reflections of the transmitted signal.

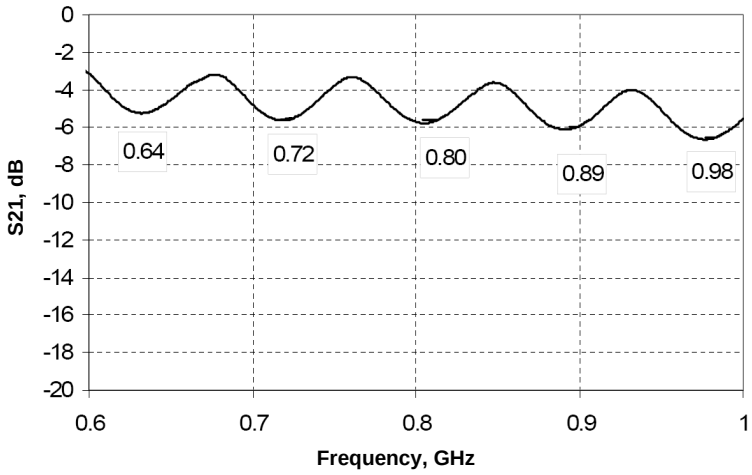

Figure 3.17: Frequency intervals between ripples in of 1m twin and earth cable

3.4.3 The Effect of Bends in Cable

Previously, powerlines are mainly tested on the ground, they are not bent or twisted. In practice, mains cables are usually laid along the corners of a room and are bent at some point, this may affect the cable's performance. Further, we need to analyse this effect because later in this thesis, a measurement campaign will be conducted on a powerline laboratory test bed, where all the cables are

bent and attached to the back of the wall, this may as well affect the actual performance of the test bed.

Figure 3.18 compares the transfer function of twin and earth cables tested stretched and folded, i.e. folded in the middle and placed close to each other, or folded twice and place all the parts closely together, at 5m and 10m respectively.

Originally, only small ripples have been observed. When the cables are folded, multiple deep notches occur above 500MHz, especially at 10m. The notches can cause nulls as deep as -60dB in the transfer function, depending on the number of times the cable is folded and how close the parts are to each other. Such deep notches are caused by the wave travelling along the line cancelling with each other. When the folded parts are closely placed, the transmitted signals cancel with each other if they are 180 degree out of phase. They can also be enhanced if they are in the same phase. That is why at some frequencies the loss is smaller than that measured stretched on the ground. In most cases, bends in the cable can degrade the channel's performance by introducing deep transmission nulls and give a low SNR level.

3.5 Transmission and Attenuation Characteristics of 2.5mm Twin and Earth Cable

Transmission characteristics of in-door powerline channel have been extensively examined below 30MHz, with channel models developed from statistical summary of measurement data or analysis of the physical configuration of the cable [43, 45, 91]. However, very few studies have considered high frequencies above 100MHz. This section analyses the attenuation characteristics of twin and earth cable, since it provides a better path for signal transmission than the three-core cable.

3.5.1 Transmission Loss

Similar to those observed in the low frequency bands, powerline channel's attenuation increases with frequency and transmission length. The attenuation characteristics of powerline can be analysed by using a channel transfer function

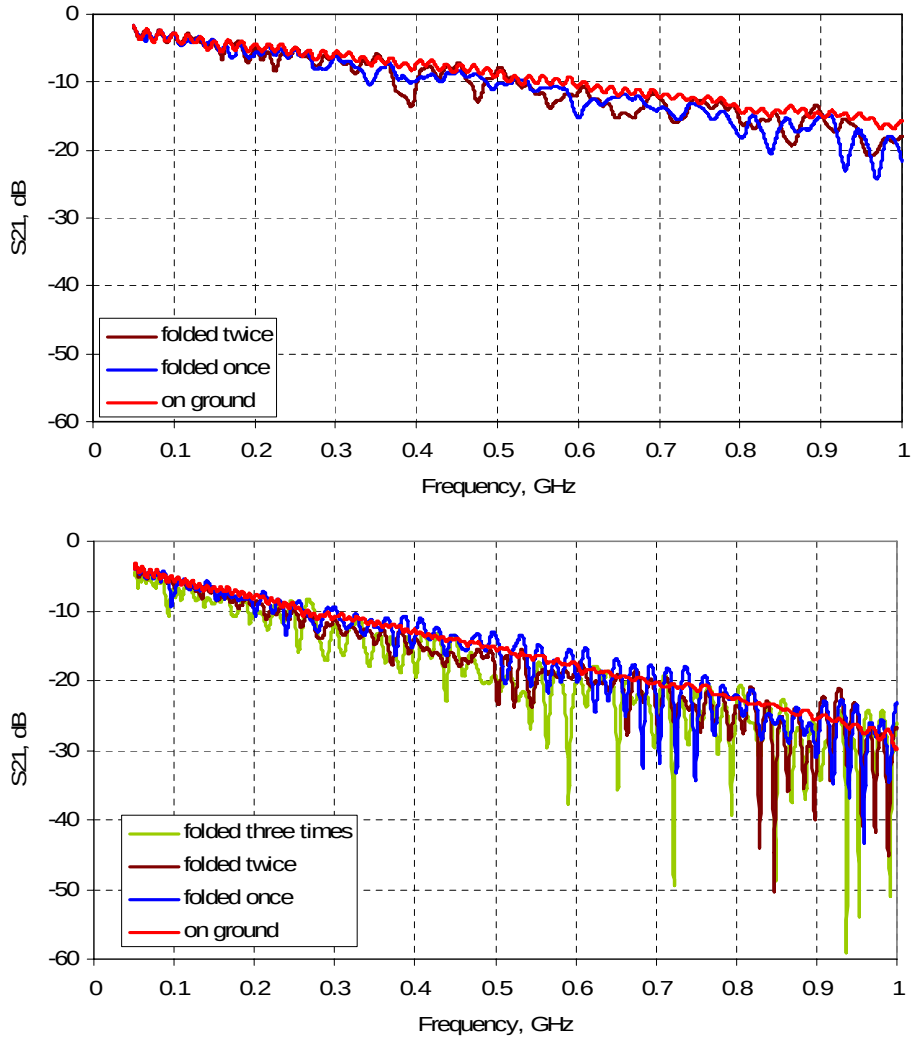

Figure 3.18: Frequency responses of 5m (the upper figure) and 10m (the lower figure) twin and earth cable, laid stretched and folded.

model, based on the transmission line theory. In the high frequency range, powerlines can be modelled as transmission lines with per-unit-length parameters: L (inductance), C (capacitance), R (resistance) and G (conductance), as illustrated in Figure 3.19.

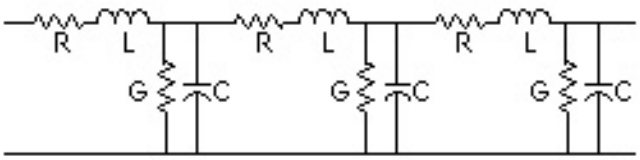

Figure 3.19: Transmission line model.

The characteristic impedance Z_0 of the powerline is given by Equation (3.8):

$$Z_0 = \sqrt{\frac{R + j\omega L}{G + j\omega C}} \tag{3.8}$$

The value of Z_0 is between 100 - 150Ω. The propagation constant of the powerline, γ, is given by Equation (3.9):

$$\gamma = \sqrt{(R + j\omega L)(G + j\omega C)} = \alpha + j\beta, \tag{3.9}$$

where α denotes the attenuation characteristics of the channel, its unit is $neper/m$. And β shows the phase changing characteristics, in rad/m. α and β can be calculated as follows:

$$\alpha = \frac{R}{2Z_0} + \frac{GZ_0}{2} \tag{3.10}$$

and

$$\beta = \omega\sqrt{LC} = \frac{\omega}{v_p}, \tag{3.11}$$

where $R/2Z_0$ describes the impact of skin effect, and $GZ_0/2$ denotes the dielectric loss within the insulation material.

At low frequency ranges, α is usually constant, but at high frequencies, it becomes a function of frequency and can be represented as [13]:

$$\alpha(f) = \eta_0 + \eta_1 f^{\varepsilon}, \tag{3.12}$$

where coefficients η_0,η_1 and ε are dependent on the cable types.

With attenuation coefficients $\alpha(f)$, the loss of a powerline channel $D_{dB}(f,l)$ at different frequencies can be calculated using [13]:

$$D_{dB}(f,l) = |20\log_{10} e^{-\alpha(f)l}| = 8.868\alpha(f)l \tag{3.13}$$

where l is the transmission distance.

Equation 3.13 only considers the attenuation of a powerline cable. But in the frequency domain measurements, the effect of the coaxial connector (mismatch) is also included. This can be eliminated by referencing to a fixed cable length l_0, which is usually 1m. So the measured attenuation $H_{dB}(f,l)$ of a powerline l can be represented as:

$$|H_{dB}(f,l)| = |H_{dB}(f,l_0)| + D(f,l-l_0) = |H_{dB}(f,l_0)| + 8.868\alpha(f)(l-l_0), \tag{3.14}$$

where $H_{dB}(f,l_0)$ is the measured transfer function of a l_0 meter powerline.

Based on the measured attenuation of powerline at different lengths, the attenuation coefficient $\alpha(f)$ of a twin earth cable can be extrapolated statistically, with the values of η_0, η_1 and ε being 0.03, 0.299 and 1 respectively. Figure 3.20 illustrates the modelled $\alpha(f)$ (twin and earth) as a function of frequency.

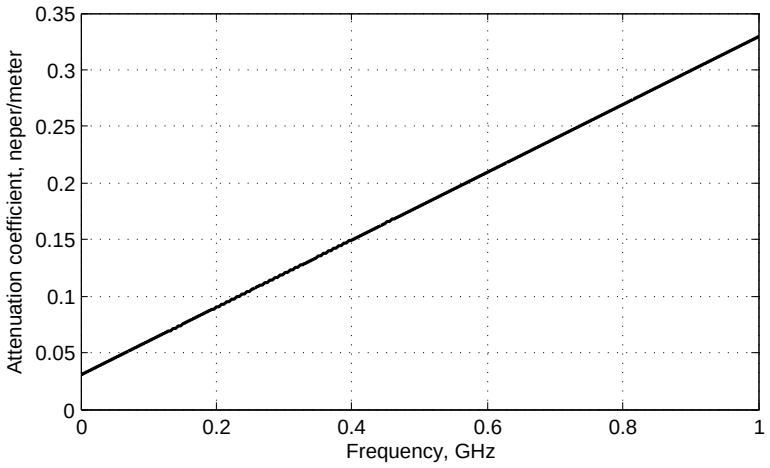

Figure 3.20: Calculated attenuation coefficient α.

Figure 3.21 compares the cable loss between the attenuation model and measurement results at 200, 500 and 800MHz. The two results show good agreement up to 30 metres. This is a reasonable distance for a home network, since there is a trade off between transmission range and operating bandwidth. For longer transmission range, a signal relay can be used to boost up the signal. Furthermore, it shows that the signal attenuation rate increases with frequency. In the frequency band below 200MHz, the signal attenuates at 0.8dB/m (Table 3.1). The signal can be transmitted over a long distance before the SNR drops to certain threshold level, however, the transmission rate may not be very high due to the limited bandwidth available. In the frequency range up to 800MHz, the bandwidth used is wider and thus higher data rate could be achieved. However, in the high frequency band, signal strength degrades more rapidly, i.e. at 800MHz, signal attenuates three times faster than that in 200MHz, therefore, the transmission distance will be decreased.

Table 3.1 lists the signal attenuation rate at different frequencies, which increases with frequency. It is noted that above 100MHz, the average attenuation rate increases at 0.26dB/(m·100MHz). If more data need to be transmitted, higher bandwidth should be exploited, therefore signal relays are required to enable long distance transmission.

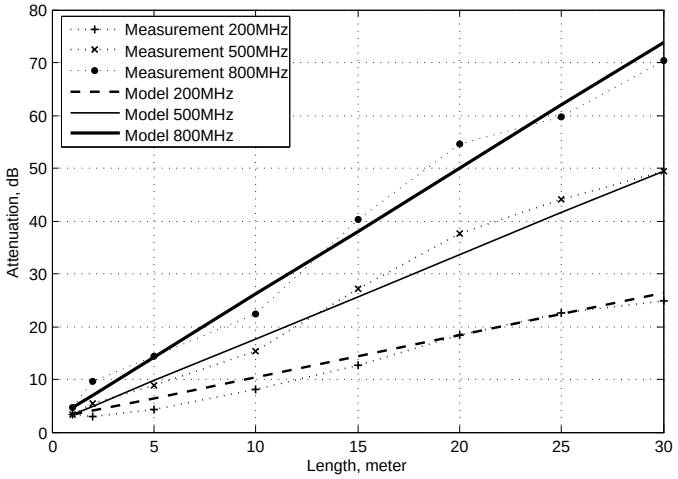

Figure 3.21: Modelled and measured powerline attenuation at 200, 500 and 800MHz.

Frequency(MHz)	100	200	300	400	500
Attenuation Rate(dB/m)	0.53	0.8	1.06	1.33	1.59
Frequency(MHz)	600	700	800	900	1000
Attenuation Rate(dB/m)	1.86	2.12	2.4	2.65	2.92

Table 3.1: Signal attenuation rate (dB/m) on twin earth cable.

3.5.2 Channel Model

A powerline channel can be represented by a transfer function. Recent approach of modelling the powerline network's transfer function can be achieved by breaking down the network topology into a cascaded 2 port networks (2PN), then replace a distributed parameter circuit with a single lumped network. The transmission matrix or ABCD matrix is used because it can represent the total transfer function of a network, simply by multiplying the transmission matrix of each sub-2PN [92].

In general, a network that has a source, and terminated with a load can be described using Figure 3.22 The dashed box represents the whole network topology, which can be the cascade of many 2PN elements:

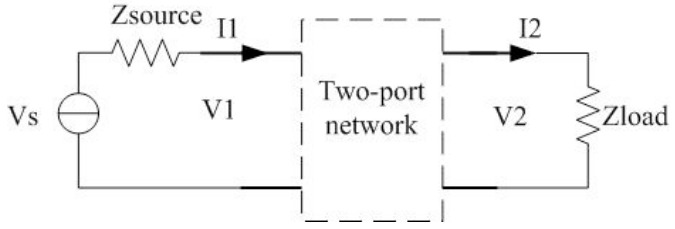

Figure 3.22: Generic two-port network.

The relationship between the current and voltage at the two ports of a 2PN is given by Equation (3.15) [9]:

$$\begin{bmatrix} V_1 \\ I_1 \end{bmatrix} = \begin{bmatrix} A & B \\ C & D \end{bmatrix} \begin{bmatrix} V_2 \\ I_2 \end{bmatrix} \tag{3.15}$$

where $\begin{bmatrix} A & B \\ C & D \end{bmatrix}$ is called the transfer matrix or $ABCD$ matrix T. The relationship between the transmitted and received voltage signals of a system can be

derived as:

$$\left.\begin{array}{l} V_s = Z_{source}I_1 + V_1 \\ V_1 = AV_2 + BI_2 \\ V_2 = Z_{load}I_2 \end{array}\right\} \Rightarrow H(f) = \frac{V_2}{V_s} = \frac{Z_{load}}{AZ_{load} + B + Z_{source}Z_{load}C + Z_{load}D} \tag{3.16}$$

Cascaded 2PNs can be used to model powerline channels with many branches, such as a T network illustrated in Figure 3.23, which consists of two transmission lines L_1, L_2, and a branch terminated by a load Z_b.

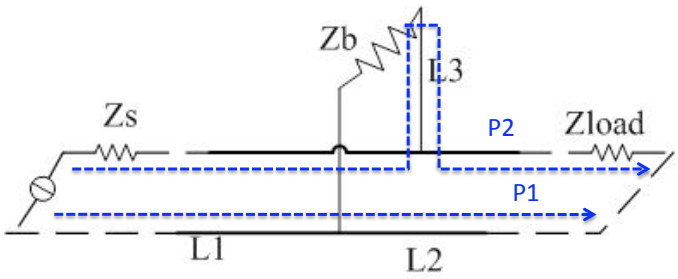

Figure 3.23: Configuration of a T-network

The total transmission matrix is [45]:

$$T_{total} = T_{TL}T_{Branch}T_{TL} \tag{3.17}$$

where

$$T_{TL} = \begin{bmatrix} \cosh(\gamma L) & Z_0 \sinh(\gamma L) \\ \frac{\sinh(\gamma L)}{Z_0} & \cosh(\gamma L) \end{bmatrix} \tag{3.18}$$

represents the $ABCD$ matrix of the transmission line, and γ is the propagation coefficient of twin earth cable, which can be calculated from Equation (3.11) and (3.12).

T_{Branch} denotes the transmission matrix of the branch, which can be modelled as a shunt impedance across the line with an input impedance Z_{in} as shown in Equation (3.19):

$$T_Branch = \begin{bmatrix} 1 & 0 \\ \frac{1}{Z_{in}} & 1 \end{bmatrix} \tag{3.19}$$

where

$$Z_{in} = Z_0 \frac{Z_b + Z_0 \tanh(\gamma L)}{Z_0 + Z_b \tanh(\gamma L)} \tag{3.20}$$

Figure 3.24 compares the measured and modelled transfer function of a 20m powerline channel, there is a 2m open circuit branch 15m away from the source. The T network can be represented using Figure 3.23, where $L_1 = 15m$, $L_2 = 5m$, $L_3 = 2m$, $Z_s = Z_l = 50\Omega$ and $Z_b = \infty$. The blue dotted lines represent the two main propagation paths, where P2 will be longer than P1. It can be seen that modelling results agrees well with the measured results. The nulls are caused by multi-path transmission. Branch L_3 totally reflects the signal on P2, causing a time delay between P1 and P2 signals. According to Equation (3.6), the frequency interval between adjacent nulls is $\Delta f = 2L_3\sqrt{\varepsilon_r}/c_0 = 47.6MHz$, which is very close to the results shown in Figure 3.24. Apart from the multi-path effect, it is noticed that the transmission loss in the T network has a similar trend to a single length 20m cable, as shown in Figure 3.14 (a).

Comparison of results proves that the channel model developed can be used to model the powerline channel with a tree topology correctly. However, in a complex PLC system with couplers, sockets and loads, this model needs to be improved for better prediction of the variable effects of the system components.

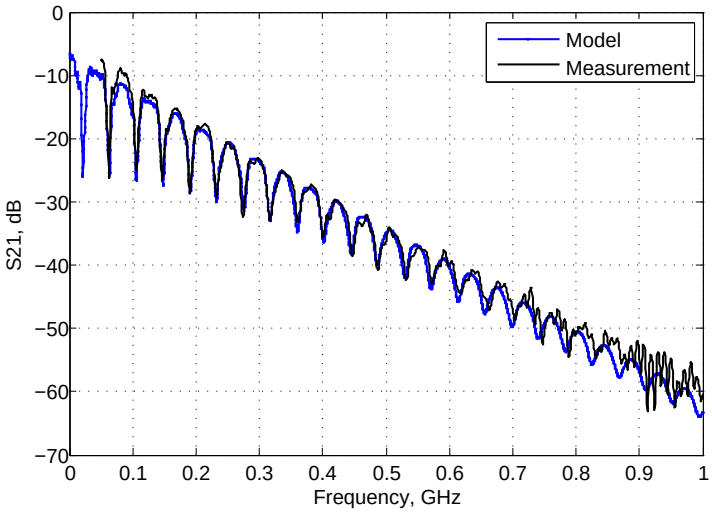

Figure 3.24: Model and measured powerline channel attenuation (T-network)

3.6 Summary

In this chapter, characteristics of signal propagation over the indoor powerline cables have been investigated in a very wide frequency range up to 10GHz. Time domain simulation shows that differential mode signal coupling is preferred to allow maximum signal transmission over the powerline. It is also noticed that the powerline channel causes potential radiated emission in the frequency range above 1GHz. The measured transfer function of the cable reveals that the transmitted signal also experiences strong attenuation above 1GHz. Thus, further channel characterisation has been carried out in the scaled down UWB band below 1GHz. The effect of cable types, impedance mismatch and cable bends have been addressed. It is noticed that 2.5mm flat twin and earth cable provides a better transmission path than three core flexible cable. Detailed analysis of signal attenuation rate and channel model of twin and earth cable in 50MHz - 1GHz range has been conducted. Results show that above 100MHz, the average signal attenuation rate increases at 0.26dB/(m·100MHz), which indicates that the powerline can potentially be utilised for UWB transmission up to 1GHz in the home network.

Chapter 4

Development of Wideband Coupler for UWB PLC

4.1 Introduction

This chapter presents the design of a RF coupler suitable to transmit wide band signals into the powerline. As previously mentioned in Chapter 3, it is possible for powerline to operate in a scaled down UWB band below 1GHz, therefore, the developed coupler should operate in a wide frequency range up to 1GHz. Moreover, the signal should be coupled into the powerline differentially, to avoid far field radiation and allow better signal transmission. So far, there is no such wideband coupler available for the study and measurement of broadband powerline channels. Therefore, it is very critical to develop a coupler that can serve such purposes.

4.2 PLC Coupling Unit Basics

One of the most important components of any PLC system is its interface (or coupler) with the power distribution network. This is by no means a simple unit considering the challenging properties of the powerline channel. Due to high voltages, varying impedances, high amplitudes and frequency dependent disturbances, the coupling unit needs to be carefully designed to provide both

the specific signal transmission function within the appropriate bandwidth, and the safety level required by the applicable domestic or international standard [93].

4.2.1 Requirements of RF Coupler for PLC

An RF coupler for PLC should consider the following aspects:

- It should not introduce a high level of loss to the system. Ideally, the transmission loss of a coupler should not exceed 3dB.
- Signals should be injected into the powerline differentially with the earth conductor connected to the ground.
- For this project, the designed coupler should provide a very flat transmission performance in the studied frequency band. It is very challenging to design a coupler that has such wide band capability.
- Safety protection. A powerline coupler is designed to be used simultaneously with AC power on. It is very critical to filter out the 220V AC power, so as not to cause damage to the users and other equipment.
- Impedance matching. This is often an important aspect in the coupler design. However, for a PLC system, the input impedance can vary from a few ohms to several kilo ohms, depending on the locations of the Tx and Rx, as well as the electrical appliance plugged into the system [36, 94]. Thus, impedance matching to a PLC system is very complex and it is usually achieved by using a transformer to provide impedance adaptation.

The above requirements show that it is very critical to develop a coupler that has such wide bandwidth and provides desirable performance at the same time. Besides, existing powerline couplers are only designed for narrowband use, below 30MHz. There is no literature available on broadband RF coupler that can operate in such a wide bandwidth, from 50MHz to 1GHz. This fact makes it even more challenging and yet important to design a novel coupler that can operate in the interested frequency band.

4.2.2 Existing Coupling Units for PLC

As mentioned earlier, there is no wideband couplers that can operate in the frequency band up to 1GHz. Most of them only provide coupling capabilities up to 30MHz. Figure 4.1 shows a prototype of the coupling unit designed by SiConnect^{TM}. The coupler is comprised of a number of passive components[1], i.e. capacitors, transformers and resistors. The RF signal is transmitted to the AC mains through an impedance matching circuit. The transformer is used for galvanic isolation between the RF signal and the AC mains, it also provides differential mode signal coupling. Finally the capacitors act as band pass filters to the signal.

The performance of the couplers in the 50MHz - 1GHz frequency range has been tested. Figure 4.2 illustrates the s-parameters of the couplers, being connected back-back. It shows that SiConnect^{TM}'s couplers, originally designed for PLC applications below 30MHz, do not provide satisfactory performance, over 10dB loss can be observed across the frequency band. Consequently this coupler is not appropriate for UWB over PLC applications in this study.

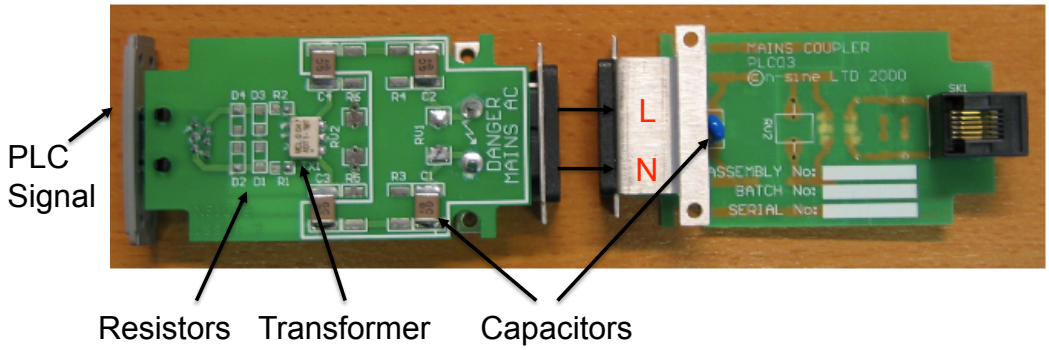

Figure 4.1: Photograph of SiConnect^{TM}'s coupler.

Another semi-conductor company Artimi^{TM}, has also developed a coupling unit, to demonstrate UWB pulse transmission over powerline. The RF coupler, as shown in Figure 4.3, is build on an RF4 Printed Circuit Board (PCB). The

[1]Components that are capable of operating without an external power source.

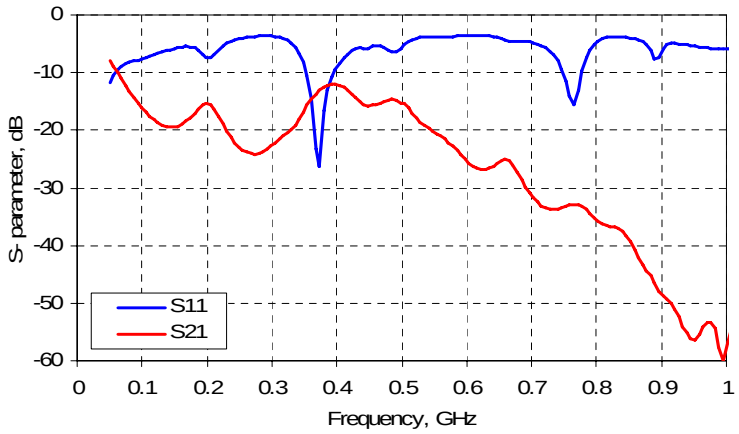

Figure 4.2: S-parameters of SiConnect^{TM}'s coupler in 50MHz - 1GHz.

UWB signal is injected into the coupler via a SubMiniature version A (SMA) connector, and travels to the powerline in common mode. The earth conductor is connected to the ground plane of the coupler for safety protection.

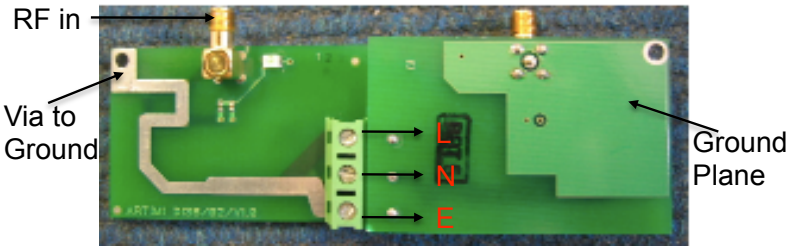

Figure 4.3: Photograph of Artimi^{TM}'s RF coupler.

Artimi et al have claimed that their coupler can operate in the FCC defined UWB frequency range of 3 - 5GHz. We hence test the s-parameters of the couplers in 50MHz - 10GHz frequency range. However, as shown in Figure 4.4, measurement results reveal that this coupler also brings in too much loss to the system. The S_{21} value is below -10dB in their claimed operating band of 3 - 5GHz. Even in the frequency range below 1GHz, its performance is not ideal either. Furthermore, it has been shown in previous study (Section 3.3.1) that common mode

signal transmission is not the preferred propagation mode in PLC, it will cause strong distortion to the transmitted signal

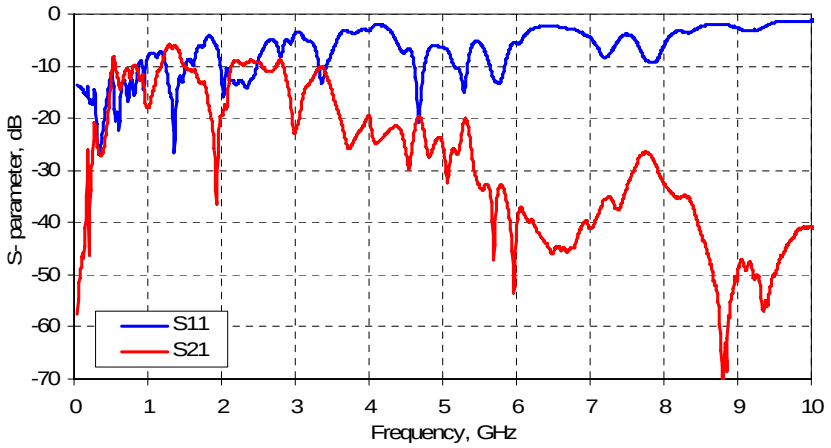

Figure 4.4: S-parameters of Artimi^{TM}'s coupler in 50MHz - 10GHz.

After examining the two coupling units developed by industrial companies, none of them is appropriate for the intended UWB over powerline applications in the high frequency range up to 1GHz. They both have short comings in terms of high insertion loss and very narrow operating bandwidth. As a result, a novel RF coupler that meets the application requirements needs to be developed.

4.3 Design of RF Coupler

4.3.1 Powerline Coupler Circuit

A typical and practical coupling unit for PLC below 30MHz, is usually a passive device providing isolation via a capacitive and magnetic network [35]. It is used to fulfill the two basic requirements, specifically galvanic isolation and differential mode signal transmission over the mains cable.

As illustrated in Figure 4.5, coupling to the mains is accomplished by means of two essential elements: the transformers and the filters, which can be realised by using coupling capacitors, coupling transformers and resistors [6, 93, 95, 96].

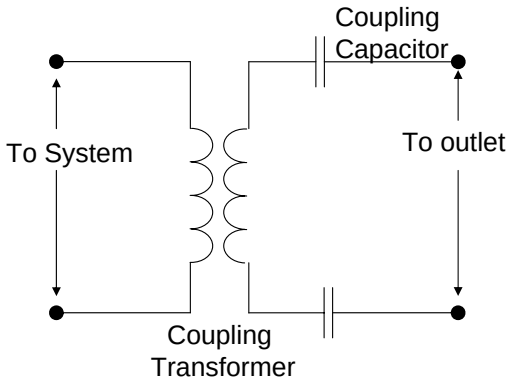

Figure 4.5: A coupling circuit for powerline communication.

- Coupling capacitors: Single and paired capacitors are used extensively in PLC to couple signals to the powerline, while blocking the low-frequency power signal [97, 98]. This requires that the capacitor to be high frequency (self-resonant point has to be higher than the upper bound of the band width [99]). More importantly, in order to avoid electrical shock, the capacitors should also be able to provide AC mains isolation after a failure and hence need to be high voltage capacitors. The X and Y range capacitors have been developed for such purposes. The requirements and essential characteristics of coupling capacitors have been standardized in American National Standards Institute (ANSI) C93.1-1972 [100].

- Coupling transformer: The transformer is an extremely important element, since the circuit performance and maximum transmission rate depends on its characteristics [101]. The function of a coupling transformer has four aspects: (1) galvanic isolation between the power circuitry and communication circuitry; (2) DC isolation between circuits while affording AC transmission; (3) voltage/current transformation, and impedance adaptation between the transmitter and powerline system; (4) differential mode signal transmission.

- Resistors: For PLC systems in general, one would try to avoid the use of resistors. It implies a loss of power, either of the communication signal or

the power waveform, i.e. 50 percent of energy will be lost on the resistor if it is 50Ω, the same as an SMA connector. However, a resistor can be used for other purposes such as a linear current-measuring device and voltage sensing device [6].

4.3.2 RF Coupler Model

Although there are not many passive components in the coupler circuitry, choosing the suitable ones, i.e. the capacitors and transformers to achieve adequate performance across a very wide bandwidth is not that trivial. At low frequencies (kilohertz range), it is sufficient to model a transformer by a magnetising and leakage inductance. At high frequencies though, the parasitic influence of a transformer has to be modelled more accurately. Figure 4.6 shows an equivalent circuit that can be used to model an RF transformer [6, 7].

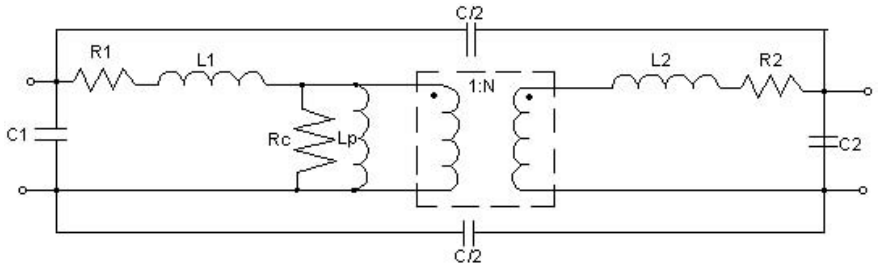

Figure 4.6: Equivalent circuit of transformer [6, 7].

Where L_1 and L_2 are the primary and secondary leakage inductances, caused by the incomplete magnetic coupling between the two windings. Because their reactance, $Z_L = j\omega L$ is proportional to frequency, these inductances increase insertion loss at high frequencies.

L_p is the magnetising inductance, which limits the low frequency performance of the transformer. It is determined by the permeability and cross sectional area of the magnetic core, and the number of turns. L_p increases the insertion loss at low frequencies.

Intra-winding capacitances C_1 and C_2, and the interwinding capacitance C, which are caused by the relative voltage difference between the turns and lay-

ers of the same winding and primary & secondary winding, also contribute to performance limitations at high frequency.

R_1 and R_2 are the resistance of the primary and secondary windings. Skin effect increases the resistance at high frequencies, contributing to the increase in insertion loss. R_c represents the loss of the conductor cores, which increases with the frequency and temperature. Core loss contributes to the increase in insertion loss at high frequencies.

In this study, a broadband transformer with small loss is very critical for the coupler to meet the requirements. Therefore, a surface mount RF Transformer ADT1.5-122+ from Minicircuit^{TM} is chosen. It has a very wide working bandwidth, from 20MHz to 1200MHz, with a flat insertion loss from 50MHz to 850MHz (0.25dB variation), as illustrated in Figure 4.7. It has a turns ratio of $\sqrt{1:1.5}$, providing an impedance matching between 50Ω and 75Ω [1].

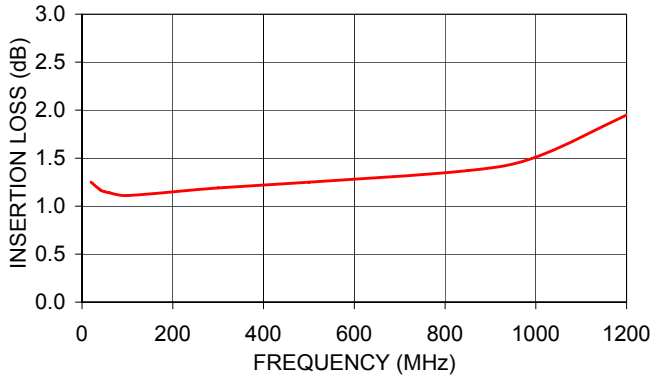

Figure 4.7: Insertion loss of ADT1.5-122+ RF transformer [8].

We also need to specify the coupling capacitor's value. So the whole coupling circuit, including the RF transformer and the coupling capacitor, is simulated in Agilent^{TM} Advanced Design System (ADS) software. Firstly, the transformer is simulated to best fit the transmission characteristics provided by the manufacturer data sheet [8]. This is done by running a few hundred simulations. We first set the minimum and maximum values of each component in the transformer model. At each simulation run ADS adjusts the component's value, i.e. increase

[1] Transformer impedance adaptation: $\frac{Z_1}{Z_2} = \frac{n_1^2}{n_2^2}$

by $0.001pF$ or $0.01nH$, to find the optimized performance. Then the whole coupling circuit is simulated to calculate the best value of the coupling capacitor (Figure 4.8). It is found out that a $100pF$ capacitor gives the best performance, as shown in Figure 4.9. The simulated coupling circuit has a very flat transmission profile in the 200 - 1200MHz frequency band and the insertion loss is small enough (less than 3dB) for signal transmission.

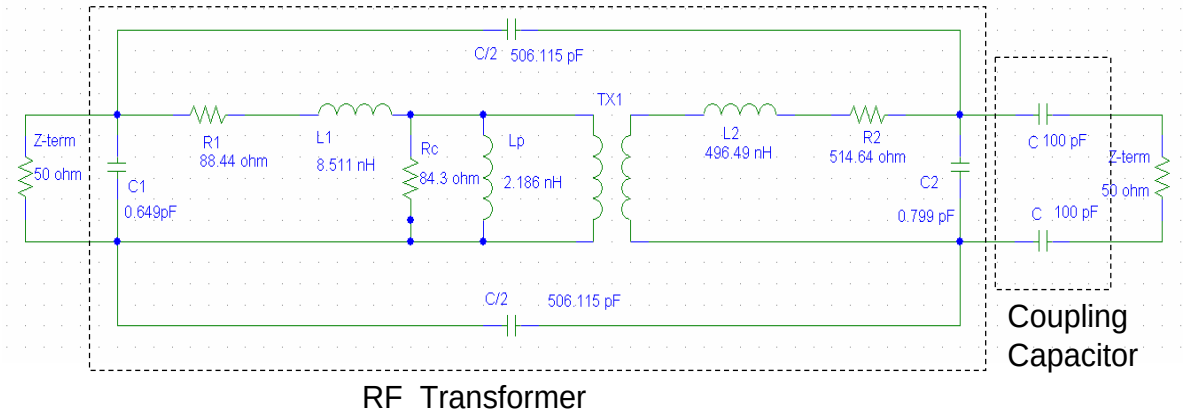

Figure 4.8: ADS circuit model for the developed powerline coupler.

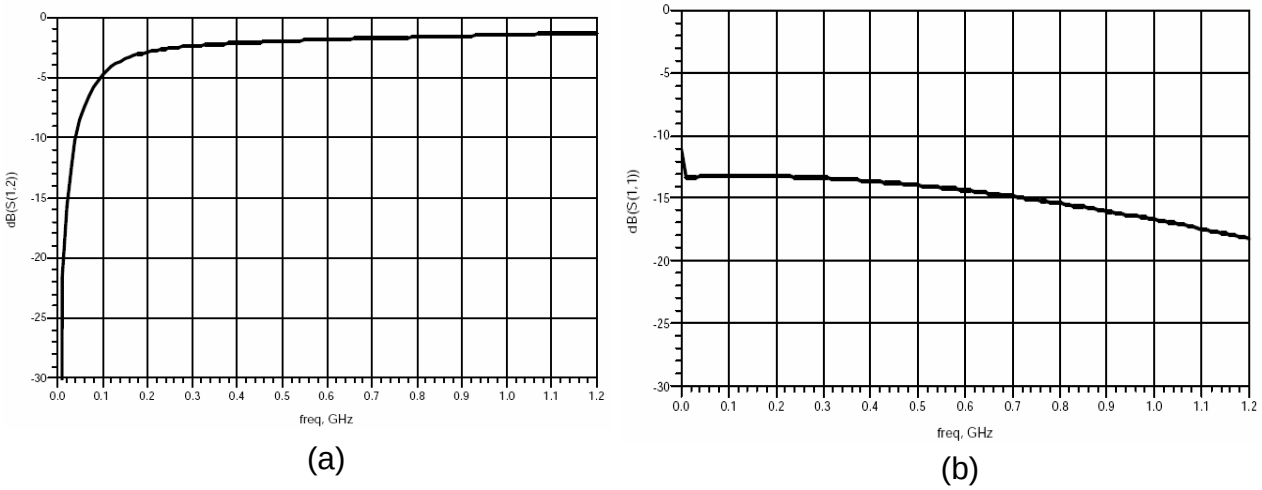

Figure 4.9: Simulated s-parameters of the coupling circuit (a) S_{21} (b) S_{11}.

4.3.3 Coupler Performance Analysis

Based on these simulation studies, a practical RF coupler is built on an RF4 PCB using an ADT1.5-122+ transformer and a pair of $100pF$ X1/Y2 ceramic disc safety capacitors, as shown in Figure 4.10. These capacitors are impulse tested up to $4000V$ and can be used in $250V$ low voltage environment. The schematic circuit of the coupler is shown in Figure 4.11. RF signals are transmitted via the SMA connector and coupled to the powerline channel differentially, where antipodal currents (equal amplitude currents flowing in opposite directions) flow on "live" and "neutral". The "earth" is connected to the earth ground of the SMA connector. AC mains power can be filtered by the coupling capacitors, safeguarding testing equipment. The resistor R_1 is removed to allow maximum energy transmission through the coupler.

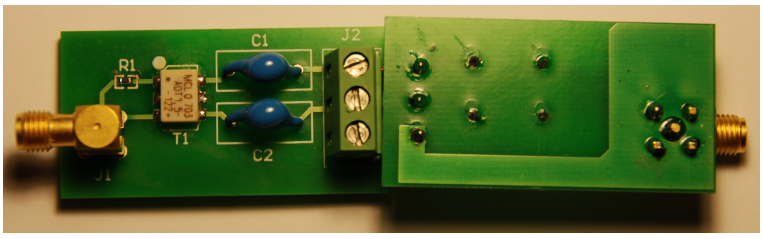

Figure 4.10: Picture of the developed coupler, front and back views.

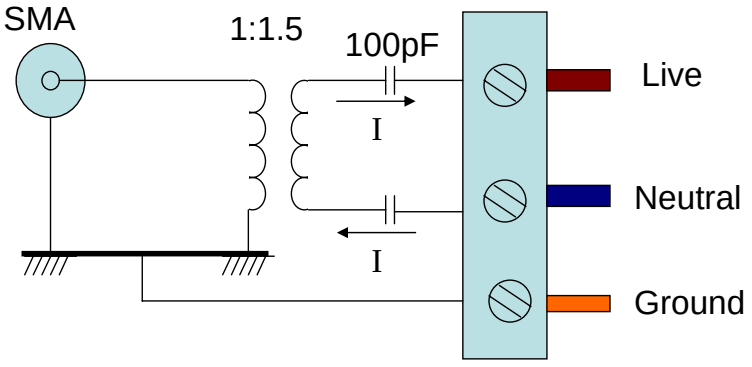

Figure 4.11: Schematic diagram of the RF coupler for UWB over PLC.

4.3.3.1 Powerline Frequency Domain Performance with Couplers

The frequency response of powerline cables with the designed couplers is tested using a network analyser. Firstly, only the coupler is tested by connecting two of them back to back, without using mains cables. As illustrated in FIgure 4.12, the measured s-parameters show good agreement with simulation results in the 200 - 900MHz frequency band, a flat insertion loss of only 4dB can be observed for the two couplers. Moreover, the 10dB bandwidth of the return loss has a very wide bandwidth, from 80 to 930MHz. Thus, this coupler provides very good performance in the desired frequency band on its own.

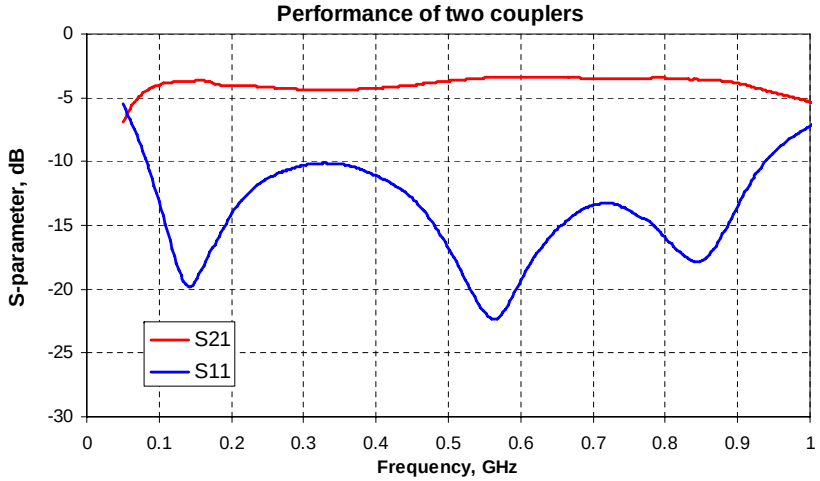

Figure 4.12: Performance (S_{11} and S_{21}) of two couplers connected back to back.

Now mains cables (2.5mm flat twin and earth and three-core flexible) are involved in the measurements and are tested in four different lengths, i.e. 1m, 2m, 5m and 10m. The frequency domain performance is measured using the Agilent^{TM} VNA HP8720ES. 1601 sample points are collected at a sweep time of 3.024 seconds, from 50MHz to 1GHz. Figure 4.13 shows the measured results.

The frequency response shows that the coupler provides good signal transfer capabilities to the powerline. The measured transfer function is smoother compared to the powerline connected directly to an SMA connector. Because the transformer provides an impedance adaptation between the powerline and the

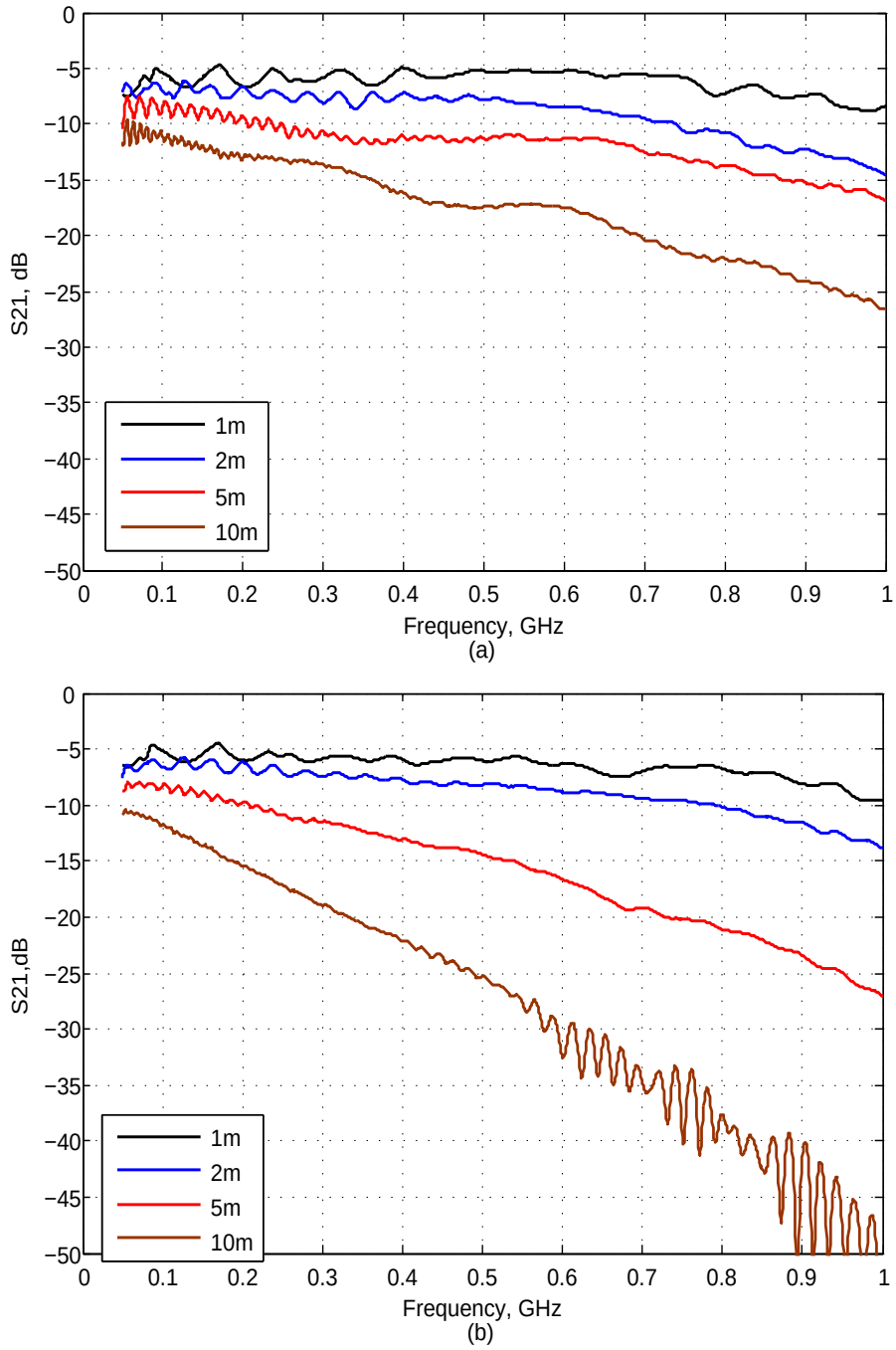

Figure 4.13: Performance of (a) twin earth (b) three-core flexible cable connected to couplers in 50MHz - 1GHz.

measurement equipment, a 50Ω impedance is converted to 75Ω after the coupler and vice versa.

Table 4.1 compares the average attenuation and the standard deviation of the powerline channel, with and without couplers. Generally speaking, the two couplers introduce an average loss of 2 to 3dB into the system. The standard deviation shows that frequency responses with the coupler produce a better performance, with fewer variations to the mean attenuation.

Still, 2.5mm flat twin earth has the best transmission path, with the existence of two couplers. An average path loss of 17.71dB can be observed at 10m, 10dB better than that of the three-core flexible powerline. This type of cable will be used to build the powerline lab test bed for system study in the following chapter.

	With Coupler Loss (dB)		Without Coupler Loss (dB)	
TWIN EARTH	Average	Std Dev	Average	Std Dev
1m	6.17	0.99	3.82	2.80
2m	9.03	2.12	6.70	3.59
5m	11.86	2.14	9.40	4.66
10m	17.71	4.42	16.04	6.70
3-CORE	Average	Std Dev	Average	Std Dev
1m	6.48	0.51	5.14	1.50
2m	8.74	0.93	8.30	2.36
5m	15.90	3.30	14.11	4.18
10m	27.94	6.83	26.41	8.62

Table 4.1: Powerline transmission loss (average attenuation and standard deviation in 50MHz - 1GHz), with and without couplers.

4.3.3.2 Powerline Time Domain Performance with Couplers

Time domain response of powerlines connected to the couplers is also studied. Using the Picosecond^{TM} (Model: 10,060A) pulse generator and Lecroy^{TM} digital oscilloscope (Model: SDA 110000), the measurement setup is shown in Figure 4.14. A short duration ($1ns$) rectangular pulse is produced by the pulse generator and transmitted through the mains cables at four different distances, including

couplers. The source pulse covers a wide frequency spectrum from DC - 1GHz. The digital oscilloscope picks up the received signal by sampling the waveform at a very high sampling rate, 40Gsamples/s, that is $0.025ns$ per sample.

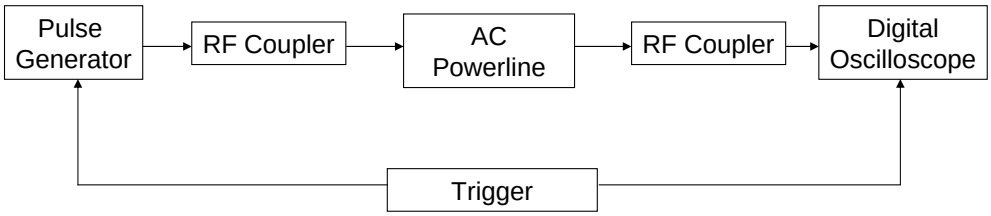

Figure 4.14: Time domain measurement set up.

Figures 4.15 (a) and 4.16 (a) illustrate the time domain wave form of the transmitted and received signal. The transmitted signal has been distorted, a differential tail appears in the received signal. This is caused by the filtering effect of the coupler: the coupling capacitor filters the AC power and also the low frequency components of the source signal. The received pulses spread into longer duration at the Rx, showing that the powerline is a weakly dispersive medium. The received wave forms from both types of cables are very similar, but the signal strength is stronger in the twin and earth cable. It is also noticed that signals travel faster in twin and earth cable. At 10m, the signal is received at $57ns$, while it takes over $60ns$ for the signal to propagate through the three-core cable. Because the dielectric material of the two cable types are different, where three-core cable has a higher dielectric permittivity than twin and earth cable.

The FFT is applied to the time domain waveform to analyse the power spectrum in frequency domain. The source pulse has a very strong DC energy and low frequency components below 100MHz, whereas in the received signal, DC and low frequency energy (below 50MHz) has been filtered by the couplers. In other parts of the signal power spectrum, the curve is very smooth without deep notches. It is noticed the high frequency signal experiences higher attenuation than low frequency components, this fact agrees with the frequency domain measurement discussed previously.

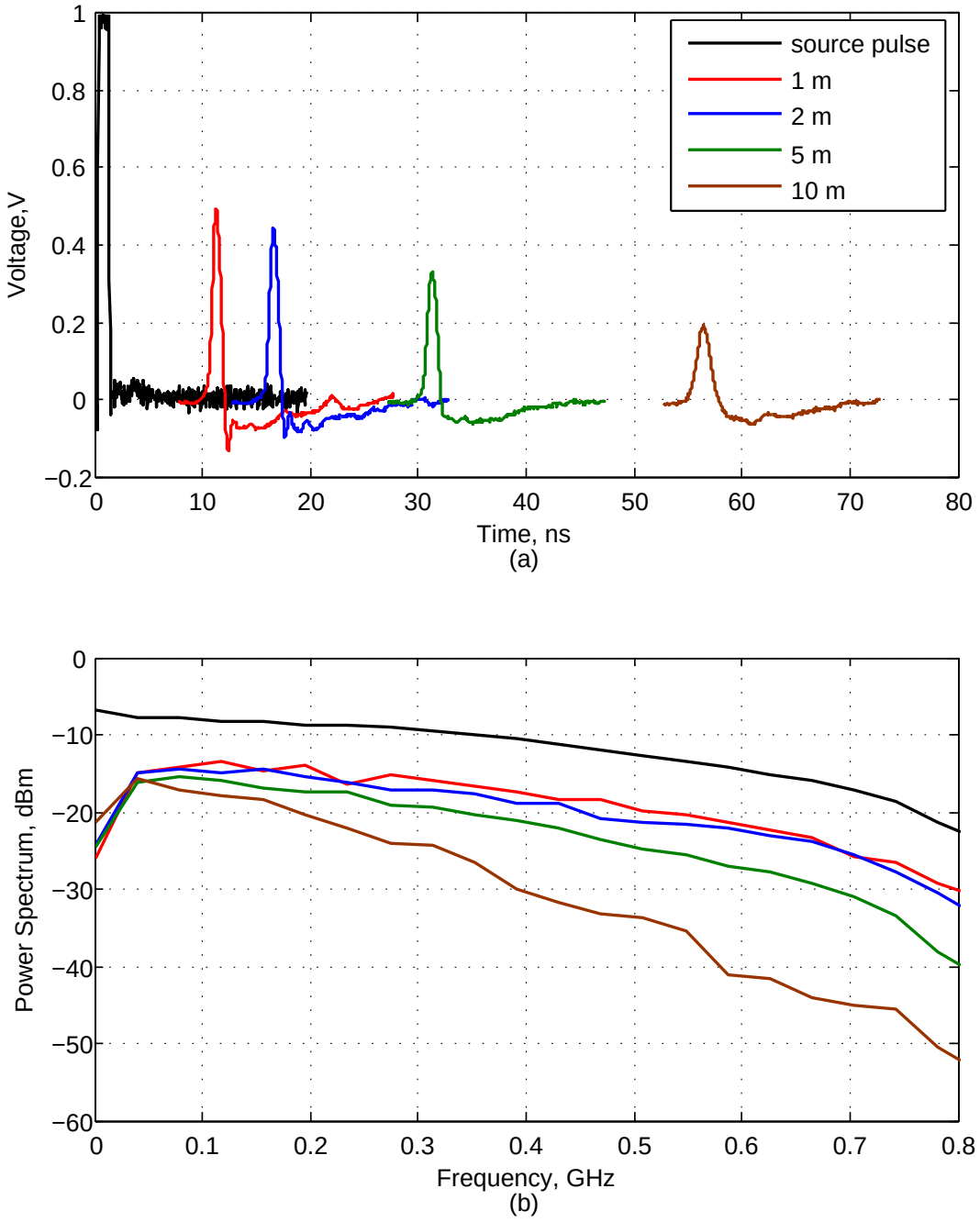

Figure 4.15: Time domain performance (a) Received wave form of twin and earth cable connected to couplers (b) Power spectrum of the time domain signal DC - 800MHz.

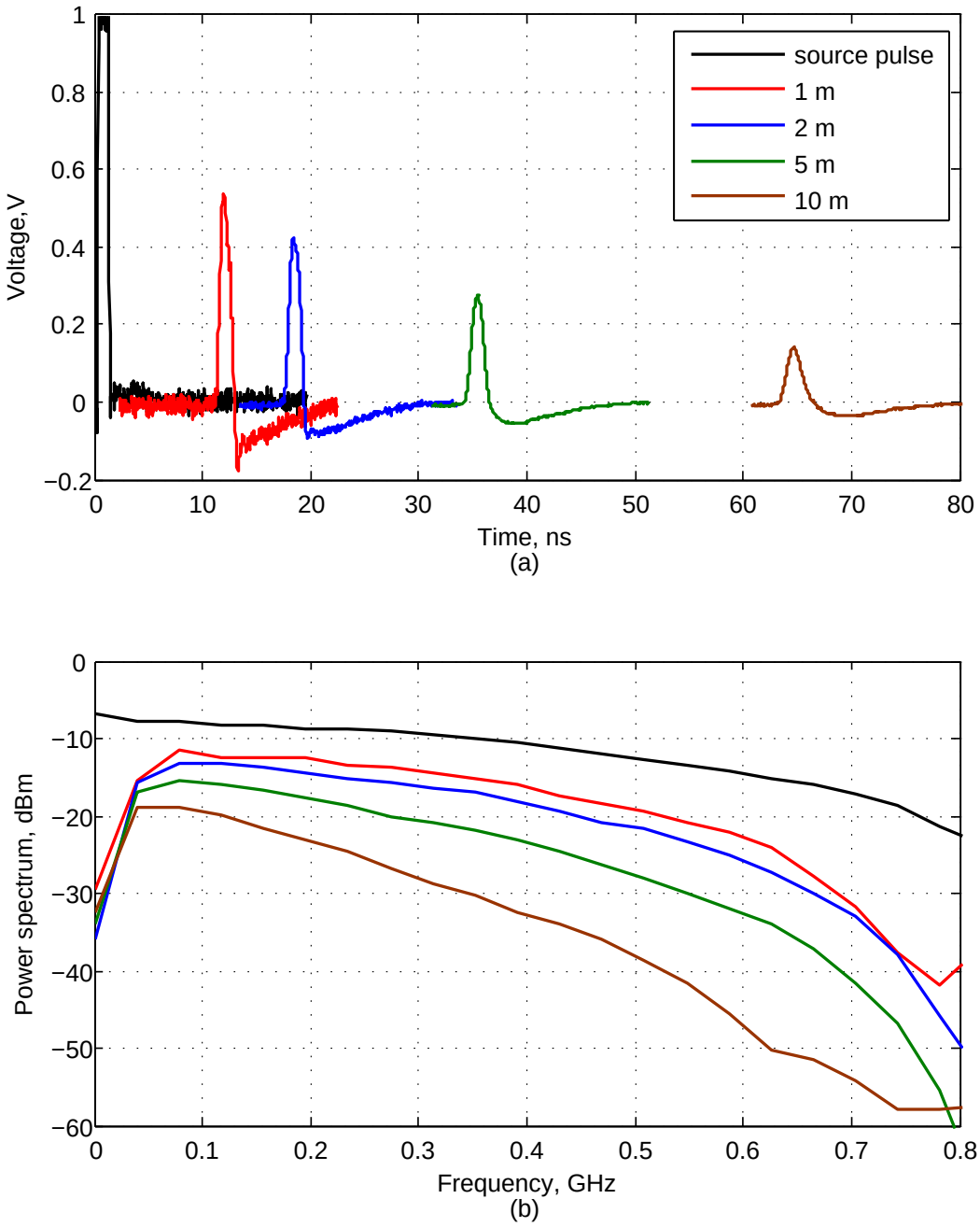

Figure 4.16: Time domain performance (a) Received wave form of three-core flexible cable connected to couplers (b) Power spectrum of the time domain signal.

4.4 Summary

Being the key component of a powerline communication system, the coupling unit needs to fulfill a number of requirements including safety protection, bi-directional signal coupling and wide operating bandwidth. Currently, there is no RF coupler that can meet the 50MHz - 1GHz bandwidth requirement.

In this chapter, the challenges of broadband coupler design have been overcome by using a number of high frequency passive components, the RF Transformer ADT1.5-122+ from Mini Circuits and the $100pF$ X1/Y2 high voltage safety capacitors.

It has been shown that the designed coupler can be used in practice, with signals being transmitted to the powerline in differential mode. It also provides wide band coupling capabilities to PLC systems up to 1GHz, with only 4dB insertion loss from two couplers. The frequency domain response of powerlines shows that ripples become less significant with the presence of the developed coupler. Moreover, the RF coupler can filter DC and low frequency AC mains signal effectively, as indicated in the time domain measurements. The experimental testing proves that the developed coupler provides a broadband interface between the communication signal and the powerline channel for PLC systems.

Chapter 5

Powerline System Characterisation

5.1 Introduction

Having completed the characterisation of powerline cables and the development of a broadband RF coupler, further experiments can be conducted on powerline communication networks. In this chapter, a powerline laboratory test bed is built and tested in Queen Mary's Antenna Laboratory. Both frequency and time domain measurements are performed in order to obtain sufficient path variation data for acceptable characterisation of broadband powerline channels. An important finding of the low pass characteristic has been addressed, leading to a thorough investigation of the channel performance in 50 - 550MHz frequency band.

The noise characteristics of the test bed has been studied, in the DC - 1GHz range. Both the background noise and the impulsive disturbance have been measured and analysed. Further, signal radiation from broadband powerline channels has been investigated. Being not specifically designed for broadband use or high data rate transmissions, the powerline may cause EMI to other radio systems. In this study, the measured radiated emission generated from a powerline ring circuit is below FCC standard limits. A conclusion can be drawn from the measurement results that it is promising to increase the operating frequency band of powerline channels for potential ultra wideband applications.

5.2 Measurement Setup

Firstly, a laboratory test bed was built according to the wiring regulations in the UK: British Standard 7671 - "Requirements for electrical installations" [102]. Unlike most in-home wiring networks, which have a tree or bus topology, UK electrical power circuits are normally described as a ring circuit, in which power is transmitted from point to point by a single length of cable linking each point to the next [103]. It starts at the main switch or fuse and goes to each device. The last device is connected back to the supply so that the whole circuit forms a continuous ring. The primary advantage is to allow more power to be supplied than it could otherwise be carried with a given size of cable [104].

The wiring circuit of the laboratory test bed is shown in Figure 5.1. AC mains at 50Hz, $240V$ is fed to the test bed through an isolation transformer, which is used to decouple two circuits and prevent the PLC signal leaking back to the mains network. A circuit breaker is used to check the current between "live" and "neutral", it is designed to protect an electrical circuit from overload or short circuit. Finally the AC power is split into three circuit rings, one for lighting and the other two for power outlets.

The lighting circuit contains twelve lamps and the one in the middle is connected to a dimmer. The power outlets are the commonly used domestic wall-mount twin sockets and normally include a switch. The cable between adjacent sockets and lamps is 5m. 2.5mm twin and earth cables are used, they are bent and laid in parallel on the back of the wall, as shown in Figure 5.2. It is necessary to label each wall outlet. So in the following measurement, all the sockets are marked as described below. The first socket ring is labelled Ring 1, each outlet in the twin socket is marked as 1A and 1B to 6A and 6B. The same rule applies for Ring 2. In order to identify a power outlet, both the ring number and the socket number are used, i.e. R1.1A represents the first wall plug in Ring 1.

For safety reasons, the coupler designed in Chapter 4 is fixed into a safety box, with one end extended to an SMA connector and the other to a plug that can be plugged into the wall socket (Figure 5.3).

Using the coupler, extensive measurements on the test bed have been carried out, in both frequency and time domain. Multi-path transmission can still happen

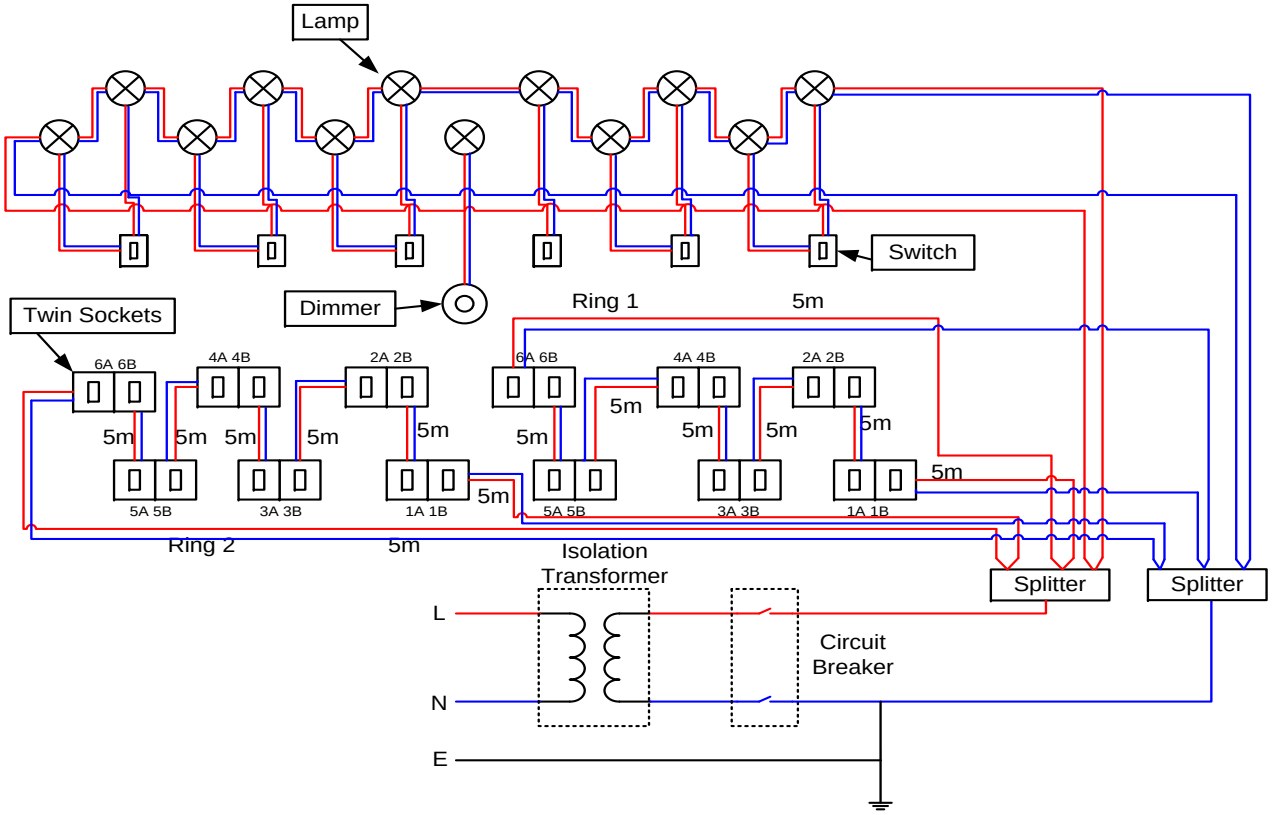

Figure 5.1: Illustration of cable wiring of the powerline test bed.

Figure 5.2: Picture of the lab test bed (a) front view (b) back view.

even if no electrical loads (which will cause impedance mismatch) are connected to it. There are always two transmission paths between a transmitting and receiving outlet pair. If we transmit from R1.3A to R1.1A, as illustrated in Figure 5.4, the signal will travel through a main path (Path 1) at 10m and meanwhile, it will also propagate along a secondary path (Path 2) at 25m. The sum of the main path and secondary path is the length of Ring 1, 35m.

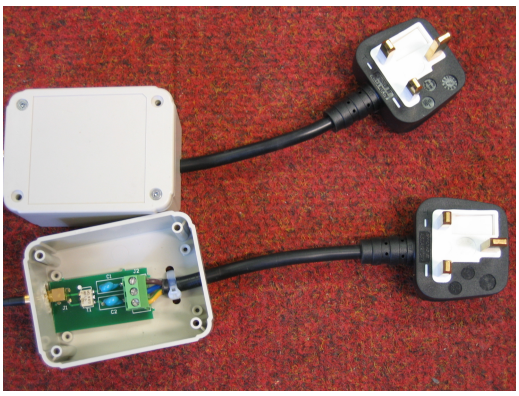

Figure 5.3: Illustration of the coupler put into a safety box for test bed measurement.

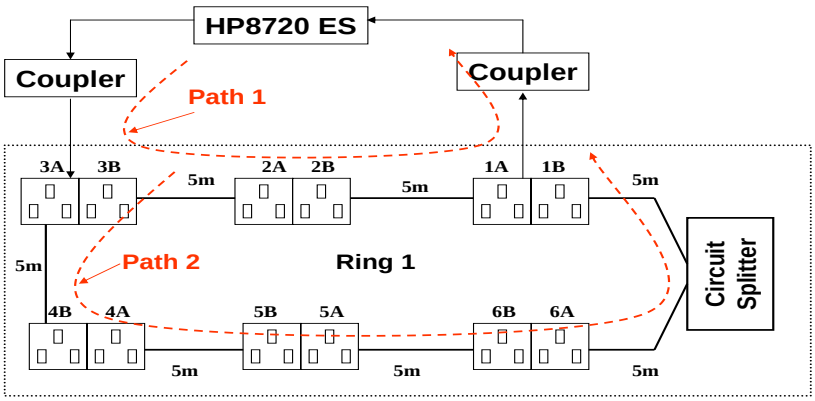

Figure 5.4: Frequency domain measurement setup: multi-path transmission in a single circuit ring, no electrical appliance is connected.

5.3 Test Bed Characterisation

5.3.1 Coupler Calibration

Performance of the coupler with safety box and plug is tested by connecting the couplers back to back. The measured insertion loss is shown in Figure 5.5. It shows that after connection to the power plug, the coupler's performance degrades, especially above 700MHz. The power plugs introduce an average loss of 4.58dB to the coupler in the 50MHz - 1GHz range. This agrees with the previous discussion that plug and socket can significantly affect the system performance. As discussed in [36] and [50], below 30MHz frequency range, the impedance from a powerline outlet varies from a few ohms to hundreds of ohms, clearly indicating the difficulties for a coupler to match to the input impedance of a powerline network.

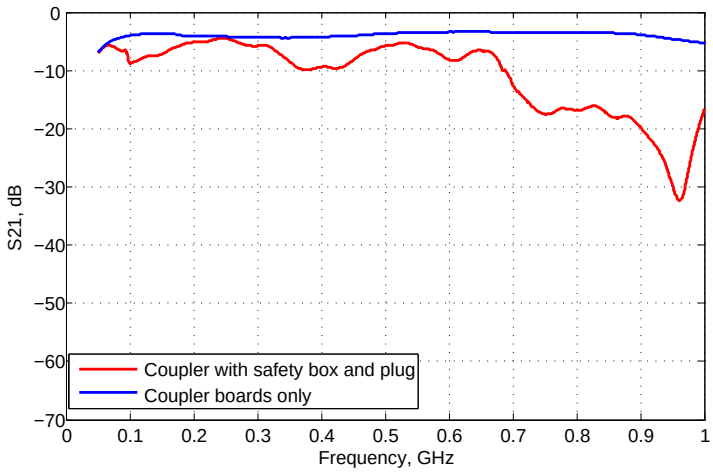

Figure 5.5: Performance of two couplers (with safety box and power plug) connected back to back.

5.3.2 Test Bed Measurement and Results

Attenuation between outlet pairs varies significantly as it is a function of frequency and distance. As a result, extensive measurements are required to obtain a thorough understanding of the complex powerline network properties.

Frequency and time domain responses between every wall outlet pair in the same circuit ring are tested first, followed by experiments on cross circuit ring transmission, with AC power on. Finally, electrical loads are connected to the test bed to assess the channel performance under interference from other appliances. In the frequency domain measurement, 1601 sample points are collected by the VNA in the range of 50MHz - 1GHz. In the time domain measurement, a $1ns$ square impulse with $1V$ voltage (DC and AC power is filtered by the coupler) is transmitted and picked up by the oscilloscope. Up to 20 sweeps are taken so the actual recordings are average data.

5.3.2.1 Same Circuit Ring (Ring 1)

1. On the same twin socket pair, 0m powerline.

   Figure 5.6 shows the frequency and time domain measurement from outlet R1.3A to R1.3B in Ring 1. They are the two outlets on a single twin socket, the main signal only travels through the twin socket. So the S_{21} curve is very similar to that in Figure 5.5, the average attenuation is 12.76dB. Time domain result shows that a differentiated pulse is received at $9ns$ and the source pulse has been dispersed and attenuated to around $300mV$. The time delay is caused by the signal traveling along the coaxial connection cable and also through the twin socket.

2. Adjacent outlet pair, 5m powerline.

   Figure 5.7 shows the response from outlet R1.3A to R1.4A. The Tx and Rx are 5m apart. The average attenuation recorded is 25.52dB, as given in Table 5.1, which lists the average channel loss starting from R1.3A, ending at other outlets in Ring 1.

   Multiple notches occur as a result of multi-path transmission, as well as the bends in the cable, which cause the attenuation to vary between 10.89dB and 88.78dB. Figure 5.8 depicts the channel response of another 5m channel, between R1.3A and R1.2A. The transfer functions of these two paths are very similar, especially in the 50 - 550MHz frequency band. In higher frequencies though, channel response starts varying with transmission paths

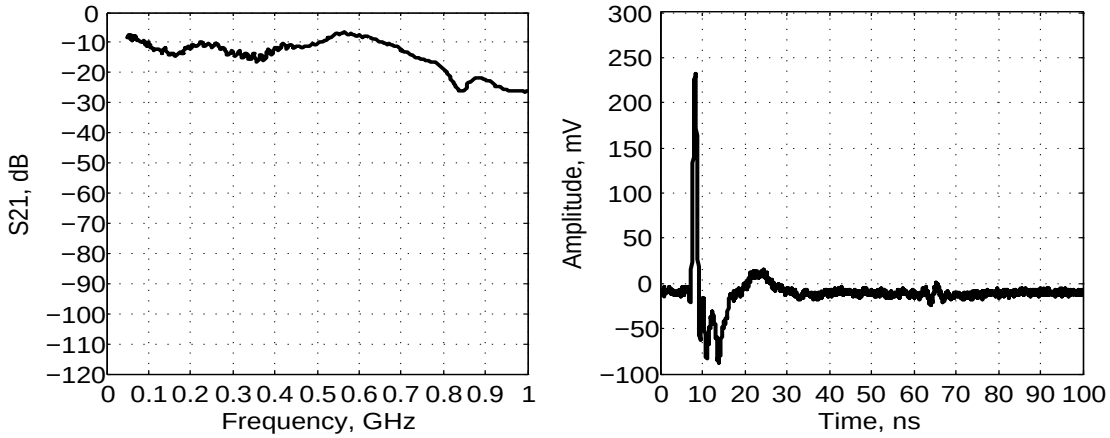

Figure 5.6: Frequency and Time domain response from R1.3A to R1.3B (0m).

and deep notches appear. It is noticed that the low frequency range provides a better transmission band, showing the low pass characteristics of the powerline channel.

The time domain results of these two channels are almost identical. In both cases, an impulse with $130mV$ is received around $40ns$. The received signal's wave form and time delay are mainly determined by the transmission distance and cable loss. Besides the main signal, there are two pulses received at $100ns$ and $180ns$. They are the multi-path signals travelling along other secondary paths in a ring. If the secondary signal is too strong, it may interfere with following signals, causing ISI.

3. Longer transmission paths, 10 and 15 meters.

   Figures 5.9 and 5.10 depict the resulting frequency and time responses of outlet pair (R1.3A-R1.5A) and (R1.3A-R1.6A) respectively. In these two paths, the shortest powerline channels are 10m and 15m respectively. It reveals that for longer transmission distances, 10m or more, channel performance degrades significantly. More severe peaks and nulls are observed in the channel response.

   Some correlations between the two channels can be noticed. For instance, it appears that the in 50 - 400MHz range, both traces attenuate with fre-

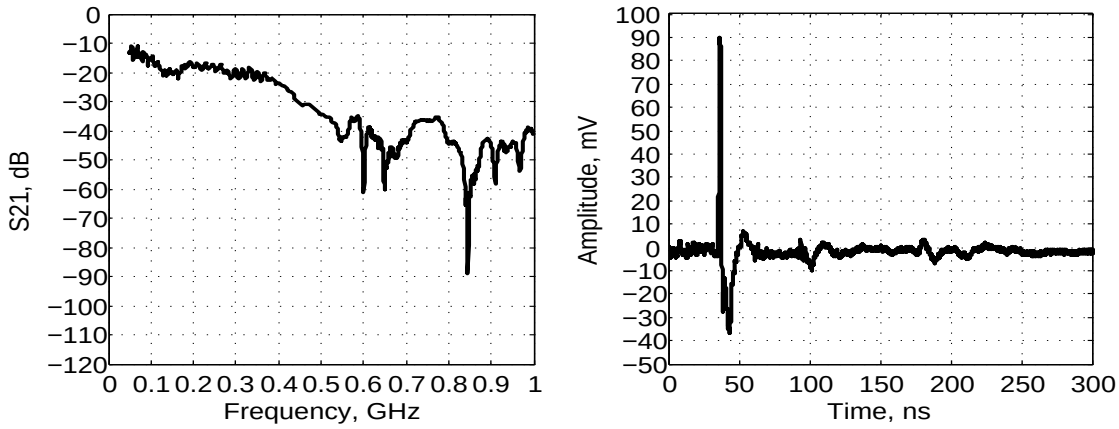

Figure 5.7: Frequency and Time domain response from R1.3A to R1.4A (5m).

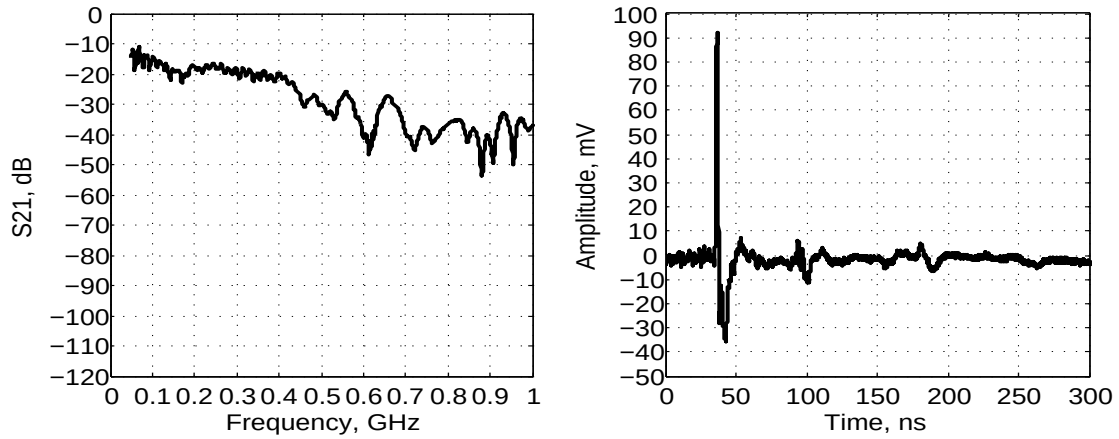

Figure 5.8: Frequency and Time domain response from R1.3A to R1.2A (5m).

quency, from 15dB to 60dB. While in 500MHz - 1GHz range, channel responses fluctuate between 40dB and 85dB. Table 5.1 shows that the average attenuation between outlet pair R1.3A and R1.5A is 32.46dB, varying between 13.47 and 84.86dB, whilst outlet pair R1.3A and R1.6A has an average attenuation of 36.23dB (4dB higher), fluctuating in the 15.16 - 85.52dB range.

The time domain results agree with frequency domain measurements. The main signal is received around $70ns$ for 10m channel and $97ns$ for 15m, signal strength has been attenuated as functions of transmission distance. Multi-path signal can be picked up by the receiver. Path R1.3A to R1.6A receives the strongest secondary signal, and it arrives $30ns$ after the main pulse.

From the time domain results, it can be proven that conducted transmission is the dominant signal transmission mode in the powerline channel. The fact that time delay increases with distance (around $30ns$ per 5m) shows that the signal is being propagated along the powerline channel, not being randomly received from radiation.

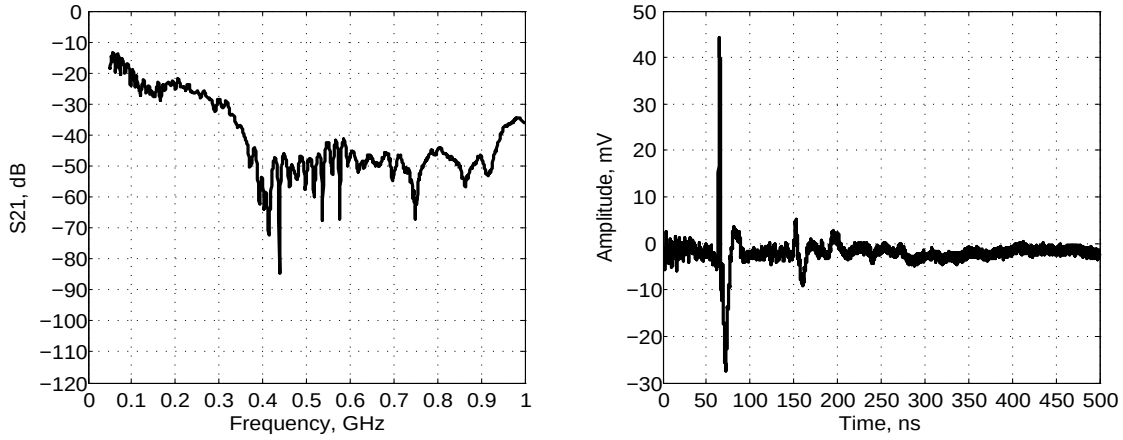

Figure 5.9: Frequency and Time domain response from R1.3A to R1.5A (10m).

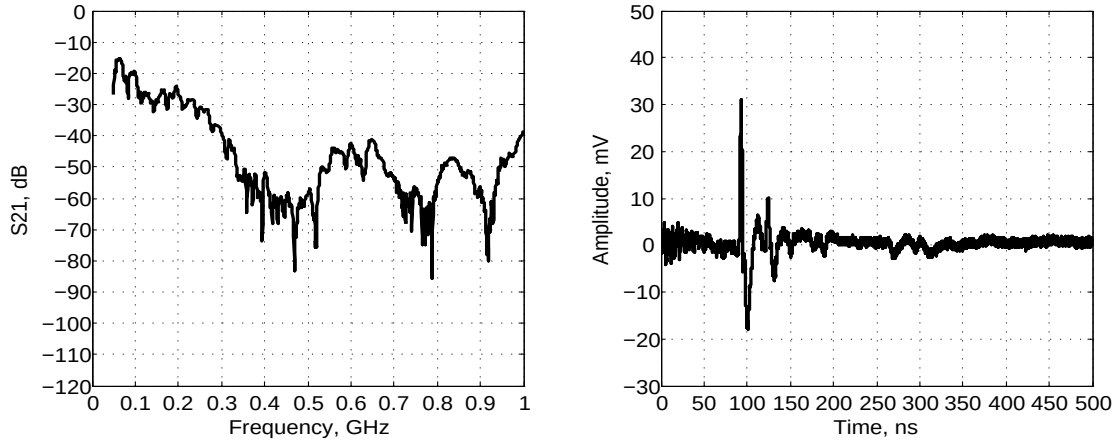

Figure 5.10: Frequency and Time domain response from R1.3A to R1.6A (15m).

4. Same transmission distance, different wall outlets.

   Figure 5.11 shows the frequency responses between outlet pair R1.3A to R1.4A and R1.4B. The length of these two paths are 5m. However, there is one more wall outlet in the R1.3A-R1.4A path. It shows that the addition of one more socket will not change the frequency response significantly. Both of the traces have similar profiles, especially below 500MHz. Variations are more obvious at higher frequencies. Thus, plugging into different outlets in the same twin socket can have similar channel response if other outlets are not connected to any equipment.

5. Symmetrical transmission.

   Figure 5.12 shows the transfer functions between outlet pair R1.3A and R1.6A, in both directions. The traces are very similar to each other as they almost overlap in the 50 - 400MHz range. In the higher frequency band, the two traces still have similar trends, despite that notches happen at different frequencies. We can observe that symmetrical transmission happens in low frequency bands, as frequency increases, the same path can have different transfer functions when transmission nulls occur at different frequencies.

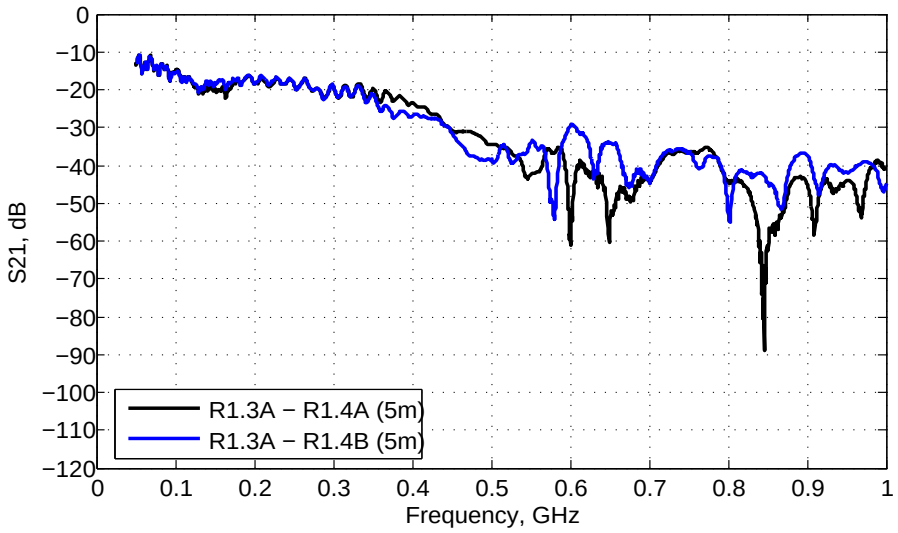

Figure 5.11: Channel response from R1.3A to R1.4A and R1.4B (5m).

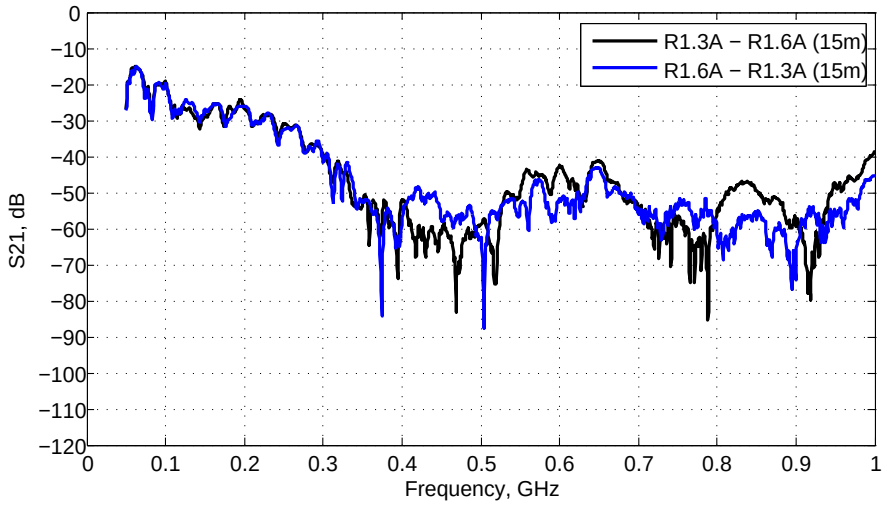

Figure 5.12: Channel response from R1.3A to R1.6A and from R1.6A to R1.3A (15m).

In summary, measurements in circuit Ring 1 reveal that the frequency variation characteristic is less obvious below 500MHz frequency band, and the signals are mainly received through conducted transmission.

Outlet Pairs		Attenuation in dB			
Name	Length(m)	Max	Min	Average	Std Dev
3A-1A	10	76.43	14.02	32.55	11.58
3A-1B	10	72.91	13.75	32.44	13.15
3A-2A	5	53.52	10.94	24.32	9.67
3A-2B	5	45.70	11.06	24.21	8.13
3A-3B	0	26.36	6.67	12.76	5.64
3A-4A	5	88.78	10.89	25.52	12.91
3A-4B	5	55.13	10.93	25.42	10.55
3A-5A	10	84.86	13.47	32.46	12.33
3A-5B	10	74.33	12.90	32.36	12.73
3A-6A	15	85.52	15.16	36.23	13.86
3A-6B	15	83.05	15.01	36.21	13.42

Table 5.1: Attenuation from outlet R1.3A to other outlets in the same circuit ring: Ring 1.

5.3.2.2 Cross Circuit Rings

Signal transmission on different circuit rings is also investigated, Figure 5.13 illustrates the transmission path for cross ring scenario.

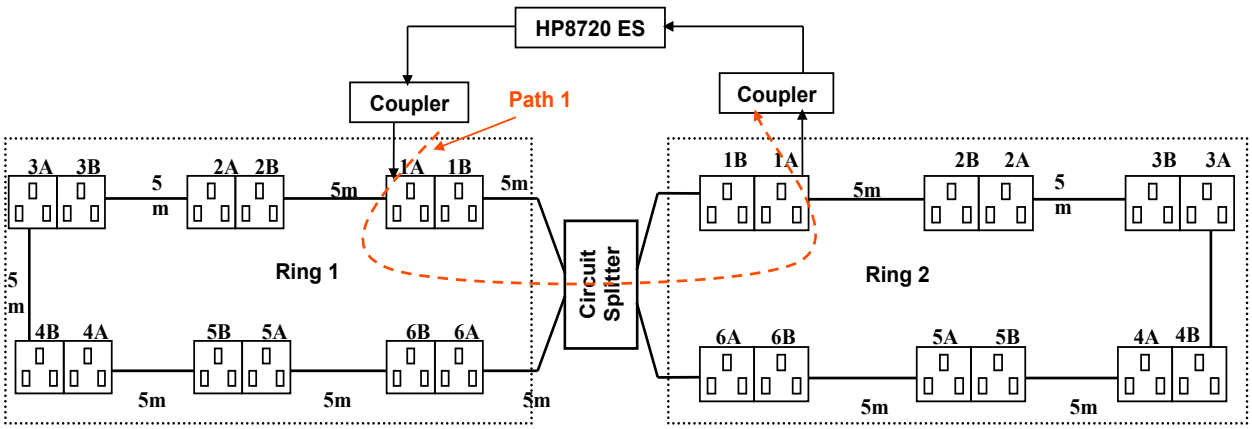

Figure 5.13: Cross ring signal transmission between R1.1A and R2.1A (10m).

Figures 5.14 and 5.15 show the measured responses between outlet pairs in dif-

ferent circuit rings, i.e. R1.3A to R2.1A (20m) and R1.3A to R2.3A (30m). From the time domain results, the source signal could hardly travel through different circuit rings, the received $5mV$ signal can be easily regarded as noise. Frequency domain measurements also prove that attenuation in cross ring transmission is much higher, the average attenuation between R1.3A and R2.1A is 52.11dB, and 55.58dB between R1.3A and R2.3A (Table 5.2). Interestingly, the transfer functions in both cases have very similar trends. Attenuation increases with frequency below 400MHz, then the channel response starts to fluctuate in the 50 - 90dB range.

Figure 5.16 shows the frequency responses of 4 outlet pairs. The signal is transmitted from R1.3A and received by different outlets in Ring 2, i.e. R2.1A, R2.2A, R2.3A and R2.4A. The minimum distance is 20m. One can see strong correlation among these traces, even though the transmission distances vary from each other. This fact shows that in cross rings transmission, the transmission distance has minor effect to the frequency responses as all the transfer functions have similar profiles. Severe nulls can be observed in the studied frequency band, showing that the powerline channel has very strong frequency selective fading effect, thus multi-carrier modulation technique is more suitable for such channel.

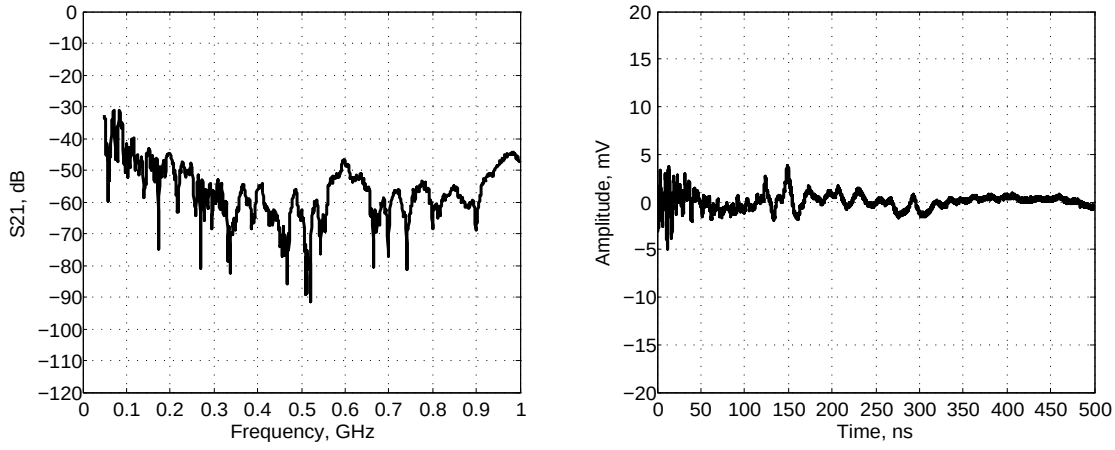

Figure 5.14: Frequency and Time domain response between R1.3A and R2.1A (20m).

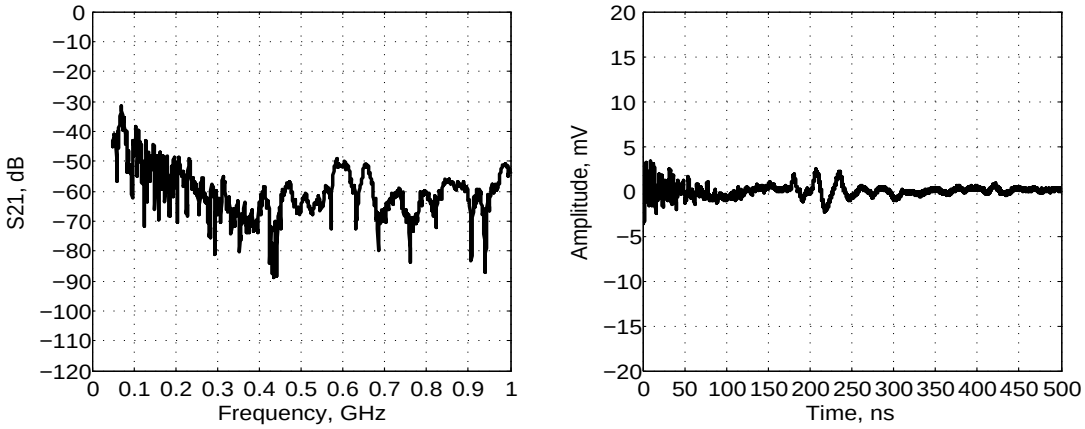

Figure 5.15: Frequency and Time domain response from R1.3A to R2.3A (30m).

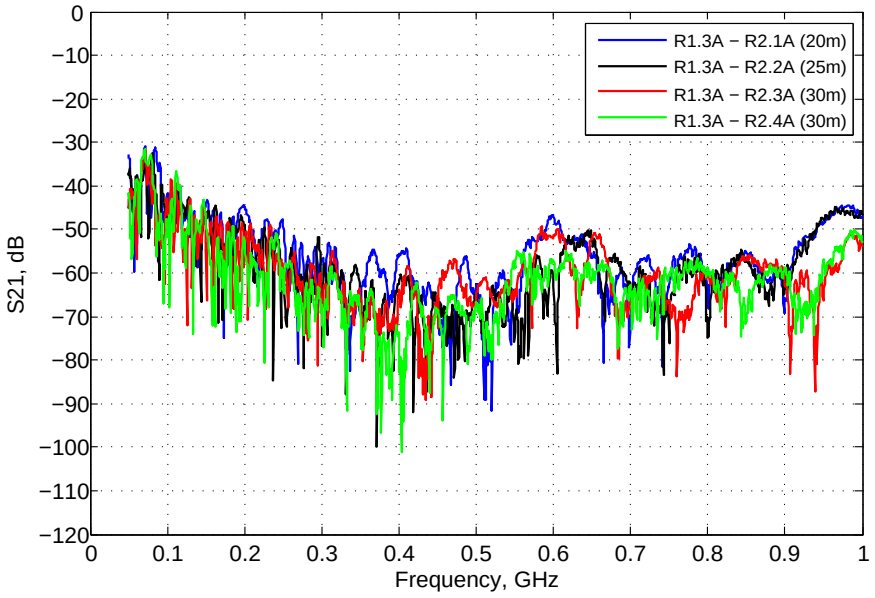

Figure 5.16: Measured channel response from different outlet pairs in cross circuit rings.

Outlet Pairs		Attenuation in dB			
Name	Length (m)	Max	Min	Average	Std Dev
R1.3A - R2. 1A	20.00	91.56	30.97	52.11	8.83
R1.3A - R2. 1B	20.00	88.98	29.90	51.89	8.02
R1.3A - R2. 2A	25.00	99.82	31.78	54.05	9.48
R1.3A - R2. 2B	25.00	98.59	31.00	54.50	8.04
R1.3A - R2. 3A	30.00	89.06	31.51	55.58	8.40
R1.3A - R2. 3B	30.00	90.22	30.63	56.52	8.61
R1.3A - R2. 4A	30.00	101.02	31.54	56.20	9.19
R1.3A - R2. 4B	30.00	93.27	30.98	56.13	8.72
R1.3A - R2. 5A	25.00	113.15	31.58	55.97	10.24
R1.3A - R2. 5B	25.00	98.32	30.69	55.72	9.58
R1.3A - R2. 6A	20.00	94.24	30.56	54.75	9.79
R1.3A - R2. 6B	20.00	97.53	30.02	54.16	9.86

Table 5.2: Attenuation from outlet R1.3A to other outlets in circuit Ring 2.

5.3.2.3 The Effect of Circuit Splitter

In previous sections, signal transmission on both single ring and cross ring has been examined. It shows that signal attenuation is much stronger in the cross circuit ring scenario. The main difference between same ring and cross ring transmission is that the signal will pass through the circuit splitter.

Figure 5.17 compares the measured responses between three outlet pairs, all of which have a transmission path of 10m, where outlet pair R1.1A-R1.3A and R1.1A-R1.6A are in Ring 1. It can be seen from Figure 5.17 (b) and (d) that both of the signals have the same delay ($70ns$), similar wave form and amplitude. The average attenuation for the two channels are 32.86dB and 35.45dB respectively. While in cross ring transmission between R1.1A-R2.1A, the main signal is attenuated more severely. Although also received at $70ns$, the source pulse has an amplitude less than $10mV$. The frequency response is also worse compared to same ring transmission, with many deep nulls across the band. The average attenuation between R1.1A-R2.1A is 45.8dB, over 10dB higher than those in the same circuit ring transmission. This shows that the circuit splitter will introduce strong losses to cross ring transmission, that signals could hardly propagate through two different mains loops.

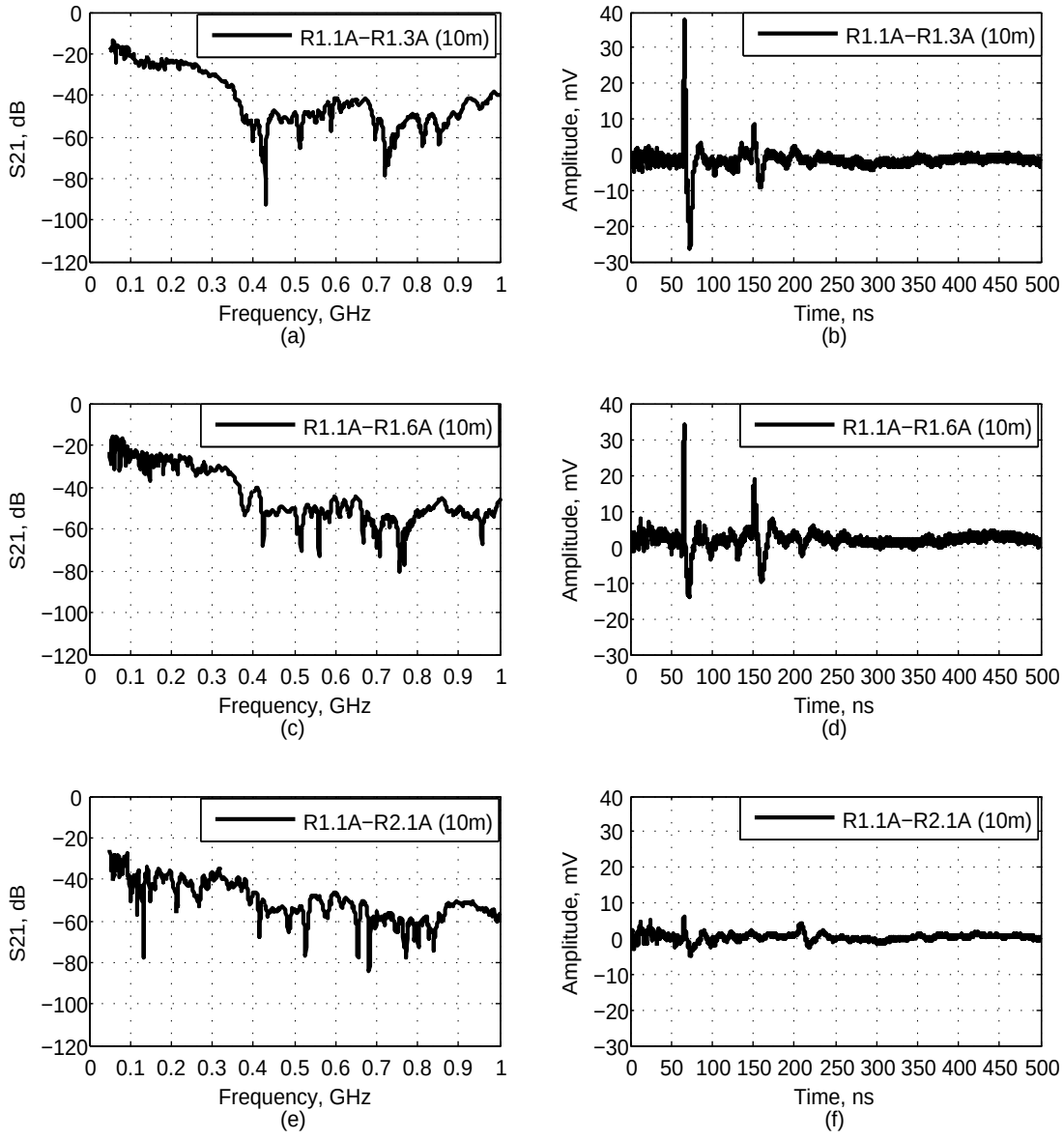

Figure 5.17: Comparison of channel response between same and cross circuit ring scenarios.

5.3.3 Channel Characteristics Analysis

5.3.3.1 Channel Attenuation vs. Distance

With the measurement on powerline test bed performance conducted, data are gathered on the attenuation characteristics, it is possible to analyse the channel loss variations in terms of transmission distance and the Tx/Rx locations.

Figure 5.18 shows the histogram of the average attenuation for all the outlet pairs in the same and cross circuit ring scenario. Table 5.3 gives the statistical data of the average attenuation in these two cases, in 50MHz - 1GHz band.

For all the outlet pairs in the same circuit ring, i.e. Ring 1, the average attenuation is 32.41dB. It can be seen from the histogram that the average attenuation of different outlet pairs spreads in three clusters, with a higher probability distribution in the 30dB - 40dB range. The histogram actually relates the average attenuation to different propagation distances. For Tx and Rx outlet pairs on the same twin socket, the average attenuation is 12.44dB, as shown in the cluster in the lower attenuation range. For outlet pairs that are 5m away, the average attenuation is 25.51dB, varying in the 24dB - 28dB range. When the outlet pairs are over 10m away, the average attenuation varies between 30dB to 40dB. It can be seen that in a ring circuit, attenuation between outlet pairs can vary significantly to the transmission distance.

However, in cross circuit scenario, the effect of transmission length is not as significant. The overall average attenuation in this case is 52.29dB. Although the transmission distance can vary from 10m to 30m, the average attenuation does not change much with distance, as previously observed in Figure 5.16. The histogram illustrates that most of the path loss falls in the 45dB to 57dB range. Compared with the same circuit loop, cross ring transmission will need to overcome 12.5dB more losses over the same distance, i.e. at 10m and 15m.

5.3.3.2 Channel Attenuation vs. Frequency

As can be observed from Section 5.3.2, frequency responses between different outlet pairs show a low pass characteristic of the powerline channel. The channels provide a good transmission band below a few hundred megahertz, i.e. 500MHz. As frequency increases, signal transmission performance degrades dramatically

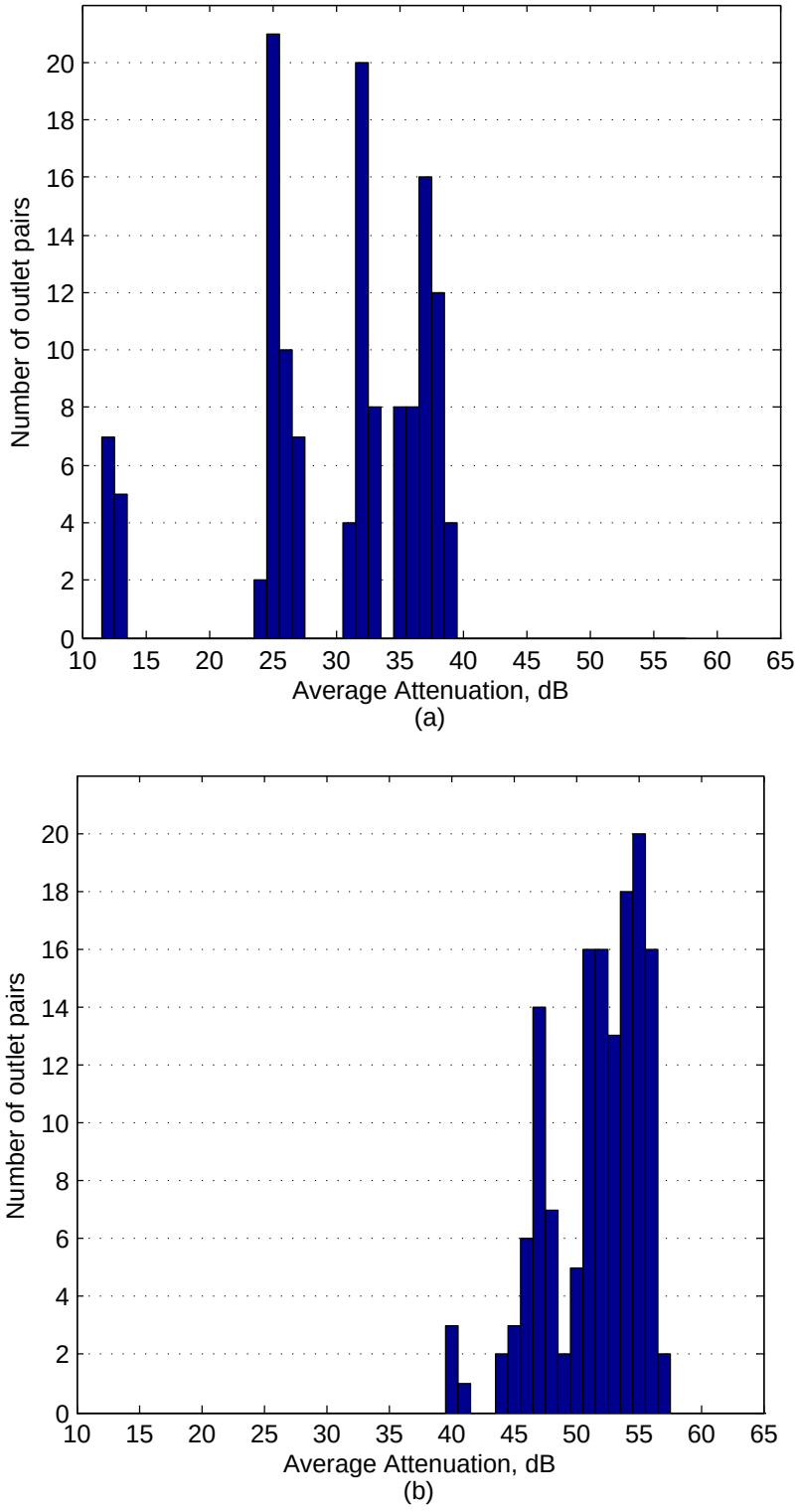

Figure 5.18: Histogram of average attenuation on different outlet pairs in (a) Ring 1 (same circuit ring) and (b) between Ring 1 and 2 (cross circuit ring).

	Attenuation (dB)			
Same Ring Scenario (Ring 1)	Max	Min	Average	Std Dev
twin socket (0m)	28.49	6.53	12.44	5.58
5m	71.26	11.62	25.51	10.19
10m	88.06	13.90	32.88	12.87
15m	87.26	15.53	37.33	12.78
Total	83.95	13.37	32.41	11.61
Cross Ring Scenario	Max	Min	Average	Std Dev
10m	85.59	24.79	45.64	9.45
15m	91.11	28.08	50.02	8.83
20m	92.72	29.15	52.54	8.60
25m	98.75	30.57	54.25	8.59
30m	95.89	31.15	55.24	8.38
Total	94.10	29.14	52.29	8.72

Table 5.3: Statistical analysis of average attenuation on different outlet pairs in same ring and cross circuit ring scenarios (50MHz - 1GHz).

and many deep nulls occur. Figure 5.19 shows the transfer functions between different outlets pairs in Ring 1 that are 10m away and up to 40 configurations have been recorded. Although measured at different locations, the loss profiles show remarkable resemblance in the low frequency range, 50 - 400MHz, in which the transmission loss increases with frequency, from 20dB to 50dB. However, as frequencies keep increasing, the channel responses vary with frequency and outlet pairs. Transmission nulls occur at different frequencies, mainly due to multi-path transmission and the effect of cable bends. Such deep nulls make it very difficult to use single carrier modulation, therefore a multi-carrier technique such as OFDM is more suitable. OFDM separates the channel into a number of narrow band flat fading sub-carriers, to overcome the frequency selective fading effect.

The average path loss at four transmission distances in Ring 1, i.e. 0m, 5m, 10m and 15m have been illustrated in Figure 5.20, from which the channel's low pass effect can be examined clearly. The channel transfer function can be separated into two parts, namely the low band and the high band. For instance, at 5m, the low band is 50 - 500MHz, with an average attenuation of 23.74dB. The high band is 500 - 1GHz. In this band, the path loss fluctuates between

30 - 40dB. The average attenuation is 14dB higher than that of the low band. Furthermore, the low band becomes narrower as distance increases. At 10m, its bandwidth is 400MHz, whilst at 15m it is narrowed to 320MHz.

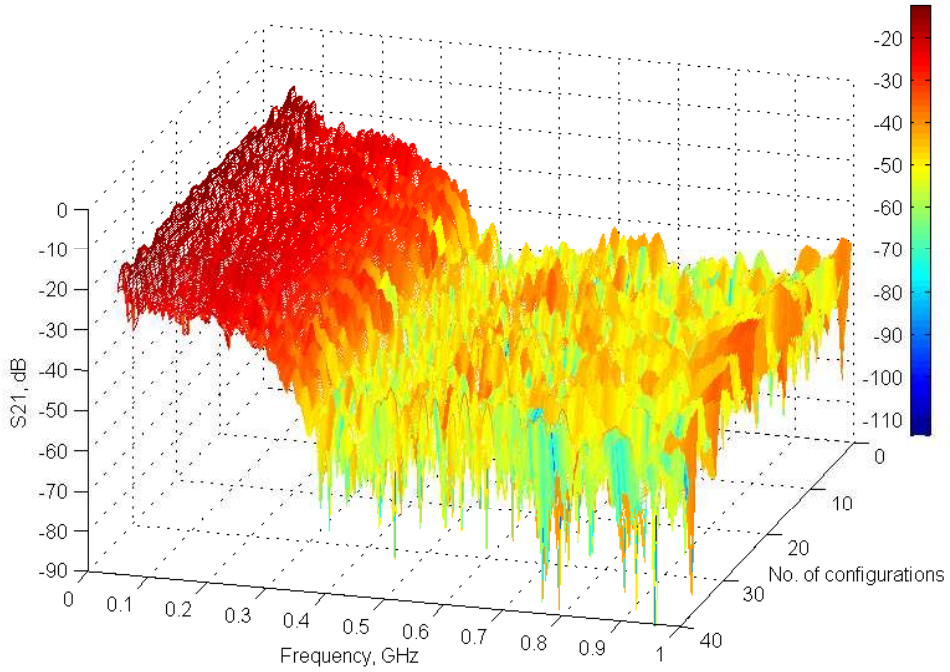

Figure 5.19: Three dimensional channel transfer function when the Tx/Rx is 10m away in Ring 1.

From Figure 5.21 and Table 5.4, the average channel loss has been analysed in three frequency bands, 50 - 550MHz, 500MHz - 1GHz and 50MHz - 1GHz. The first two bands are set at 500MHz to meet the FCC UWB standard. It can be seen that in the same circuit ring scenario, 50 - 550MHz band has the lowest transmission loss, and the attenuation rate is much smaller compared to other frequency bands. In the cross ring transmission, the signal experiences much higher attenuation in all transmission bands, while still the 50 - 550MHz band maintains the best performance. This indicates that the 50 - 550MHz frequency range can be possibly exploited for high data rate transmission in PLC systems.

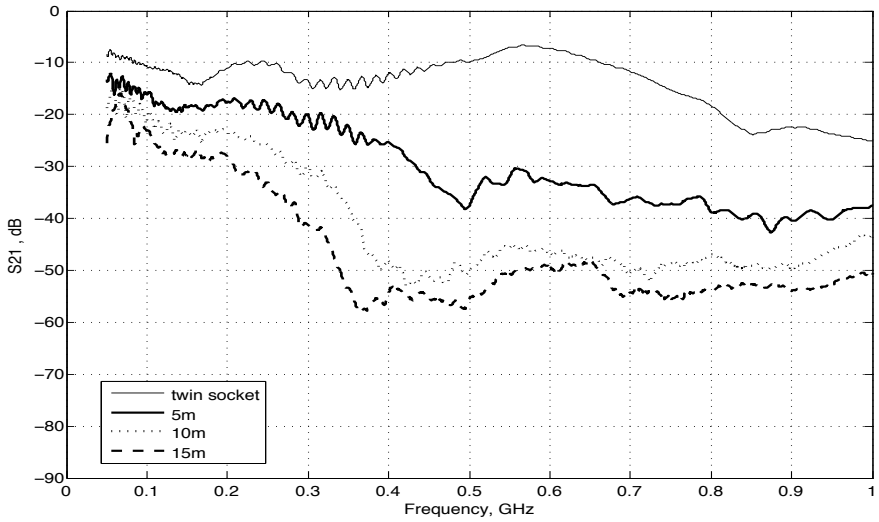

Figure 5.20: Average attenuation of different transmission distances in Ring 1.

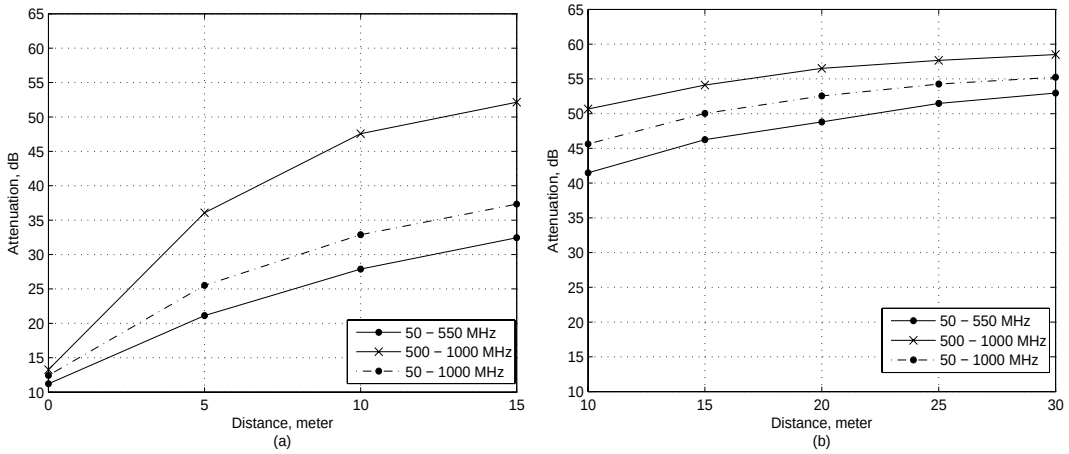

Figure 5.21: Average attenuation in different frequency bands in (a) same ring (Ring 1) and (b) cross ring situations.

	Attenuation (dB)					
	50 - 550MHz		500MHz - 1GHz		50MHz - 1GHz	
Same Ring Scenario	Average	Std Dev	Average	Std Dev	Average	Std Dev
twin socket (0m)	11.22	2.06	13.27	7.44	12.44	5.58
5m	21.13	8.29	36.08	6.69	25.51	10.19
10m	27.88	15.42	47.56	7.01	32.88	12.87
15m	32.45	17.60	52.15	6.33	37.33	12.78
Cross Ring Scenario	Average	Std Dev	Average	Std Dev	Average	Std Dev
10m	41.48	9.93	50.66	10.47	45.64	9.45
15m	46.25	11.76	54.12	8.96	50.02	8.83
20m	48.81	12.30	56.52	8.04	52.54	8.60
25m	51.46	12.40	57.67	7.50	54.25	8.59
30m	52.96	12.06	58.51	6.47	55.24	8.38

Table 5.4: Comparison of average attenuation of different outlet pairs in same and cross circuit ring scenarios in three different frequency bands.

5.3.3.3 Frequency Response with Electrical Appliances

Previous sections show that 50 - 550MHz range provides a suitable transmission band for UWB over PLC, without any electrical appliances attached to it. In realistic environments, the powerline channel is subject to different types of interference generated by household appliances. We therefore test the channel response by connecting different electrical loads to it, such as a hair dryer or a mobile charger. The channel frequency responses have been examined again, with loads connected at different locations, i.e. near the Tx/Rx or in the middle of the path. As an example, Figure 5.22 and 5.23 illustrate the recorded S_{21} between outlet pair R1.3A and R1.5A, from 50MHz to 600MHz.

It can be seen that both devices affect the channel performance. The nulls become deeper when the appliances are switched on and attenuation increases at some frequencies. For example, the hair dryer causes a few transmission nulls below 200MHz, while signal transmission is less affected in the high frequency range, where the S_{21} curves are similar to those measured without loads. More interestingly, the transmission performance might be improved sometimes, i.e. when we connect the loads in the middle of the path at R1.4A.

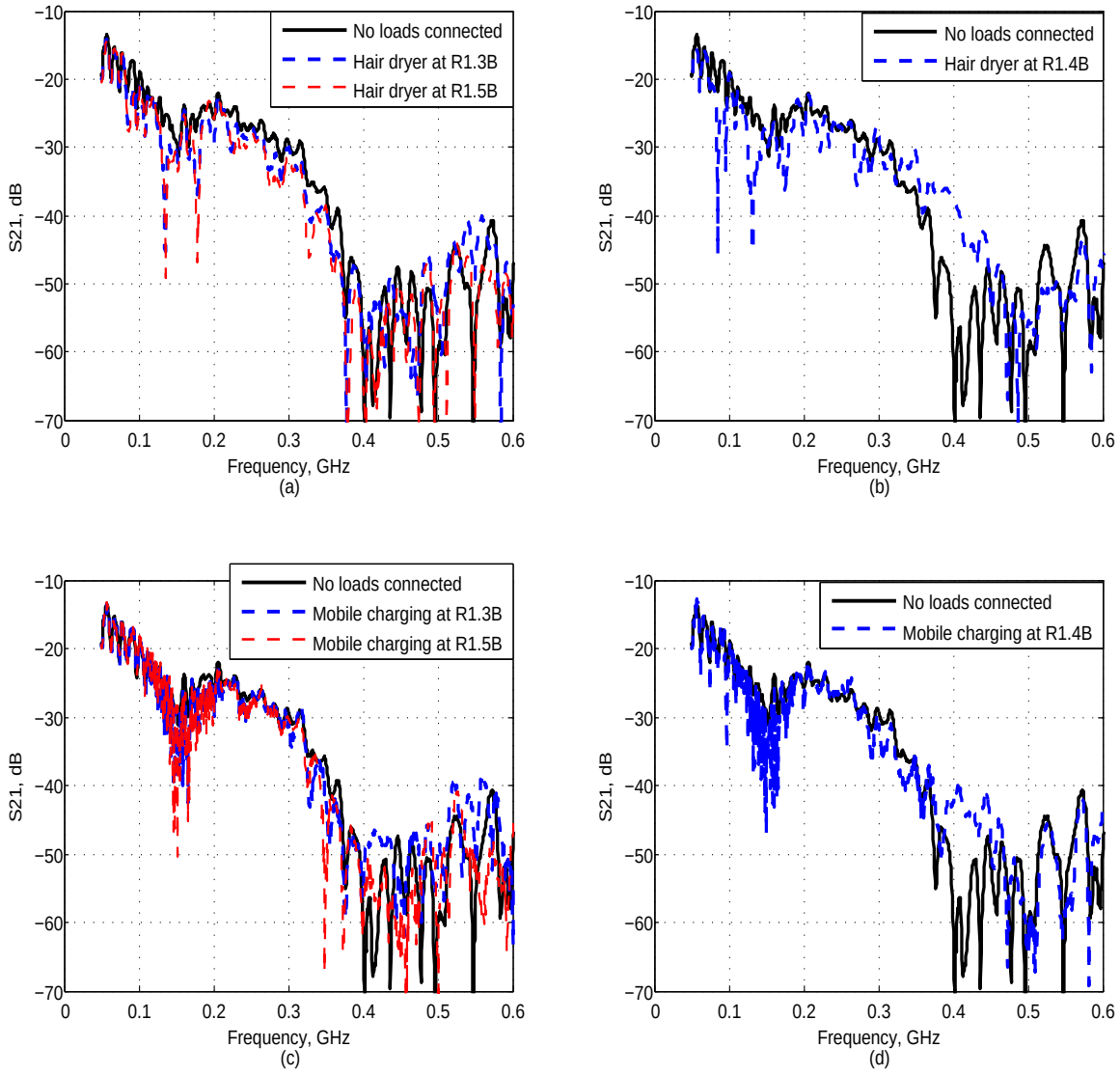

Figure 5.22: Channel transfer function between R1.3A - R1.5A (10m) when a hair dryer was connected to the (a) Tx or Rx (b) middle of the path, or charging a mobile phone at the (c) Tx or Rx (d) middle of the path.

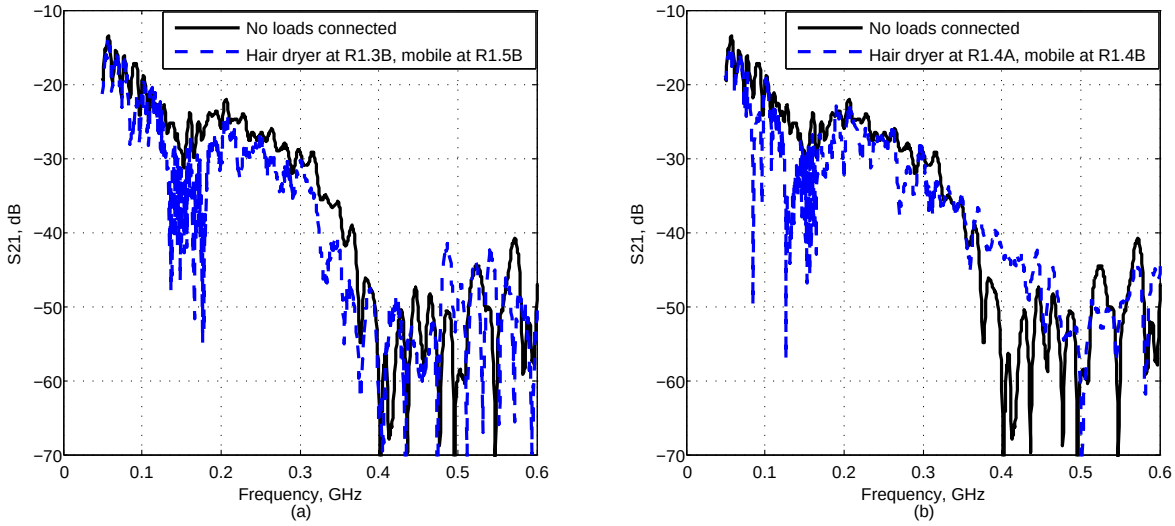

Figure 5.23: Channel transfer function between R1.3A - R1.5A (10m) when a hair dryer and a mobile charger were both connected to the (a) Tx and Rx (b) middle of the path.

On the other hand, when charging the mobile phone, many transmission nulls appear in 130 - 170MHz range and the same effect is also observed when it is in the middle of the path. This may due to the periodic impedance change of the phone when charging [105]. Moreover, as shown in Figure 5.23, similar loss profiles can be obtained when we connect both of the appliances to the channel.

In summary, interference caused by electrical loads is mainly in the low frequency range, below 200MHz. As frequency increases, the deteriorating effect to the channel is less significant as switching on the loads does not introduce new transmission nulls to the S_{21} curve. All the traces have a profile similar to that measured without any loads. Therefore, high frequency range is more robust to interference and a very wide bandwidth can still be used when other equipments are connected.

Table 5.5 compares the increase in average attenuation when electrical loads are connected to the path. It can be seen that the 5m path is most affected by the interference from household appliances. For longer transmission paths, the hair dryer causes more losses than charging the mobile phone, although the mobile charger introduces severer transmission nulls in 130 - 170MHz range. The

worst transmission case happens when both appliances are turned on, which adds another 3dB loss to the original channel.

	S_{21}	Increase in Attenuation (dB)								
Hair dryer location	o	Tx	Rx	Middle	o	o	o	Tx	Rx	Middle
Mobile charger location	o	o	o	o	Tx	Rx	Middle	Rx	Tx	Middle
R1.3A - R1.4A (5m)	20.97	2.56	2.74	–	2.19	2.17	–	4.08	4.33	–
R1.3A - R1.5A (10m)	28.55	1.92	2.22	1.47	0.85	0.86	0.87	2.83	2.81	2.46
R1.3A - R1.6A (15m)	32.12	2.10	2.00	1.57	0.78	0.79	1.04	2.92	2.83	2.43

Table 5.5: Increase in the average attenuation (50 - 550MHz) when electrical loads are connected ("o" means the appliance is not connected).

5.4 Noise Characteristics

Besides signal distortion due to cable loss and multi-path propagation, noise is another crucial factor influencing digital communication over powerline networks. Being different from many other communication channels, powerline channel does not represent an AWGN environment. As mentioned earlier, the powerline noise can be classified into five types: coloured background noise, narrow band noise, periodic impulse noise synchronous to the mains frequency, asynchronous periodic noise and random impulsive noise [106, 107].

The first three types of noise usually remain stationary over periods of seconds and minutes and may be summarized as background noise. However, the last two types, known as impulsive noise, are time variant in terms of microseconds and milliseconds, will cause the system's noise floor to be perceptibly higher and introduce bit or burst errors in data transmission [108].

5.4.1 Background Noise

The background noise of the AC powerline network can be measured with all the appliances turned off [95]. We measure the background noise with mains power on, and no electrical devices are connected to the test bed. A Spectrum Analyzer

R&S^{TM} FSP40 [109] is used to capture the noise PSD, with the resolution bandwidth of 30KHz. The sweep time is set at 1.15 seconds and 501 sweep points are collected in the DC - 1GHz frequency band. The measurement result is obtained by averaging 50 runs. The recorded noise seems to remain stationary almost over the whole observation period.

Figure 5.24 illustrates the background noise from DC to 1GHz. The best and worst background noise PSD was recorded by using the "Hold" function of the spectrum analyzer, the dynamic range is about 10dB. In the frequency band below 100MHz, the channel suffers very high background noise, narrow band interference caused by the ingress of broadcast stations (i.e. FM and AM radio) increases the noise floor in DC - 100MHz (Figure 5.25).

The measured background noise PSD has a flatter profile above 100MHz with less narrow band interference, providing a better environment for data transmission. The calculated average noise PSD is -102.76dBm/Hz across the frequency band, this indicates that UWB over PLC will benefit from the low level of noise interference in the high frequency band.

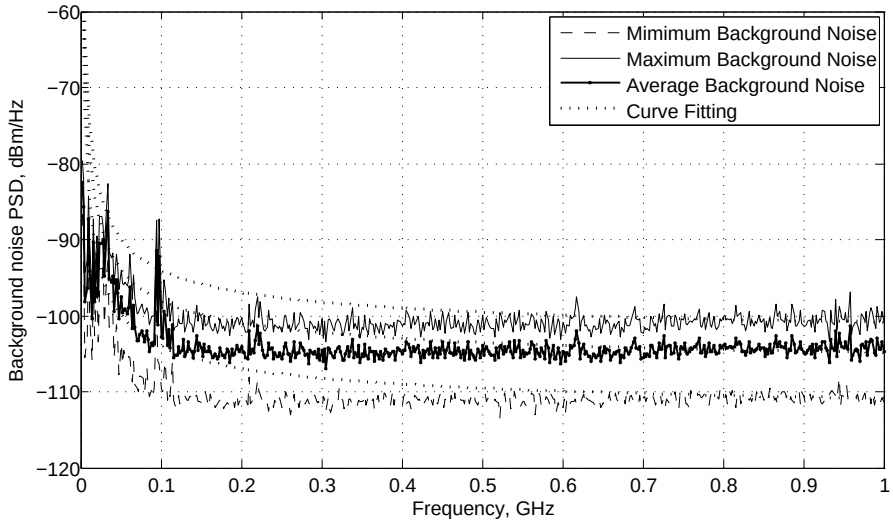

Figure 5.24: Measured Background noise of powerline channel, DC - 1GHz.

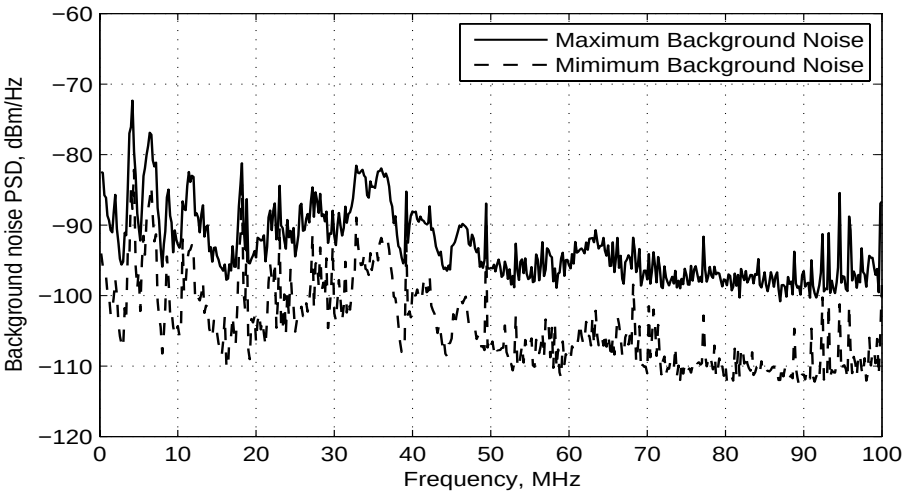

Figure 5.25: Measured Background noise of powerline channel in DC - 100MHz: strong narrow band interference can be observed.

5.4.2 Impulsive Noise

The impulsive disturbance caused by switching events in the powerline system has also been examined. Unlike background noise, this type of disturbance will cause more deteriorating effects to the system. As shown by Dostert in [108], the impulses have durations of some microseconds up to a few milliseconds with random arrival times. The PSD of this noise can reach values of more than 50dB above the background noise.

The impulse transients from the test bed have been measured by the Lecroy Digital Oscilloscope. No electrical loads are connected to the test bed when measuring the noise generated from switching on/off the lights and dimmers. In order to capture the impulse transients, the single trigger function is used. It captures a single impulse when it detects a voltage higher than a certain threshold level, which is $0V$ in our measurements.

5.4.2.1 Impulsive Noise Properties

- **Time Domain Analysis**

  We first test the impulsive noise generated from switching on the dimmer

in the lighting circuit, the impulses have been captured at different times, as shown in Figure 5.26. Although the lighting circuit and the sockets are in different rings, very strong disturbance can still be picked up by the Rx.

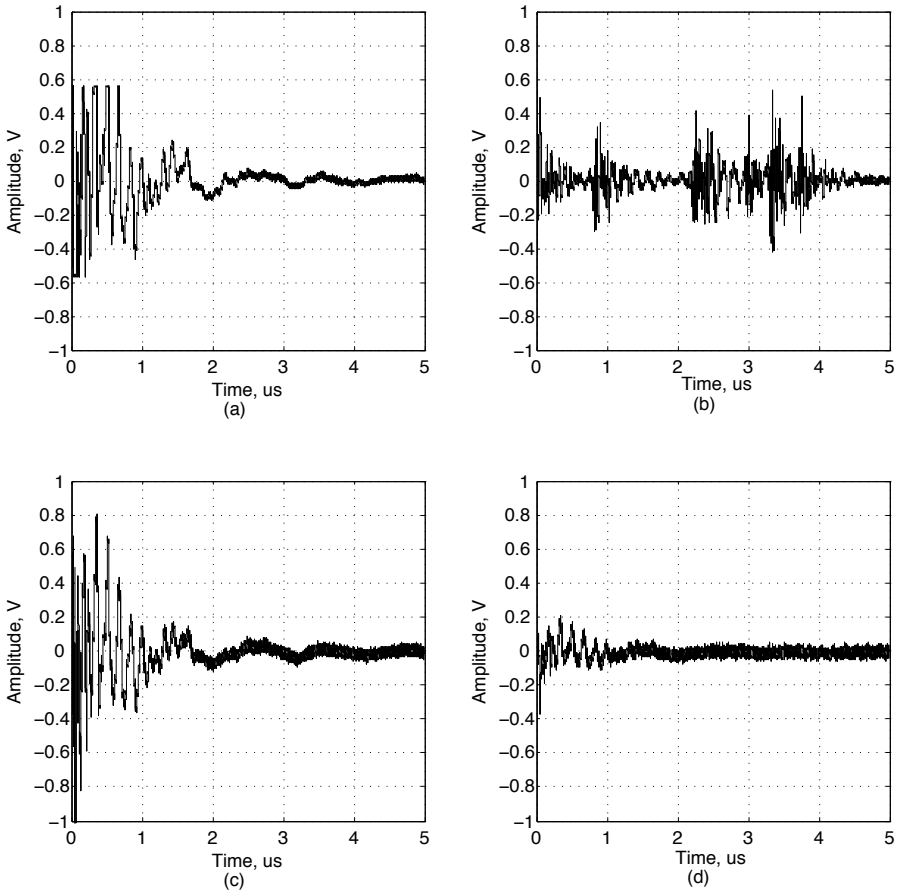

Figure 5.26: Measured impulsive noise transients when switching on the dimmer.

It can be seen that the impulsive noise has been randomly generated every time a switching event happens. The shape of the impulses is often similar to damped sinusoids or superimposed damped sinusoids [107]. The impulses have very high voltages and long durations up to a few microseconds. Furthermore, unlike the background noise, which is quite stable during the measurement, the impulse noise characteristics, i.e. amplitude, duration

and power are very different between each switching event. The same impulsive noise property has also been observed when switching on the lights in the network, as shown in Figure 5.27.

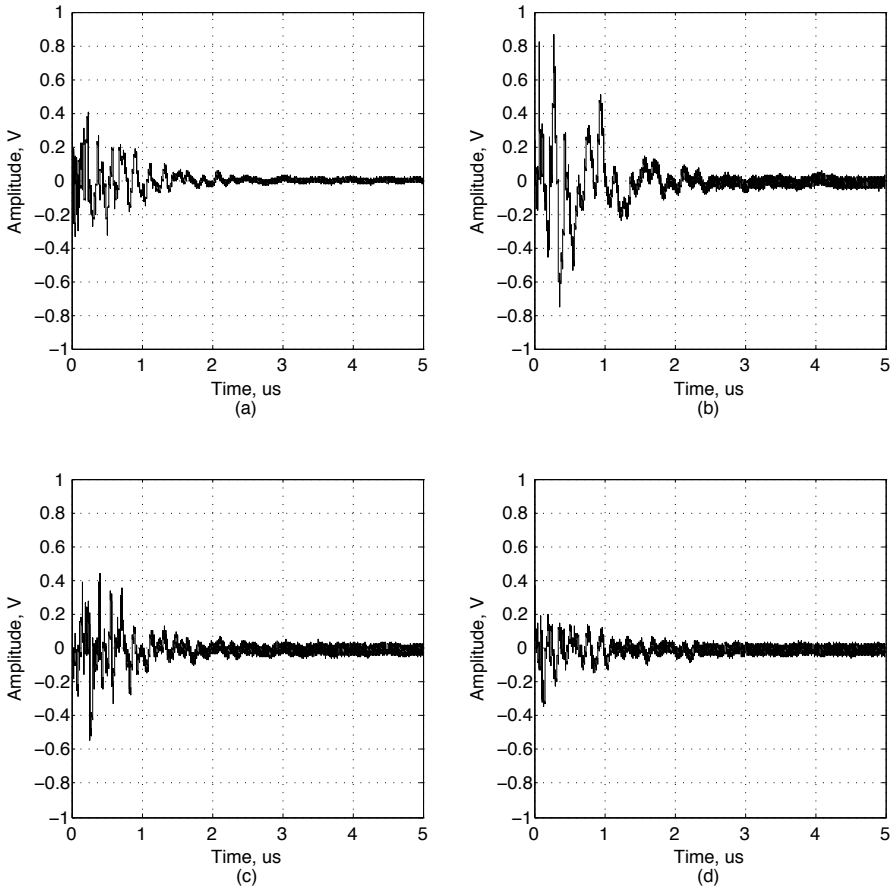

Figure 5.27: Measured impulsive noise when switching on the lights.

Based on the measured noise impulses, it is possible to analyse the time domain characteristics. Table 5.6 lists the parameters of the impulse examples from Figure 5.26 and 5.27, where the duration and power are calculated when 90% of the total energy has been received[1]. The duration of impulses varies from less than $1\mu s$ to a few μs, and their amplitudes can be as high as $1.13V$. The power of the impulses are dependent on the pulse width,

[1] $power = \frac{1}{T_2-T_1}\int_{T_1}^{T_2} s^2(t)dt$, $energy = \int_{T_1}^{T_2} s^2(t)dt$

pulse shape, as well as the amplitude. The maximum impulse power has reached to 50.83dBm[1] and it has a pulse shape shown in Figure 5.26 (b).

Pulse Information		Duration, μS	Amplitude, V	Power, dBm
Dimmer On	(a)	0.99	0.57	20.15
	(b)	3.75	0.54	50.83
	(c)	0.91	1.13	20.04
	(d)	2.72	0.37	3.4
Light On	(a)	1.01	0.4	12.47
	(b)	0.98	0.87	19.17
	(c)	0.96	0.54	13.97
	(d)	1.61	0.37	7.72

Table 5.6: Characteristic parameters of the impulses from Figure. 5.26 and 5.27.

It can be seen that the impulsive noise has very high amplitude and power. During its occurrence, strong disturbance to the PLC system is possible. The impulsive noise can be modelled as a periodically repeated rectangular signal $imp(t)$ (Figure 5.28), with random amplitude, duration and inter-arrival time t_p [44, 110]:

$$imp(t) = A_i \cdot rect_{d_i}(t). \tag{5.1}$$

Where A_i and d_i denote the amplitude and duration of the impulse.

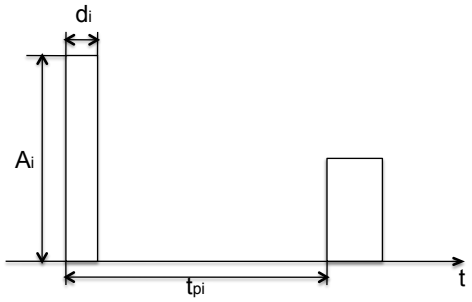

Figure 5.28: Impulsive noise modelled as random period rectangular signals.

[1] $power_{dBm} = 10log(power_{watts} \times 10^3)$

Statistical analysis of these parameters can help better understand the impulse characteristics and develop suitable impulsive noise model. In this study, 100 samples of impulses generated by switching on the lights and dimmer have been collected and analysed. The cumulative probability distribution (CDF) of impulse parameters, i.e. amplitude, duration and power are shown in Figure 5.29 - 5.31.

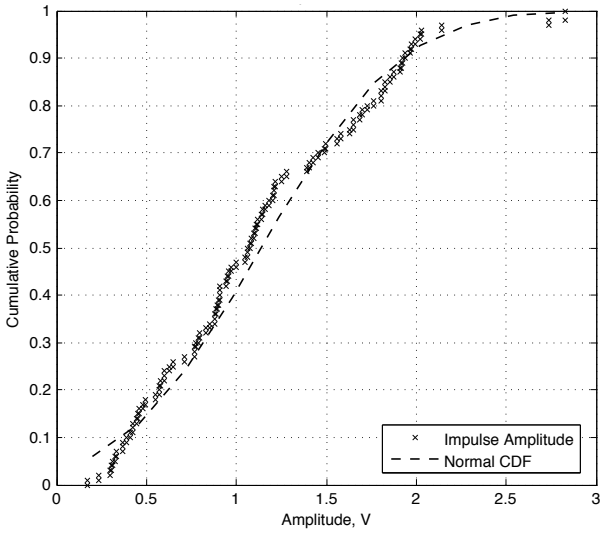

Figure 5.29: Measured impulsive noise amplitude fitted to normal distribution.

The measured data is statistically analysed by means of fitting to well-known empirical distributions [111]. The amplitude and power can be fitted to the normal distribution[1], where $\mu = 1.14$, $\sigma = 0.61$ for amplitude data and $\mu = 15.93$, $\sigma = 6.99$ for power data. The majority of impulse amplitude is between 0.5 - $2V$ and the power is between 5 - $23dBm$. While for impulse duration, log-normal distribution[2] ($\mu = 0.426$, $\sigma = 0.55$) provides a better fit than normal distribution, that is, the natural logarithm of the duration is normal. Statistical analysis of the sampled data show that the random impulsive noise generated by switching on/off the lights has parameters that

[1]CDF Normal Distribution: $F(x : \mu, \sigma) = \frac{1}{\sigma\sqrt{2\pi}} \int_{-\infty}^{x} exp(-\frac{(u-\mu)^2}{2\sigma^2})du$

[2]CDF Log-normal Distribution: $F(x : \mu, \sigma) = \frac{1}{\sigma\sqrt{2\pi}} \int_{-\infty}^{x} exp(-\frac{(lnu-\mu)^2}{2\sigma^2})du$

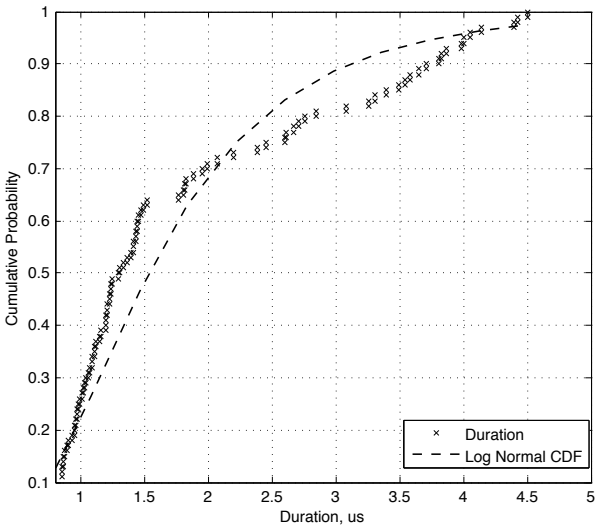

Figure 5.30: Measured impulsive noise duration fitted to log-normal distribution.

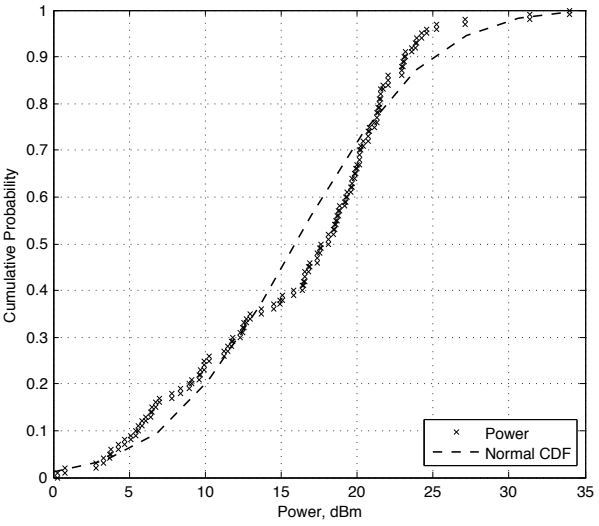

Figure 5.31: Measured impulsive noise power fitted to normal distribution.

can be modeled using empirical distributions. There is another parameter called inter-arrival time t_p, which determines the density of impulsive noise disturbance, is dependent on human activities during different times of the day. It requires a much longer observation period of the PLC network to obtain enough sample data for analysis.

- **Frequency Domain Analysis**

  From the time domain measurements, it can be seen that the impulsive noise has long duration and high power, this will significantly increase PLC system's noise floor. Analyses on the PSD will give a more precise assessment of its impact on a communication system, therefore, the PSD of the captured impulses are shown in Figure 5.32 and 5.33, where the blue curves are the measured maximum background noise level.

  The impulses have very high power in the low frequency range, most of the energy concentrates below 200MHz. Further, impulse with higher power has higher PSD level across the frequency range. For example, the pulse in Figure 5.26 (b) has the highest power and this is also reflected in the PSD profile, most of its frequency components have power levels stronger than other signals. It is noted that the impulses generated by switching on the dimmer have higher PSD than that measured when switching on the lights. As from Figure 5.33, above 200MHz, all the signal's PSD are below -100dBm/Hz, while the pulses recorded from dimmer switching events still can reach up to -90dBm/Hz at certain frequencies.

Compared to the background noise measured in the previous section, the impulsive noise will increase the noise floor of PLC systems, up to 30dB rise can be observed when strong impulse transient happens, and most of such increase is below 200MHz, interference to the high frequency signal is less significant. Properties of the impulse examples indicate a higher probability of bit and burst errors for high speed PLC applications. Therefore, more investigations are needed to understand the behavior of the impulsive noise and their patterns, in order to find appropriate countermeasures [39, 107].

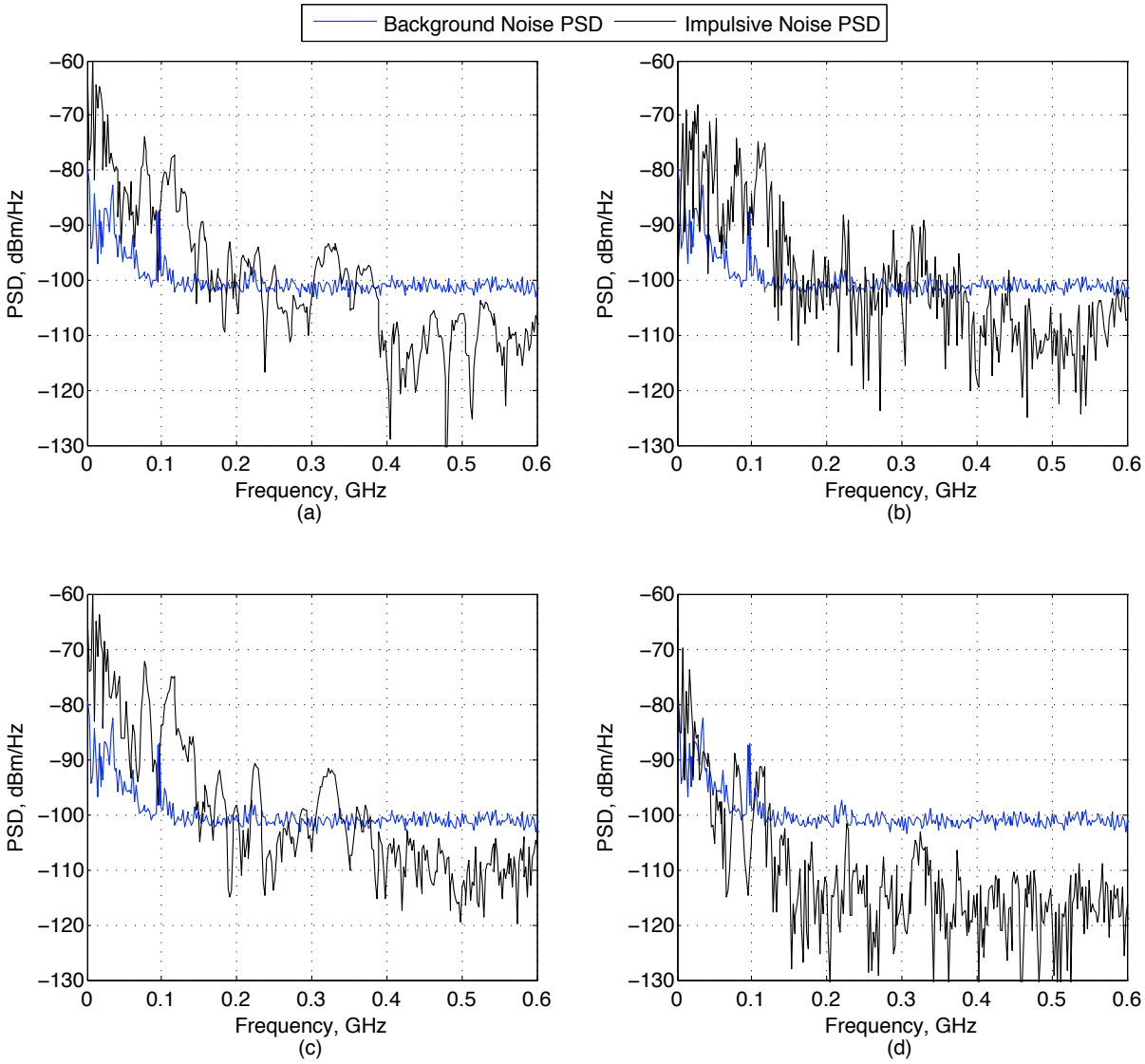

Figure 5.32: PSD of the measured impulsive noise from Figure 5.26.

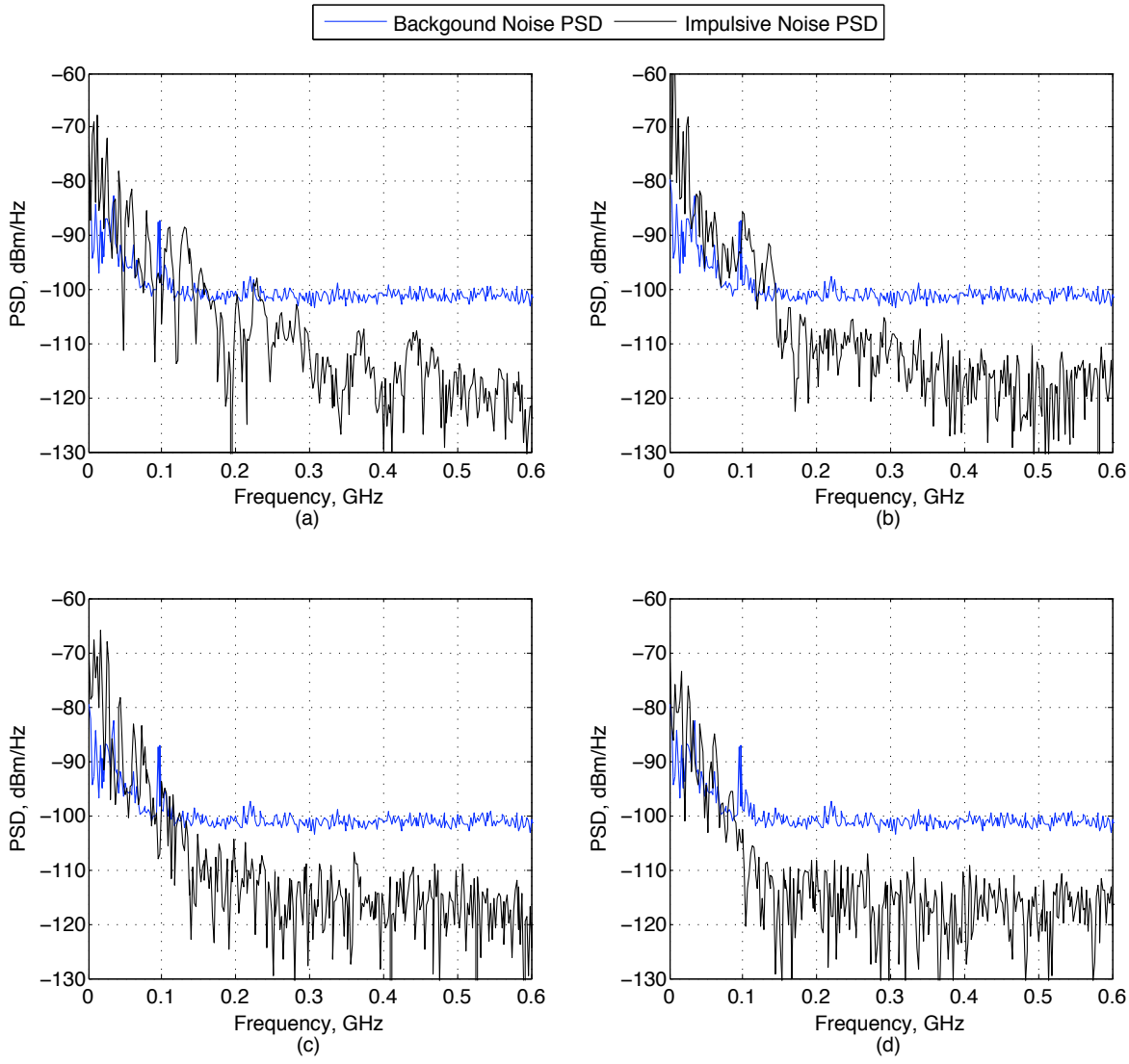

Figure 5.33: PSD of the measured impulsive noise from Figure 5.27.

5.5 EMC Issues

In previous sections, signal transmission characteristics of the indoor powerline channels have been studied thoroughly in the high frequency range. It has been proven that the powerline channel provides a good transmission band in the 50 - 550MHz range.

However, in the operating frequency range of 50 - 550MHz, the potential UWB over PLC application may cause electromagnetic radiation that will adversely affect the performance of the established radio communication systems. Because indoor powerlines are not designed for broadband use or high data rate transmissions, they will act as long antennas as frequency increases [50]. This will cause unintentional RF emissions, which may possibly increase the existing HF background noise floor via signal radiation.

Increase of the noise floor by the widespread use of powerline systems will bring up problems for radio users, such as FM, DAB, TV Broadcast, mobile communications and military communication [112]. Many efforts have been devoted to answer questions regarding how much electromagnetic interference does the powerline channel emit and how much emission is allowed for PLC systems. However, these studies are mainly focused on the 1.6 - 30MHz range, for high frequency use though, very few studies have been done [61]. Thus, it is necessary to find out what is the radiated emission from powerlines above 30MHz, so as to assess the potential deployment of UWB over PLC systems in terms of electromagnetic compatibility.

5.5.1 Measurement Setup

In this study, we are interested to find out the emission level from powerline systems in the high frequency range above 30MHz. This is achieved by field measurements from an exemplar powerline transmission circuit.

The measurement needs to follow the measurement guidelines proposed by international regulatory bodies, including CISPR 22, ITU-T and the FCC. The field strength should be measured at 3m distance to the powerline, using a measurement bandwidth of 9KHz below 30MHz and 120KHz when measuring above

30MHz. The field strength limits proposed for broadband wireline telecommunication networks has been given in Figure 2.4, from 1MHz to 1GHz.

A number of factors can affect the radiated emission from a powerline system, including the power injected to the lines, the electrical characteristics of the lines, the structure of the networks and the length of signal lines with respect to the HF wavelength, as well as the density of the PLC network [3]. Therefore, as a starting point, we build a simple powerline ring circuit for EMC measurement. It is a single circuit ring with 4 twin sockets, each being $0.7m$ apart. 2.5mm flat twin and earth cable is used. The cables and the sockets are fixed on a $0.8m^2$ wooden frame as illustrated in Figure 5.34.

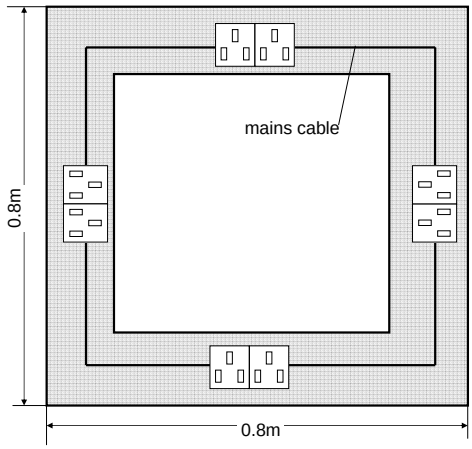

Figure 5.34: Illustration of the powerline circuit ring for EMC measurement.

Radiated emission from the powerline circuit has been measured at the test field in The Open University, Milton Keynes, UK. The test field has been built for standard EMC measurements in outdoor environment. It has a 9m×4m ground plane, which is constructed from four 9×1.2m sheets of wire mesh (Figure D.1 in Appendix C). As illustrated in Figure 5.35, the testing powerline circuit frame was placed in the middle of the test site, 0.8m above ground. The receiving antenna is set 3m away from the powerline circuit and aligns with the center of the frame.

The Lecroy pulse generator is used to input continuous pulses to the powerline circuit, through the RF coupler. The pulse generator is set to its maximum level,

that is, a $1ns$ pulse with $10V$ amplitude is transmitted continuously, at an interval of $10us$. In the receiving end, the electrical field is measured by two antennas operating in different frequency ranges: R&S KH116 Bi-conical (20 - 300MHz) and R&S HL223 Log-periodic (200MHz - 1.3GHz) antennas. The output of the antennas is swept by an R&S EMI Test Receiver ESVS10 (20MHz - 1GHz), with 120KHz resolution bandwidth. Finally, the receiver outputs the data to computer software, which loads the antenna factor data and displays the actual electrical field from the powerline circuit under test. Photographs of the measurement system are also shown in Appendix C.

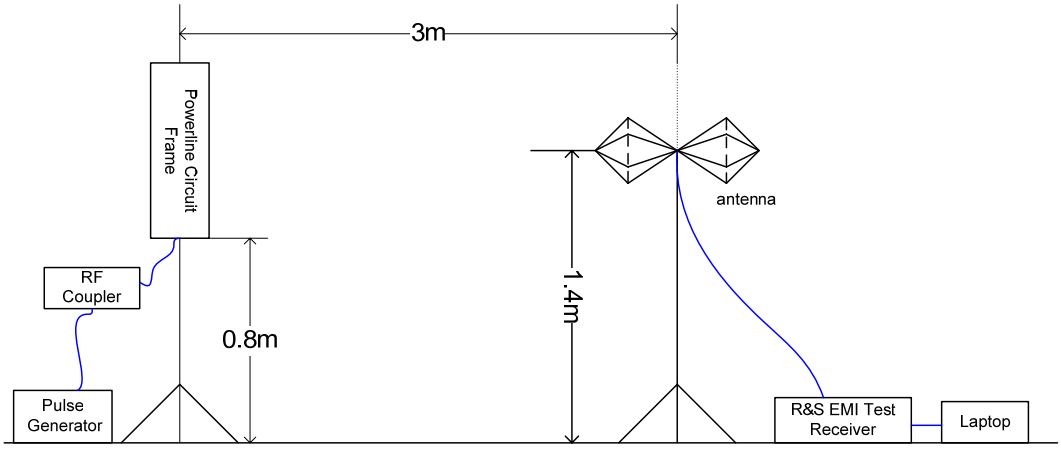

Figure 5.35: EMC radiated emission test site.

5.5.2 Results Analysis

Firstly, the background noise floor is measured in the 30MHz - 1GHz frequency range, by measuring the electrical field from the surrounding environment, when the equipment under test (EUT) is not operating. As illustrated in Figure 5.36, the background noise is quite small across the whole frequency range, with an average level between 12 and 30dBuV/m. The local radio systems can be clearly identified as their field strength is much stronger than the noise floor. FM radio signals operating around 100MHz radiates very strong signal up to 80dBuV/m,

DAB digital radio transmitting around 220MHz is also received, and in the 400MHz to 600MHz range is the terrestrial TV broadcasting channel, as well as the Global System Mobile Communications (GSM) network operating above 900MHz.

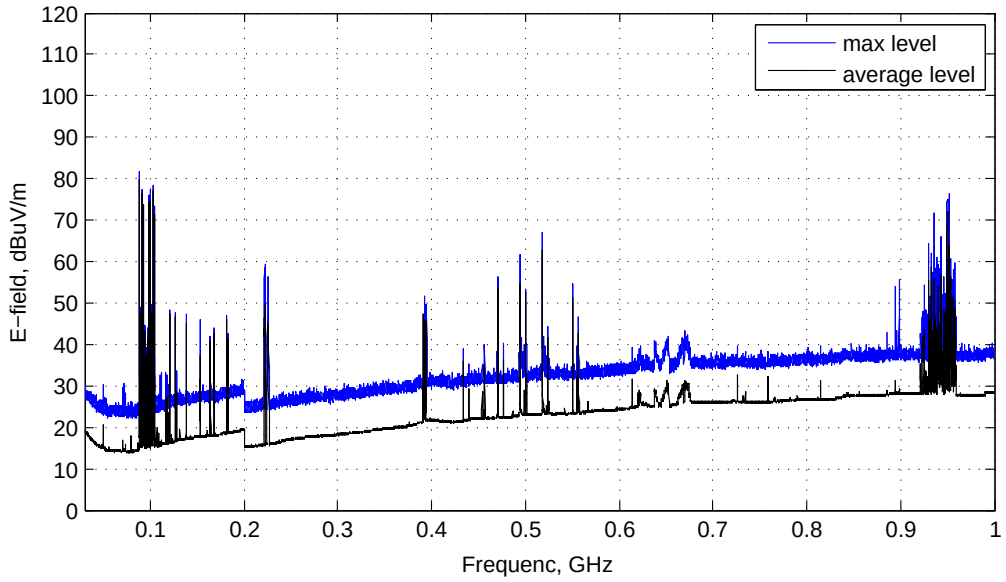

Figure 5.36: Tested background noise level of the test site.

Now we can test the radiated emission from the powerline circuit by feeding the pulse signals into the circuit. Figure 5.37 shows that the noise floor rises when the powerline circuit is transmitting. The maximum electrical field varies between 30dBuV/m and 50dBuV/m. The strongest radiated emission has been recorded in the 100 - 200MHz range, it reaches the maximum level of 50dBuV/m. Some of the narrowband radio systems in this band will be affected as the noise floor is relatively high compared to the transmitted energy from these systems. In other frequency bands, the maximum noise floor mainly resides below 40dBuV/m, except for the 450 - 550MHz range. Nevertheless, it can be noted that the background noise floor with powerline circuit transmitting is still below the FCC Part 15 emission limit for wire-line communication systems. Other radio systems can operate normally simultaneously as their radio emission levels are more than 20dB higher than the increased noise floor.

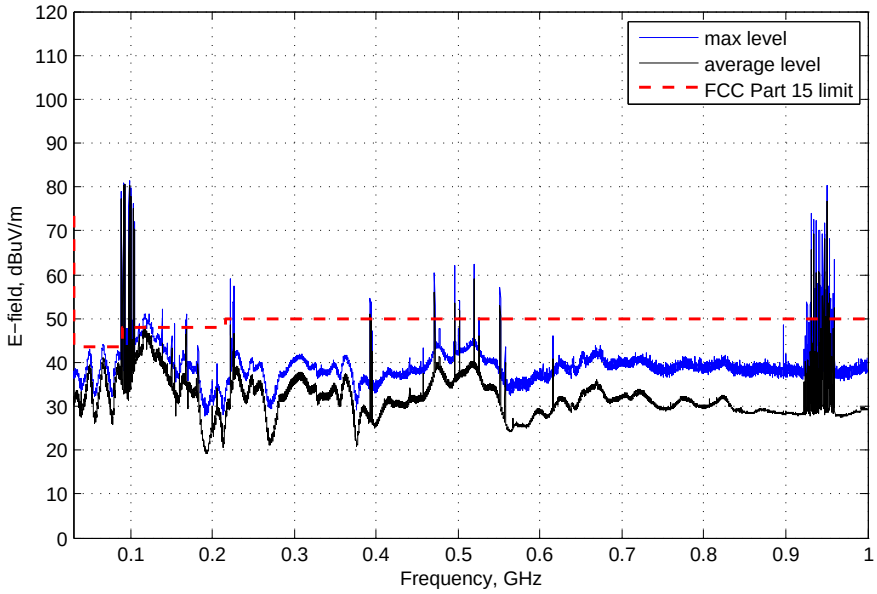

Figure 5.37: Radiated emission when signals are being transmitted to the powerline circuit - without electrical loads.

It is noted from previous measurements that loads connected to the powerline network will affect the system's transmission performance, as the input impedance and the transmission current will be changed. This may as well affect the radiated electrical field from the PLC system. Therefore, we also measure the electrical field from the powerline circuit, when a hair dryer and a mobile charger are connected to it.

It can be seen from Figure 5.38 that the powerline circuit causes less emission with the presence of loads, the maximum electrical field strength varies in the range of 30 to 40dBuV/m. Disturbance from the powerline circuit in this case is well below the FCC limit and a good performance on other radio systems can be maintained.

In order to see how much radiation has been generated from the powerline circuit, we compare the electrical field in the frequency bands where other systems are not transmitting. As from Figure 5.39, the average increase in the noise floor is more significant in the 30 - 50MHz and 250 - 350MHz range, where the noise floor rises over 10dB when there is no electrical load connected to the circuit.

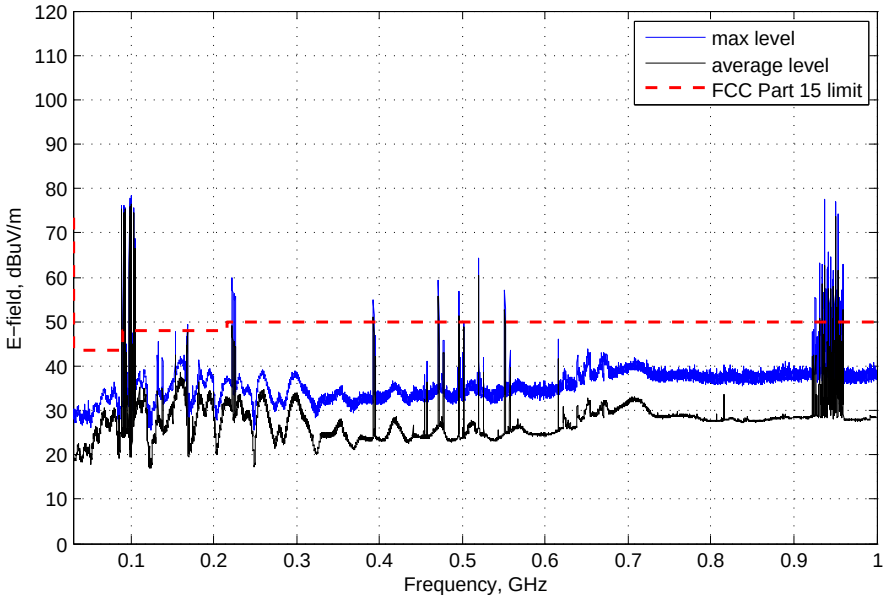

Figure 5.38: Radiated emission when signals are being transmitted to the powerline circuit - with electrical loads.

In higher frequencies above 500MHz, radiation from the powerline circuit is less remarkable. This is because in high frequency range, the transmitted power of the source pulse is smaller compared to that in the low frequency range. Despite such increase, we can see that radiation from the powerline circuit still meets the FCC emission limit. Moreover, during these measurements, the transmitted pulses have been set to $10V$, this gives a very high instant transmit power to the system. Radiation can be controlled by reducing the transmit power, i.e. the emission signal will be reduced by 10dB if a $1V$ pulse is transmitted.

For comparison purpose, we also measure the conducted transmission along the EUT (Figure 5.40). The doted lines show the background noise when no signal is transmitted. Strong FM and GSM signals can be picked up by the powerline circuit and the noise floor has a flat peak level profile at 15dBuV/m. The solid curves illustrates the conducted transmission signal when the $10V$ pulses are being transmitted. Most of the signals are received via conducted transmission, i.e. below 600MHz, the received signal is 30dB higher than the noise floor.

Initial studies give encouraging results for potential UWB over PLC applica-

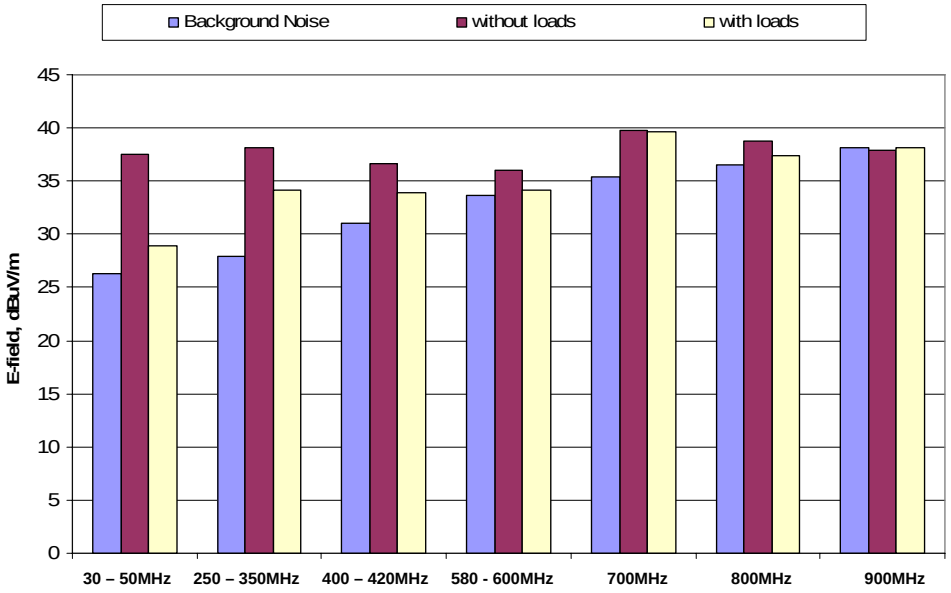

Figure 5.39: Noise floor variations caused by signal radiation from the powerline circuit.

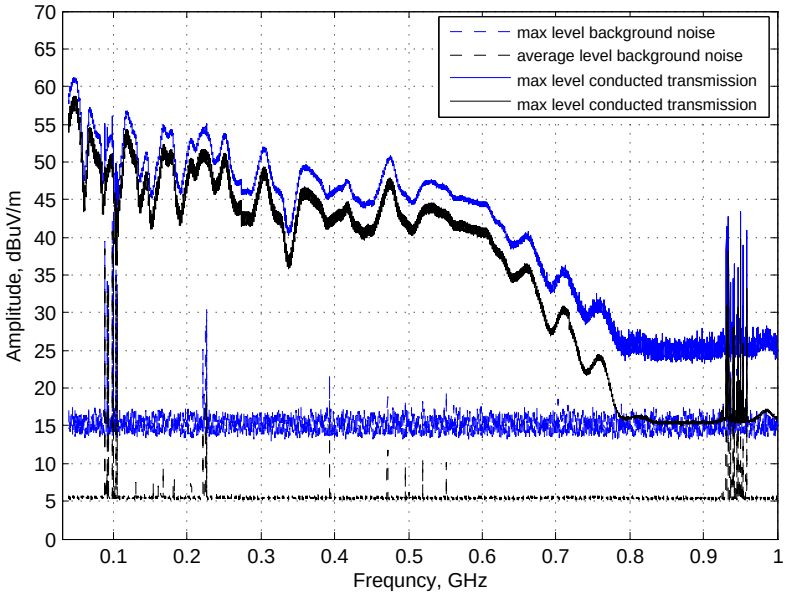

Figure 5.40: Conducted transmission over the powerline channel.

tions, as the radiation from powerline is below regulatory standards. However, the emissions caused by powerline channel is related to many factors including system topology, equipment connected to the network, measurement positions and the total transmit power [89]. Therefore, further measurements of the radiated emission from a more complicated PLC network is necessary, in order to establish a full empirical model for the behavior of broadband PLC systems and define the signal power level for potential UWB over PLC applications.

5.6 Summary

A test bed for indoor powerline communication system has been developed and its transmission characteristics have been investigated thoroughly. Broadband transmission over indoor powerline network has been experimentally proven possible. Time domain results show that a short duration impulse does travel along the cable, proving that a signal is not randomly picked up from a wireless link. On the other hand, frequency domain measurements show that the powerline channel exhibits frequency selective fading and low pass characteristics in 50MHz - 1GHz band. In the same circuit ring transmission scenario, signal loss increases with transmission distance, while in cross ring transmission, most of the signal has been attenuated by the house access point, therefore, UWB over PLC applications is more suitable for in-home networking over the same circuit ring. Further, analysis on channel transfer function reveals that 50 - 550MHz frequency band is more suitable for UWB over PLC, because the transmission loss is much smaller than other high frequency bands, and it is not affected significantly by other electrical loads connected to the system. Therefore, 50 - 550MHz frequency band has been defined as the operating band for potential UWB over powerline applications.

The noise characteristics of the test bed have been examined as well. Measurement of the background noise gives positive results, since there is not much narrow band interference above 100MHz. Whereas the impulsive noise generated by switching events will cause more disturbance to the PLC system. This type of noise can significantly increase the system noise floor as they have strong power

and long duration. Study of the impulsive noise is still an important topic and measures are required to overcome this type of interference.

As the operation frequency increases, broadband powerline systems may cause electromagnetic disturbance to other radio systems or raise the background noise floor. Therefore, the radiated emissions from a simple powerline ring circuit of 2.8m has been tested. Experimental results show that the powerline circuit does cause radiation emission above 30MHz, when a $10V$ pulse of $1ns$ duration is transmitted at $10us$ interval. Nevertheless, the measured emission level is below the FCC Part 15 limit across the frequency band. And it is noted that the radiated signal becomes smaller when other electrical loads are connected to the system. The conducted emission measurement also shows that most of the signal propagates through the powerline channel, instead of being received from random radiation. These investigations strengthen the potential of the proposed UWB over PLC technology.

Chapter 6

Ultra Wideband Communications for PLC Network

6.1 Introduction

In previous chapters, the transmission characteristics of powerline channel in a home system have been studied experimentally, as well as the radiated emissions from a single ring circuit. It is shown that UWB communication over the indoor powerline channel is highly feasible in the 50 - 550MHz frequency band. However, the potential transmission rate is not clear. Therefore, data transmission over the measured powerline channel will be examined in this chapter, in order to answer questions regarding system bandwidth and transmission rate.

Firstly, key system parameters such as link budget and SNR are analysed with their underlying statistics. The theoretical channel capacity has been obtained using the so called "water-filling" algorithm.

Further, data transmission is modelled in the PHY layer, based on the Multiband-OFDM UWB standard proposal. This proposal is submitted to the IEEE 802.15.3a standard group for WPAN communications. System performance parameters such as Bit Error Rate (BER) and transmit power have been obtained to predict the performance of UWB over PLC technologies and their potential applications in the home network.

6.2 Theoretical Channel Capacity Consideration

Increasing channel capacity is one of the objectives of this project. According to Shannon's channel capacity theorem, channel capacity can be increased either by using a wider bandwidth, or by increasing the SNR level, i.e. the transmit power. In most cases, the system bandwidth is fixed, therefore, SNR becomes the critical factor for channel capacity.

6.2.1 Link Budget

In the design of high speed communication system, a top-level link budget analysis is often used by engineers to determine the feasibility of any given system. A link budget calculation is also an excellent way to understand the various factors which need to be traded off to realize a given cost and level of reliability for a communication link. When evaluating a communication system, there exist five important factors: the available transmit power, bandwidth of the system, the loss of the communication link, the noise characteristics of the channel and the required reliability [113].

For a digital communication system, link budget is typically specified as an E_b/N_0 (ratio of energy per bit to noise PSD) requirement for some distance or percentage of the coverage area [68], which can be calculated as:

$$\frac{E_b}{N_0} = TxPower(dBm) - Atten(dB) - [noise(\frac{dBm}{Hz}) + 10log(R(bps))] \tag{6.1}$$

where $TxPower$ is the transmitted power, $Atten$ is the measured channel attenuation, which includes all the loss experienced by the signal between the Tx and Rx, $noise$ is the noise PSD and R is the system data rate. E_b/N_0 is a measure of the required energy per bit relative to the noise PSD and it can be converted to SNR by using:

$$SNR = (E_b/N_0) \times (R/B), \tag{6.2}$$

where B is the system bandwidth.

With the attenuation and background noise characteristics collected from measurement, link budget can be obtained by using equation (6.1). Table 6.1 compares the link budget of a 10m transmission link in three transmission bands:

50 - 550MHz, 500MHz - 1GHz and 50MHz - 1GHz. Channel attenuation is the average attenuation value listed in Table 5.4. The noise PSD is the average value calculated from the measured background noise.

Assuming the system data rate is 1Gbps, 50 - 550MHz band provides the best communication link, it gives an E_b/N_0 of 14.66dB when the total transmit power is 30dBm. At the same transmit power and system data rate, the link budget achieved in 50 - 550MHz band is 4.5dB better than that in the 50MHz - 1GHz frequency band, and 18dB better than the 500M - 1GHz band.

	Transmission Band 50 - 550MHz				
Total Transmit Power, dBm	10	20	27	30	37
Channel Attenuation, dB	27.88	27.88	27.88	27.88	27.88
Noise PSD, dBm	-102.34	-102.34	-102.34	-102.34	-102.34
Bit rate, dB	90	90	90	90	90
Bandwidth, dB	87	87	87	87	87
E_b/N_0, dB	-5.54	4.66	11.66	14.66	21.66
SNR, dB	-2.54	7.66	14.66	17.66	24.66
	Transmission Band 500MHz - 1GHz				
Total Transmit Power, dBm	10	20	27	30	37
Channel Attenuation, dB	47.56	47.56	47.56	47.56	47.56
Noise PSD, dBm	-103.28	-103.28	-103.28	-103.28	-103.28
Bit rate, dB	90	90	90	90	90
Bandwidth, dB	87	87	87	87	87
E_b/N_0, dB	-24.28	-14.28	-7.28	-4.28	2.72
SNR, dB	-21.28	-11.28	-4.28	-1.28	5.72
	Transmission Band 50MHz - 1GHz				
Total Transmit Power, dBm	10	20	27	30	37
Channel Attenuation, dB	32.88	32.88	32.88	32.88	32.88
Noise PSD, dBm	-102.76	-102.76	-102.76	-102.76	-102.76
Bit rate, dB	90	90	90	90	90
Bandwidth, dB	90	90	90	90	90
E_b/N_0, dB	-10.12	-0.12	6.88	9.88	16.88
SNR, dB	-10.12	-0.12	6.88	9.88	16.88

Table 6.1: Comparison of average E_b/N_0 and SNR of 10m transmission in Ring 1, in 50 - 550MHz, 500MHz - 1GHz and 50MHz - 1GHz frequency bands.

6.2.2 Theoretical Capacity of Background Noise Channel

6.2.2.1 Water Filling Algorithm

With all the measurements and analyses, theoretical channel capacity under background noise can be calculated, based on the well known water-filling algorithm under several practical assumptions [114]. Suppose that $N(f)$ and $H(f)$ are the PSD of the background noise and the broadband channel transfer function respectively and the total signal power is limited. From [115], channel capacity can be defined as:

$$C = \int_W log_2(1 + \frac{S_x(f)|H(f)|^2}{N(f)})df \tag{6.3}$$

where $S_x(f)$ is the PSD of the signal power, and W is the channel bandwidth. The broadband channel can be split into a set of flat fading channels, in which the channel transfer function can be regarded as constant with AWGN, thus the channel capacity can be determined as the sum of the sub-channels' capacity.

It is well-known that the water-filling algorithm can be used to determine the optimal transmission power distribution over the sub-channels. Given the total transmission power P, the optimal transmission PSD can be obtained as [82]:

$$S_x(f) = \begin{cases} L - \frac{N(f)}{|H(f)|^2}, & f \in W \\ 0, & otherwise \end{cases} \tag{6.4}$$

where

$$P = \int_W S_x(f)df \tag{6.5}$$

L is a parameter that depends implicitly on the specified power and channel parameters by:

$$L = \frac{1}{W}\{P + \int_W \frac{N(f)}{|H(f)|^2}df\} \tag{6.6}$$

$S_x(f)$ should always be non-negative. If the calculated $S_x(f)$ is negative it will be set to zero, meaning no power is allocated to the sub-channel.

$S_x(f)$ can be optimized through the following steps:

1. Assume there are N sub-channels, each with bandwidth $\Delta f = W/N$. The carrier to noise ratio of each sub-channel can be obtained as $|H_n|^2/\sigma_n^2$, where H_n is the channel transfer function in sub-channel n and σ_n^2 is the average noise power within that sub-channel, $\sigma_n^2 = N(f)\Delta f$.

2. Calculate the initial power allocation for each sub-channel in the bin (here bin is referred to the collection of all the sub-channels with none zero transmit power) S_n using Equation (6.6) and (6.4).

3. Check if there is any sub-channel that has negative power allocation. If yes, set the power to zero and remove this sub-channel from the bin, then go back to step 2. Move forward until all the sub-channels are allocated with none negative power.

4. Finally, calculate the channel capacity using Equation (6.3).

6.2.2.2 Channel Capacity of Powerline System

For example's sake, consider the capacity of a powerline channel in the test bed, i.e. from outlet R1.3A to R1.5A (10m). The respective frequency response and the background noise PSD are shown in Figure 6.1.

Assume the total transmit power is 5W (37dBm) and there exist 843 sub-channels with frequency interval $\Delta f = 593.75kHz$ [1]. In this ideal case, when the powerline network is not subject to other interference caused by switching events or electrical appliances, the optimised transmit power and bit allocation of each sub-channel is shown in Figure 6.2. Water filling algorithm optimises the power allocation by closing sub-channels with poor SNR, to achieve the best power utilization.

Channel capacity can be calculated from Equation (6.3), based on the transmit PSD. It is noticed that the number of bits allocated at each frequency varies significantly, from zero bits to the maximum of 12bits/Hz. More bits are allocated to the sub-channels with higher SNR. Fewer bits are transmitted above 400MHz when the channel attenuation is around 50dB. The total channel capacity obtained in this case is 3.26Gbps, which can be increased by transmitting more power. However, the increase of transmit power should not violate the EMC regulations of the country, which sets an important limit for the usable bit rate [116].

[1] The frequency interval is set as the sampling interval of the network analyser, which records the powerline frequency response at an interval of 593.75KHz. During this frequency interval, the channel response is regarded as constant.

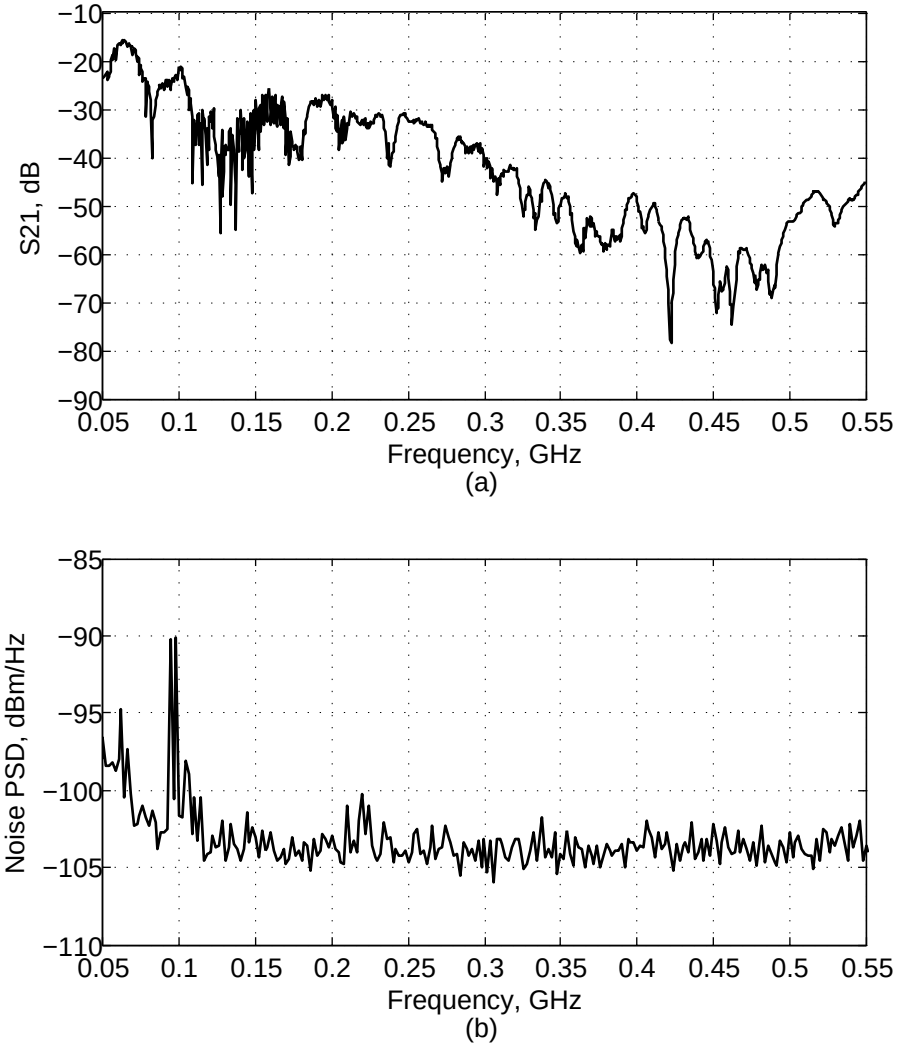

Figure 6.1: Channel response and average noise PSD between outlet pair R1.3A - R1.5A (50MHz - 550MHz).

For comparison purpose, power allocation is also calculated in the frequency range 500MHz - 1GHz, for the R1.3A to R1.5A (10m) channel. The channel transfer function and noise PSD are illustrated in Figure 6.3. With the transmitted power set at 5W, the optimised transmit power and bit allocation are shown in Figure 6.4. Although the noise level is relatively lower, the channel suffers much higher attenuation, this gives very low SNR in some sub-channels. Therefore, these sub-channels are totally shut down and no power is transmitted.

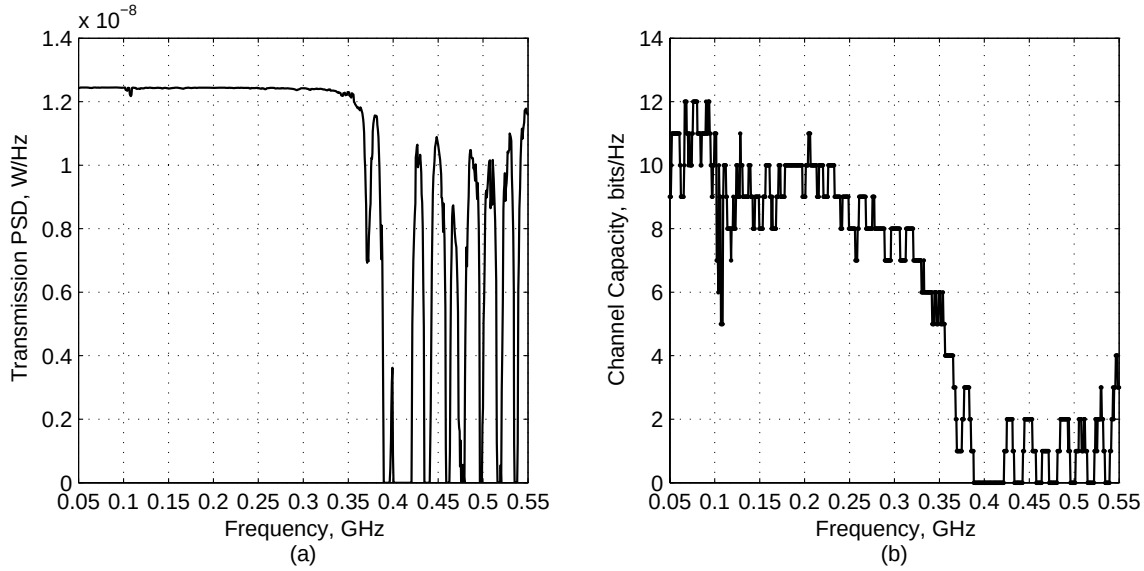

Figure 6.2: Optimized power and bit allocation of a 10m link between R1.3A and R1.5A in 50 - 550MHz range (total transmitted power: 5W).

Using this frequency band, the theoretical data rate is smaller, at 1.1Gbps. Further, the number of information bits transmitted in each sub-channel decreases significantly, hence reducing the channel efficiency. Comparison result once again proves that 50 - 550MHz is the preferred frequency band for potential UWB over PLC applications.

Broadband powerline channel capacity is highly variable to the channel frequency response, network topology, as well as the transmission distance. Different transmission outlet pairs with variable distance will result in different transmission rates. As shown in Figure 6.5, the bit allocation for two transmission paths (R1.3A to R1.2A and R1.3A to R1.6A) can be quite different. The 5m path supports higher data rate because of the smaller channel loss. While in the 15m channel, a number of sub-channels have been turned off[1] due to the low SNR level. According to Figure 6.6, which illustrates the percentage usage of the sub-carriers, the number of sub-channels can be used is related to transmission

[1]A sub-channel is regarded as "off" when no information is transmitted, it is possible that the Tx power is non-zero.

range and power. In order to achieve 50% usage of the sub-channels, the required transmit power is 24dBm for 15m and only 15dBm for 10m transmission.

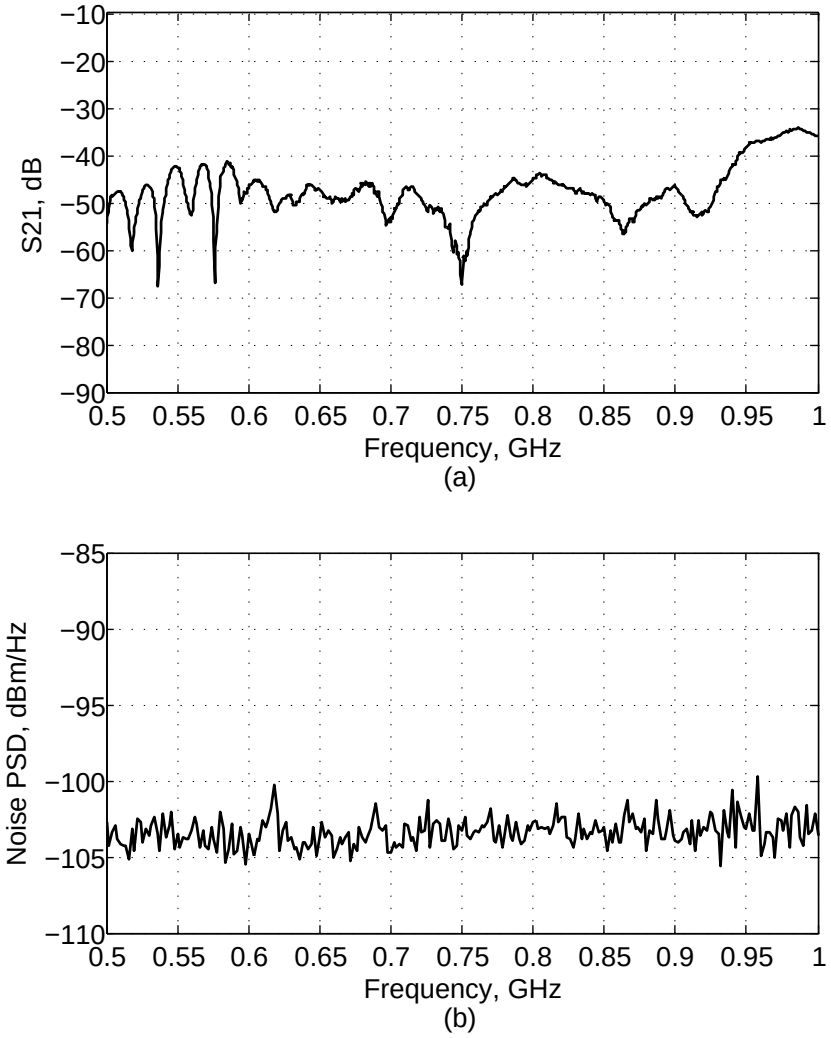

Figure 6.3: Channel response and average noise PSD between outlet pair R1.3A - R1.5A (500MHz - 1GHz).

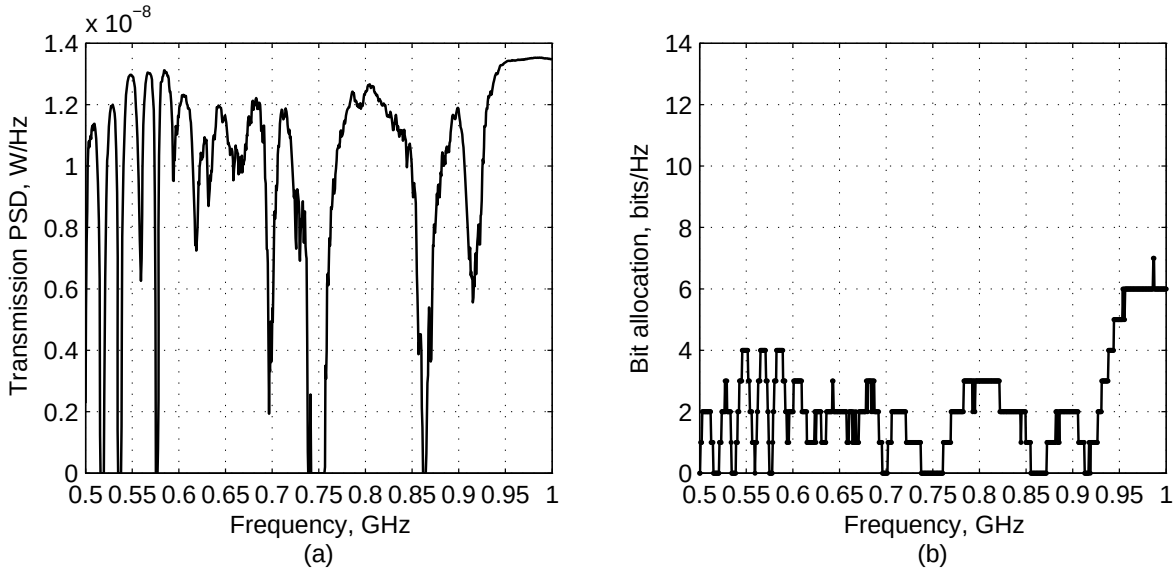

Figure 6.4: Optimized power and bit allocation of a 10m link between R1.3A and R1.5A in 550MHz - 1GHz range (total transmitted power: 5W).

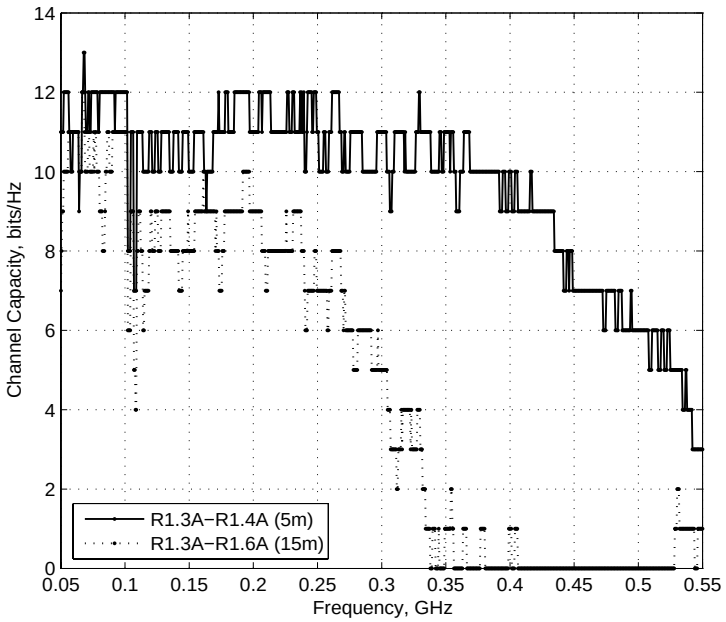

Figure 6.5: Comparison of bit allocation of two different transmission paths: 5m and 15m in 50 - 550MHz frequency range (total transmitted power: 5W).

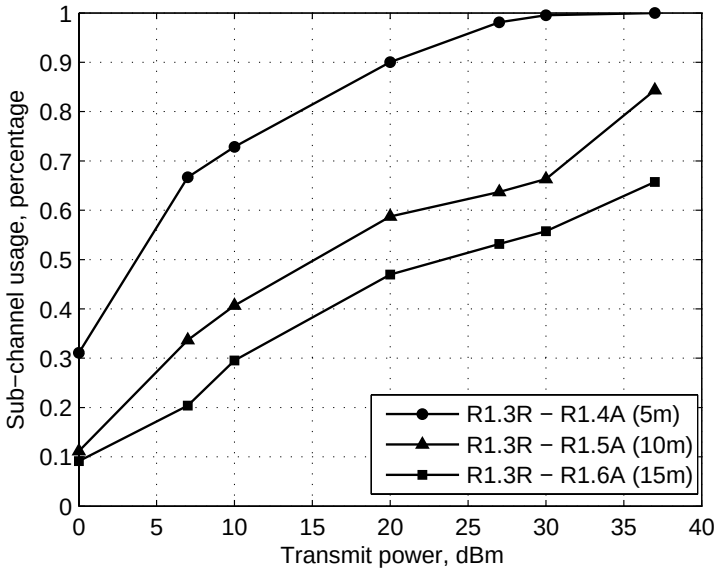

Figure 6.6: Percentage usage of the sub-channels vs. transmit power.

Table 6.2 compares the channel capacity for different transmission paths in Ring 1, under the background noise environment. Very high channel capacity can be obtained over the studied channels, especially when no electrical loads are connected. Even when electrical loads are connected to the path, the available capacity is still very high, all the channels can achieve 1Gbps capacity at 27dBm transmit power.

It can be concluded that the indoor powerline channel has high potential for fast speed data transmissions, in the 50 - 550MHz band. Nevertheless, the transmission rate is closely related to the available power and thus the electromagnetic interference (EMI) to other radio systems. In this case, the proposed UWB over PLC technology occupies 500MHz bandwidth, so the transmitted PSD is very low because total power is spread into a wide frequency band, thus reducing potential EMI. Further, EMI can also be avoided by notching out specific frequencies where existing radio systems are operating.

Total Transmit Power (dBm)	10 (10mW)	20 (100mW)	27 (500mW)	30 (1W)	37 (5W)
5m without loads	1.17	2.66	3.78	4.28	5.47
5m with hair dryer	0.59	1.68	2.67	3.12	4.21
5m with mobile charger	0.70	1.69	2.59	3.02	4.07
5m with both appliances	0.51	1.40	2.30	2.73	3.83
10m without loads	0.55	1.38	2.06	2.39	3.26
10m with hair dryer	0.28	0.88	1.52	1.83	2.64
10m with mobile charger	0.33	0.98	1.60	1.90	2.74
10m with both appliances	0.25	0.80	1.37	1.67	2.49
15m without loads	0.36	0.99	1.57	1.84	2.52
15m with hair dryer	0.19	0.63	1.10	1.34	2.01
15m with mobile charger	0.22	0.68	1.19	1.43	2.11
15m with both appliances	0.18	0.56	1.01	1.24	1.89

Table 6.2: Channel Capacities at different transmission paths and distance (same circuit ring), Gbps.

6.3 Multiband-OFDM Model for PLC

In the previous section, high channel capacity of the indoor powerline channel has been proven possible in 50 - 550MHz range. However, it is very difficult to achieve the maximum transmission rate in practice. A number of factors such as the transmit power, modulation scheme and noise will affect the system transmission rate. Therefore, a system level model is required to predict the transmission rate and the related system performance.

6.3.1 MB-OFDM Physical Layer Specification

Operating in the 50 - 550MHz frequency band, potential UWB over PLC application satisfies the bandwidth requirement of the Multiband-OFDM UWB proposal, which is submitted to the IEEE 802.15.3a WPAN standards group in September 2003 [117].

As defined by FCC regulations, UWB is a wideband signal that occupies more than 500MHz or has a fractional bandwidth of at least 20% [66]. To achieve such broadband signal transmission, MB-OFDM UWB radio divides the 3.1 - 10.6GHz

band into 14 sub-bands, each occupying 528MHz. As illustrated in Figure 2.8 in Chapter 2, the first 12 sub-bands are grouped into four band groups, while the last two are grouped into the fifth band group. Currently, only Band Group 1 is mandatory for UWB communications.

In each 528MHz sub-band, MB-OFDM UWB standard defines mandatory data rates of 53.3, 106.67, 110 and 200Mbps in the PHY. Figure 6.7 shows the transmission front end of a MB-OFDM system. The source data is encoded using convolutional coding at different code rates, according to the system data rate required. The coded data is interleaved to allow recovery from impulsive noise. After serial to parallel data conversion, quadrature phase shift key (QPSK) constellation map is used to map the data groups into complex signals. IFFT operation is performed on the complex signals to form an OFDM symbol, with cyclic prefix and guard interval added to it. The transmitted signal is then converted back into serial sequence and is ready for transmission, it will be hopping in the three sub-bands in Band Group 1 [118]. In the receiving end, reverse of the transmission operation is performed to recover information data. Details of the MB-OFDM PHY are given in Appendix B.

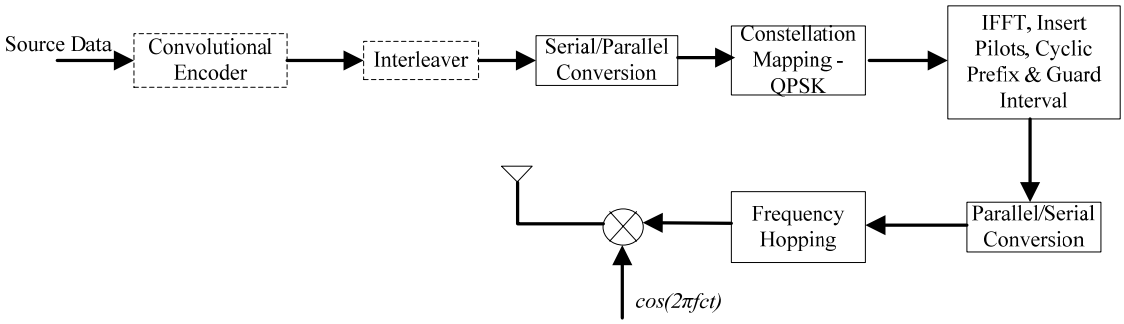

Figure 6.7: Transmission front end for an MB-OFDM UWB system.

Similar to other OFDM systems, UWB uses OFDM to mitigate the effects of multipath. Parameters of the OFDM symbol in MB-OFDM standard are given in Table 6.3. The OFDM modulator is implemented using a 128 point IFFT in 528MHz frequency band, with 122 active sub-carriers. There are 100 data carriers (each carries 2 bits of data using QPSK), 12 pilots and 10 guard sub-carriers. The

remaining 5 high frequency taps and the DC tap are set to zero, creating a time domain sequence of 242.42ns. After the IFFT, a 32 length zero-padded prefix (60.61ns in time) is added to the beginning and a 5 length zero-padded guard suffix (equating to 9.47ns) is added to the end of the IFFT output, creating a 165 sample time domain sequence of 312.5ns [119, 120]. For mandatory data rates below 200Mbps, a time-domain spreading operation is performed with a spreading factor of 2. That is, the same information is transmitted over two OFDM symbols.

Parameter	**Value**
Total Bandwidth, B	528MHz
Number of IFFT points, N	128
Sub-carrier frequency spacing, Δf	4.125MHz(=B/N)
Time period for each sub-carrier, T_{sub}	1.89ns(=$1/B$)
Number of data sub-carriers, N_{SD}	100
Number of defined pilot sub-carriers, N_{SDP}	12
Number of guard sub-carriers, N_{SG}	10
Number of total sub-carriers used, N_{ST}	122(=N_{SD}+N_{SDP}+N_{SG})
IFFT/FFT period, T_{FFT}	242.42ns(=$1/\Delta f$)
Cyclic prefix duration, T_{CP}	60.61ns
Guard interval duration, T_{GI}	9.47ns
MB-OFDM Symbol Duration, T_{SYM}	312.5ns(=T_{FFT}+T_{CP}+T_{GI})

Table 6.3: PHY parameters of MB-OFDM system.

6.3.2 Simulation Model for PLC

In order to perform a system level simulation of OFDM transmission over the powerline channel, we use a modified MB-OFDM model in Matlab Simulink published in [121]. It models the end to end PHY UWB data transmission at 200Mbps. By replacing the standard UWB channel with the powerline channels, it is possible to analyse system performance such as BER of a realistic powerline communication environment.

Figure 6.8 illustrates the modified MB-OFDM transmitter and receiver system model in Matlab Simulink. The source data are encoded using convolution coding

and interleaved before being sent to the OFDM transmitter. Frequency hopping is disabled so the simulation is in baseband. The time domain signal is up sampled by a rate of 6, therefore the system sample rate is one sixth of the sub-carrier time period, $T_{SYM}/(165 \times 6) = 0.315ns$. Further, the transmission channel has been replaced by the Channel Impulse Response (CIR) of the measured powerline channel, in 50 - 550MHz range.

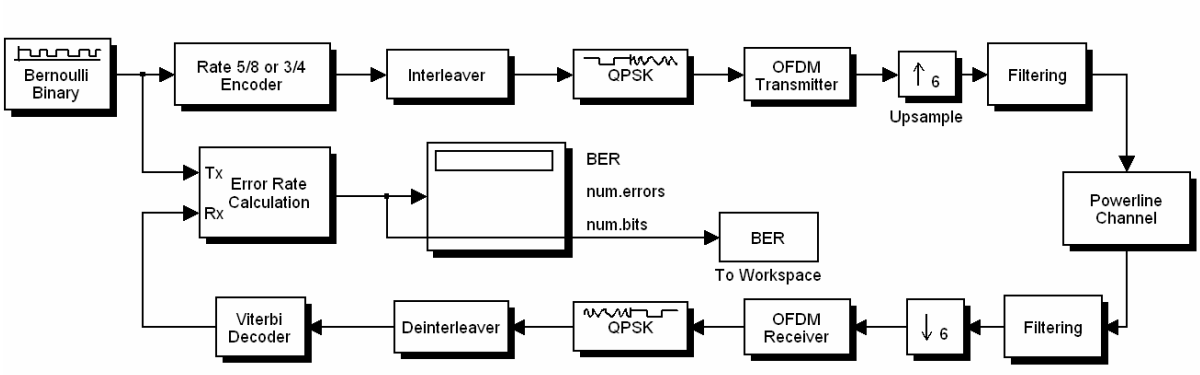

Figure 6.8: PHY Channel model for MB-OFDM UWB over Powerline.

It is shown in Chapter 5 that the frequency responses of the powerline system have been recorded using a VNA. Therefore, the CIR for system level model can be calculated using IFFT. The time steps of the CIR is fixed according to the sampling frequencies in the measurement, where $\Delta f = 593.75kHz$. In order to obtain the same sampling rate as the MB-OFDM system model, the time domain transfer function of the powerline channel is interpolated to conform with the sampling time of the simulator, $\Delta t = 0.315ns$. Further, the pass-band CIR is transformed into the base-band, this is done by:

$$h_{base-band}[t_n] = h_{pass-band}[t_n] * exp(j2\pi f_c t_n), \tag{6.7}$$

where $f_c = 314MHz$ is the center frequency of the measured powerline channel transfer function, and $h_{base-band}[t_n]$ and $h_{pass-band}[t_n]$ are the time domain CIR in base-band and pass-band respectively. $t_n = n\Delta t$ is the time samples defined in the model. Equation (6.7) shifts the CIR from f_c to base-band, this can be explained

in the frequency domain. Assume $H_{base-band}(f)$ and $H_{pass-band}(f)$ represents the frequency response of the powerline channel in base-band and pass-band,

$$H_{base-band}(f) = H_{pass-band}(f - f_c). \tag{6.8}$$

The right part of (6.8) can be converted to the time domain using fourier transform [122],

$$H_{pass-band}(f - f_c) \Longrightarrow h_{pass-band}[t] * exp(j2\pi f_c t), \tag{6.9}$$

thus relating the base-band CIR to its pass-band counter part. Figure 6.9 illustrates the calculated time domain CIR of different powerline channels in the test bed.

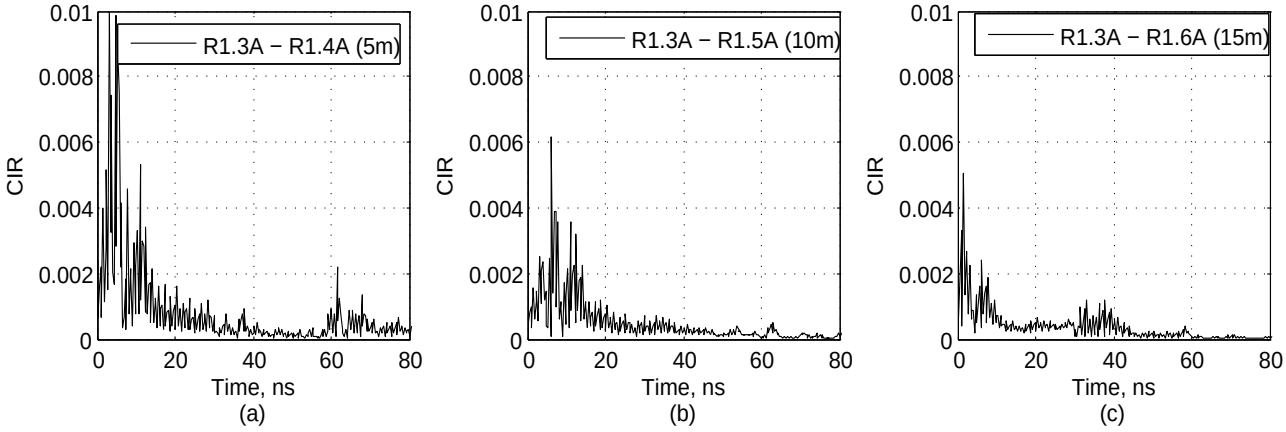

Figure 6.9: Normalised CIR of powerline channel.

By inputting the powerline channels' CIR into the Matlab simulation model, the system compares the transmitted and received data to calculate BER, given a specific value of the E_b/N_0. Two transmission rates have been simulated in this study, at 200Mbps and 240Mbps. This is achieved by varying the number of information bits transmitted per OFDM symbol and the convolutional encoding rates. The convolutional coding has a basic rate of 1/3 and the constrain length of 7 is used for FEC. Further code rates of 5/8 and 3/4 are achieved through bit puncturing. Table 6.4 gives the detailed information on data rate, modulation and coding rate of the two PHY transmission mode.

For example, at 200Mbps transmission rate, 125 bits of information is sent to the 5/8 convolutional encoder, generating 200 bits of data. After QPSK, 100 complex data is obtained and passed on to the OFDM transmitter, occupying the 100 data carriers. Other auxiliary information is also added to the OFDM symbol, to form a 165 sample time symbol in time domain. The same information data is transmitted on 2 OFDM symbols, as the time spreading gain is 2. This gives the system data rate of $(125bit/312.5ns) \times (1/2) = 200Mbps$.

Data rate (Mbps)	Modulation	Code Rate	Spreading Gain	OFDM Symbol Time (ns)	Coded bits per OFDM Symbol	Info bits per OFDM Symbol
200	QPSK	5/8	2	312.5	200	125
240	QPSK	3/4	2	312.5	200	150

Table 6.4: Rate dependent parameters of MB-OFDM model.

6.4 Performance Analysis

6.4.1 BER Performance

As a measure of performance the BER variation versus different E_b/N_0 value under the measured powerline channel is simulated, using the modified MB-OFDM model. The simulation stops when either of the following criterion is met: there are in total 1 million number of information bits have been transmitted or the number of error bits received has reached 100.

Firstly, the BER performance under background noise is simulated, with no electrical loads connected to the powerline channel. As shown in Figure 6.10 (a), all the simulated channels can achieve very low transmission error rates up to 10^{-5} at 200Mbps, under 30dB E_b/N_0 level. System performance degrades on longer transmission range and higher data rate. At higher system data rate of 240Mbps, good BER performance lower than 10^{-4} can still be obtained.

When electrical loads are connected to the transmission channel, system performance degrades accordingly. Figures 6.11 - 6.13 compare the BER performance

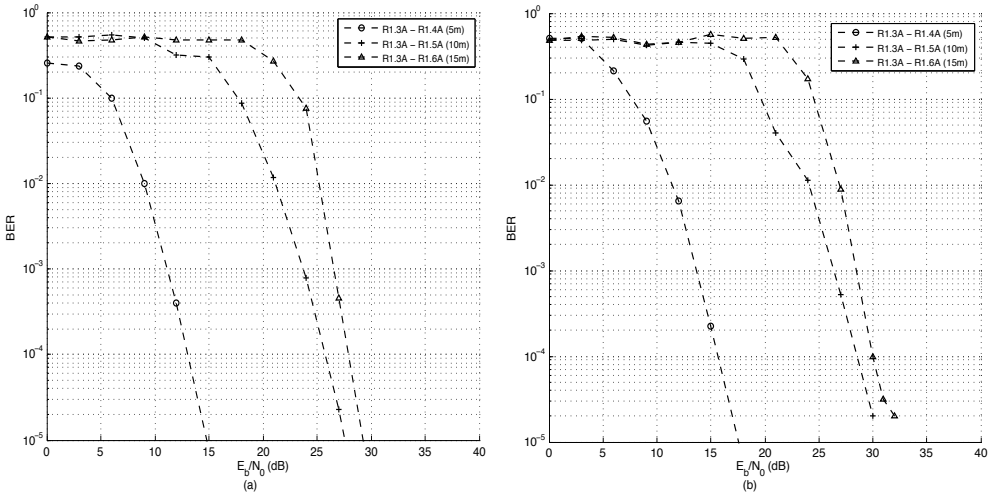

Figure 6.10: BER vs. E_b/N_0 for three different powerline channels in the test bed at (a) 200Mbps and (b) 240Mbps.

of three typical transmission distances (i.e. 5m, 10m and 15m) under different scenarios, such as connecting a hair dryer or a mobile charger to the channel. It can be seen that the connected appliances can introduce more transmission errors to the system, as they bring in more multi-path transmissions to the original channel.

The worst transmission occurs when both of the hair dryer and the mobile charger are connected and switched on, since the interference from both appliances are added to the channel. This agrees with previous results shown in Table 5.5, that the highest channel attenuation happens when both of the electrical loads are connected. It is also noticed that charging the mobile phone can cause more deteriorating effect to the system than using the hair dryer. Therefore, in order to achieve the best transmission over an indoor powerline channel, it is better to avoid connecting electrical appliances like mobile charger between the Tx and Rx. In general, transmission channels with electrical loads require up to 10dB more energy to achieve the same BER performance as those without loads.

From the simulation results, BER performance lower than 10^{-4} can still be obtained over the powerline channels studied, at 40dB E_b/N_0 level. This has greatly improved the performance of existing broadband PLC technology. It has

been shown by Guerrini in [123] that, up to 70dB SNR is required for HomePlug AV system to provide raw data rate of 189Mbps (BER target at 10^{-3}) in the powerline channel, under AWGN and narrow band interference. While in the MB-OFDM model, the data rate is much higher and the SNR has been reduced up to 30dB, under the same noise condition. It indicates that the proposed UWB over PLC technology has high potential in providing fast speed transmission in the home network. Moreover, such system performance can be further improved by adaptive modulation schemes or advanced information coding, in which a lot of active researches are being done [124, 125, 126, 127].

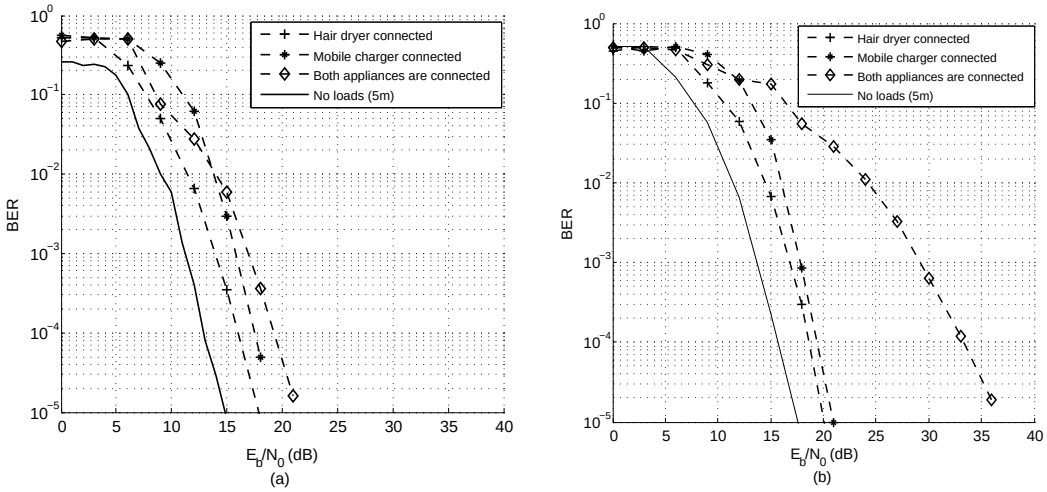

Figure 6.11: BER vs. E_b/N_0 for 5m with electrical appliances connected, (a) 200Mbps and (b) 240Mbps.

6.4.2 Transmit Power Level

The total transmit power from the powerline system can also be estimated to see how much energy is required. Given the value of E_b/N_0 and the PSD of background noise N_0, the average energy per bit E_b is available. The total received power P_{rx} is:

$$P_{rx} = E_b \cdot R, \tag{6.10}$$

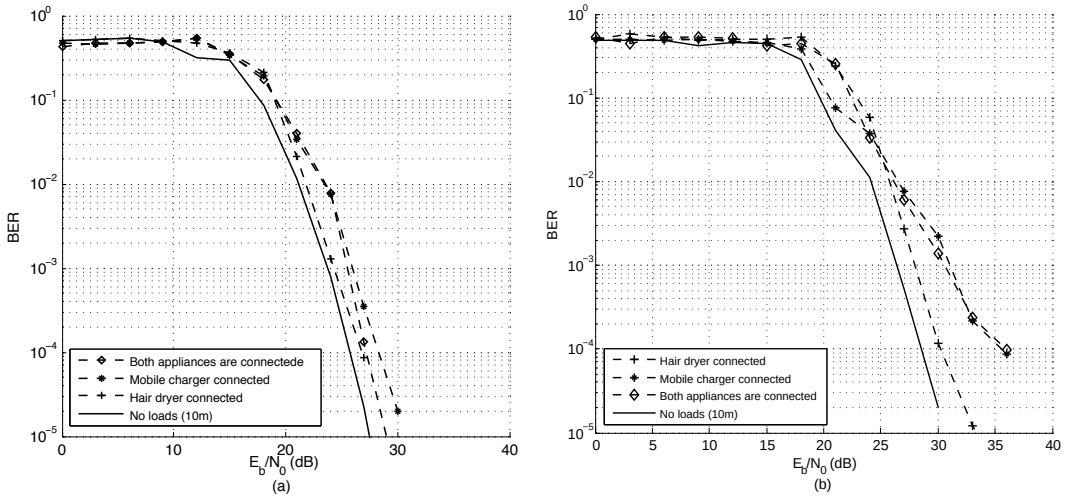

Figure 6.12: BER vs. E_b/N_0 for path 10m with electrical appliances connected, (a) 200Mbps and (b) 240Mbps.

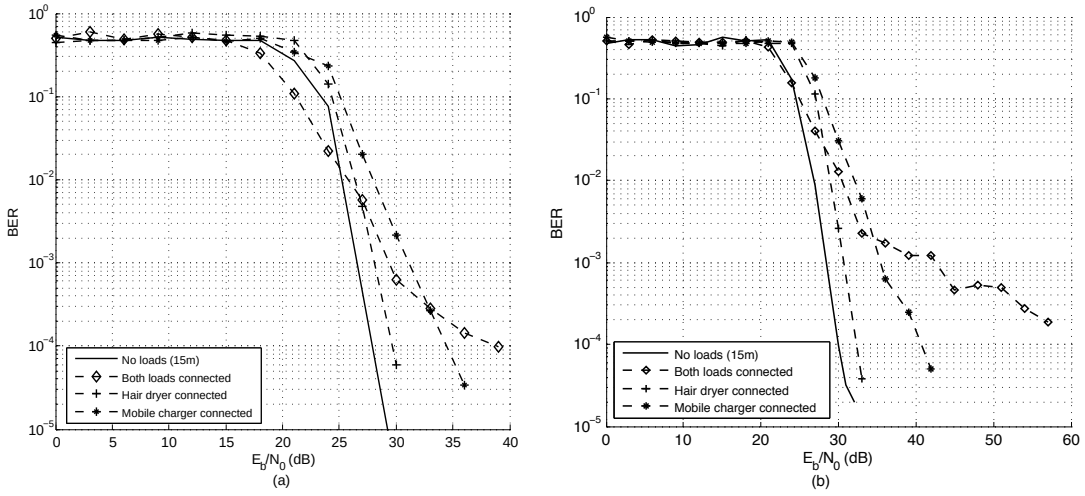

Figure 6.13: BER vs. E_b/N_0 for 15m with electrical appliances connected, (a) 200Mbps and (b) 240Mbps.

where R is the system data rate, which is 200Mbps or 240Mbps in this model. The total transmitted power P_{tx} can be estimated using:

$$P_{rx} = \int_W |S_{21}(f)|^2 P_{tx}(f) df, \tag{6.11}$$

where $S_{21}(f)$ is the transfer function of the channel and W is the system bandwidth. Assuming the transmit power is the same across different frequencies, P_{tx} is:

$$P_{tx} = \frac{P_{rx} W}{\int_W |S_{21}(f)|^2 df}. \tag{6.12}$$

It can be seen that the total transmit power is related to channel loss, system data rate and noise level. Take for example the 10m channel, the E_b/N_0 value is 25.5dB (for 10^{-4} BER at 200Mbps), the total transmit power is:

$$P_{tx} = 25.5dB + N_0(dBm) + R(dB) - |S_{21}|^2_{average}(dB). \tag{6.13}$$

Where the measured background noise is -102.34dBm/Hz as given in Table 6.1, and the average channel attenuation is the measured transfer function as listed in Table 5.4, at 27.88dB. This gives the total transmit power at 34.04dBm or -52.96dBm/Hz, as the operating bandwidth is 528MHz.

Table 6.5 lists the simulated energy per bit-to-noise ratio and PSD required to achieve BER performance better than 10^{-4} on the powerline transmission system. The best case occurs when the powerline channel is not subject to interference from other electrical loads, whilst most of the worst cases happen when both of the loads are connected to the channel. The transmitted signal PSD varies from -70dBm/Hz to the worst case scenario of -13dBm/Hz, when 240Mbps data rate is transmitted over a 15m channel with both of the electrical loads switched on. If the PSD threshold is set at -40dBm/Hz, we can allow over 80% of the studied powerline channels to operate under the BER constraint. It can be seen that longer transmission distance and higher data rates always require more power to boost up the SNR level and the transmitted PSD.

The BER performance analysis presented above is targeted for very high bit rate transmission over indoor powerline channels, over 200Mbps. The maximum data rate available in the market place is only up to 200Mbps, which already uses advanced coding and modulation schemes, i.e. 1024QAM and bit loading

Distance	Data Rate (Mbps)	Best Case		Worst Case	
		$E_b/N_0(dB)$	PSD (dBm/Hz)	$E_b/N_0(dB)$	PSD (dBm/Hz)
5m	200	13	-72.21	19.5	-65.71
	240	15.5	-69.71	33	-52.21
10m	200	25.5	-52.96	28	-50.46
	240	28	-48.46	36	-40.46
15m	200	28	-45.89	39	-34.89
	240	30	-43.89	60	-13.89

Table 6.5: Transmit power and PSD of powerline system, BER level: 10^{-4}.

are exploited for 200Mbps Homeplug AV [16]. There is very limited space for existing technology to up grade their system data rates, because the available operating bandwidth sets an upper limit to the channel capacity. In the proposed PHY model for broadband PLC, QPSK constellation map is used to provide good BER performance at high data rates that existing techniques struggle to achieve. Much higher data rates can be obtained if higher constellation maps and adaptive bit loading algorithms were used, which can also improve the system transmission performance. Therefore, the potential data rate for UWB over Powerline Communication is very high and thus the demand for future applications can be met.

6.5 Summary

Theoretical channel capacity and system level performance of the measured powerline channel in the test bed have been analysed and simulated in this chapter, under background noise disturbance. Link budget analysis reveals that 50 - 550MHz frequency range gives a good SNR for data transmission, because in this band, channel attenuation is smaller than that in high frequency ranges, and the background noise is also very low. Thus, very high channel capacity up to Gigabits per second can be achieved in theory, by optimising the allocation of transmitted power and the number of bits per carrier.

However, the theoretical data rate is very difficult to obtain due to the limitations in practice. Therefore, we also conduct system level simulation of data transmission, to predict the transmission rate and its performance. The PHY model used for this study is the MB-OFDM UWB proposal submitted to the IEEE 802.15.3a standard group. By using the modified MB-OFDM simulator in Matlab Simulink, different transmission paths over the indoor powerline network have been modeled. The BER performance versus energy per bit-to-noise ratio shows promising outlook for UWB over PLC to deliver high data rate services in a home network. Different transmission distances have been analysed at two transmission rates, namely 200Mbps and 240Mbps, both under normal background noise environment and under the interference from other electrical appliances.

The transmit power and signal PSD are analysed based on the simulated and measured results. The transmitted PSD is dependent on the system data rate, noise level and transmission distance. It is shown that BER performance better than 10^{-4} can be achieved at power level as low as -40dBm/Hz, for high data rate transmission up to 240Mbps. Improvements on the PHY model can be done in the future to increase the data rate and better the BER performance by advanced data modulation and coding.

Chapter 7

Conclusions and future work

7.1 Summary

Data transmission over powerline has become increasingly popular recently, because of its ability to provide in-home networking and internet access to customers. By exploiting the ubiquitous mains network, it makes laying expensive cables a thing of the past. At the same time, UWB communication emerges as a renewed technology that is capable of providing fast speed wireless transmission for consumer electronic devices in a short range. Current studies on UWB are related to wireless communication, wired UWB communication also starts to attract attention. A few projects have been carried out on transmitting UWB signal over coaxial cables, UWB over powerline has also been looked into below 100MHz, in order to increase the data rate. However, limited research has been done to exploit higher frequency band (>100MHz) UWB transmission over the mains cable. Therefore, a novel study of UWB transmission over powerline to achieve gigabits per second data rate is carried out in this thesis.

One of the most important aspects of this research is the characterisation of powerline channel in the high frequency band, while the majority of existing studies only try to understand the channel characteristics below 30MHz. Therefore, in this thesis, signal transmission over indoor mains cables in ultrawide-band has been studied. Based on the simulation and measurement results, it is noticed that the indoor powerline cable, namely the 2.5mm flat twin and earth provides

a suitable transmission channel in frequency band below 1GHz, as the signal degrades at a rate of $0.26dB/(m \cdot 100MHz)$ in the proposed frequency band.

As a result, a wideband RF coupler working in 50MHz - 1GHz frequency range is required to couple the transmitted signal to the powerline. The challenges of coupler design lie in the wide frequency band, bi-directional signal coupling and minimum insertion loss to the system. Moreover, existing powerline couplers are only designed for narrowband use, below 30MHz. It is noted that couplers used in PLC below 30MHz consists of a number of passive components, such as transformers and filters. Therefore, the newly developed coupler is built on a coupling circuit, by using a broadband RF transformer and a pair of $100pF$ safety capacitors. Eventually, much wider bandwidth has been achieved by the developed RF coupler, from 50MHz to 1GHz.

With the key components, a measurement campaign on a powerline network test bed simulating the UK in-home powerline environment has been conducted. The test bed is thoroughly tested to understand the signal transmission characteristics in both frequency and time domain, as well as under the interference from household appliances. It is shown that the powerline channel is more robust to interference generated from electrical appliances in the higher frequency range. Analysis of background noise also show that frequency range above 100MHz provides a more benign environment with less narrow band interference to the system. Such results have been enhanced by the radiated emission measurements. It is proven that radiation generated by a signal powerline circuit is below the field strength limits set by standard organisations such as the FCC, meaning that the electromagnetic disturbance caused by PLC systems will not degrade the performance of existing radio systems. On the other side, studies of the impulsive noise generated by switching events show that impulsive disturbance still presents a challenge for potential UWB PLC applications, as it may raise the system noise floor.

Statistical analysis of the channel loss reveals that the frequency band 50 - 550MHz is a better transmission path for UWB PLC. Evaluations of key system parameters - SNR under background noise and channel capacity show that sufficient link budget can be obtained in this band for gigabit per second data

transmission. Since the proposed frequency band for UWB over PLC technology is 500MHz, it satisfies with the bandwidth requirement for MB-OFDM proposal. Therefore, system level data transmission has been analysed in the PHY, by applying the MB-OFDM UWB standard. Different transmission rates above 200Mbps have been simulated with regards to BER performance verse E_b/N_0. Results showed that higher than existing available bit rates can be achieved by potential UWB over PLC applications, with the transmitted PSD level as low as -40dBm/Hz.

7.2 Key Contributions

The main contributions in this thesis are detailed in the four sections below:

- ***Characterisation of Powerline for UWB Transmission in 0 - 1GHz***
  - Two types of mains cable: 2.5mm flat twin and earth and three-core flexible cable have been studied for UWB transmission in 0 - 10 GHz range. Simulation and measurement results reveal that the properties of powerline channel are not suitable for data transmission above 1GHz, due to high level of attenuation. Nevertheless, it is noted that in frequency band below 1GHz, powerline channels show high potential for in-home applications.
  - 2.5mm flat twin and earth cable provides a better path for transmission in high frequency band, the signal attenuation rate is $0.26dB/(m \cdot 100MHz)$ above 100MHz operating frequency band. Moreover, differential mode signal coupling should be used as it allows more energy to be transmitted and suppresses radiation.
- ***Design and Development of A Broadband RF Coupler***
  - A broadband RF coupler has been designed, it provides insertion loss less than 3dB/coupler in 50MHz - 1GHz frequency range. It provides galvanic isolation between AC power and communication signal, which is transmitted to the powerline system in differential mode.

  - The developed coupler is built on a RF4 PCB board, by using passive components including transformer and capacitors. It has a simple structure for manufacture. Further, it provides unique broadband transmission performance for PLC applications above 30MHz.

- ***Characterisation of Powerline Network Transmission System***

  - A powerline test bed simulating the UK indoor wiring environment has been tested in Queen Mary's Antenna lab. An exhaustive measurement campaign in both frequency and time domain has been carried out. Analyses on channel loss with regards to distance and frequency reveal that same circuit ring transmission in 50 - 550MHz is more suitable for the implementation of UWB over PLC. Further, interferences from other electrical appliances are also evaluated, it is noted that powerline channel is more robust to such interferences in the high frequency range.
  - Measurement of the noise signal confirms that the background noise above 100MHz has less narrow band interference to PLC systems. Whereas the impulsive noise resulted from the switching events will increase the noise floor significantly, especially below 200MHz. Thus, counter measures should be sought to avoid severer transmission errors.
  - Standard emission measurements of a powerline circuit ring show that in very high frequency range of 30MHz - 1GHz, signal radiation caused by a powerline channel is below the emission limits set by FCC Part 15 regulatory standard. The average electrical field generated by the powerline system is below 40dBuV/m.

- ***System Level Simulation of UWB Data Transmission over Powerline Channel***

  - Link budget and SNR have been analysed under coloured background noise environment, it is shown that a 500MHz bandwidth from 50 to

550MHz provides the best link budget for data transmission. Analysis of channel capacity proves that transmission rates up to 1Gbps is highly feasible in the proposed frequency band.

- Very high data rate transmission over the powerline has been proven possible, by applying the PHY standard of MB-OFDM proposal submitted to the IEEE 802.15.3a standard group.
- Transmission rates at 200Mbps and 240Mbps have been simulated over the measured powerline channels. BER performance shows that up to 240Mbps data rate can be transmitted over the indoor powerline channels, even under the interference from other electrical appliances. The required transmission power is also very small, at BER level of 10^{-4}, a transmit PSD level as low as -40dBm/Hz can support high data rate transmission over 80% of the analysed channels.

7.3 Recommendations for Future work

Based on conclusions drawn and the limitations of the work presented, further work can be carried out in the following areas:

- The powerline as a transmission medium has been extensively studied in high frequency band above 30MHz. A channel model has been used to model the powerline network with T-network topoplogy, based on the measured signal attenuation parameters. Development of a complex channel model which can predict the effects of other system components, i.e. sockets and plugs, will improve our understanding of the channel characteristics in high frequency range.
- The impulsive noise will cause more deteriorating effects to the PLC system than background noise. It has time variant properties that its amplitude, duration will change in each switching events. A thorough understanding and modelling of this type of noise will assist system designers to develop suitable DSP techniques for error correction.

- More transmission environments can be tested (i.e. flats, houses, offices and trains) to see signal transmission variations to network topology, appliances connected and different times during the day. This could pave the way for the widespread use of UWB over powerline technology.

- The EMC measurement in this study is the beginning of UWB PLC emission analyses. Radiated emission from PLC systems can be very complicated, which is dependent on many factors including network topology, transmit power, measurement locations, etc. Further investigation on this topic can provide a guideline for future system deployment and regulation establishment.

- In the PHY data transmission model, uniformed modulation scheme is used for each OFDM sub-carrier. Higher data rate can be obtained if more advanced signal processing technique is used. Adaptive modulation and coding such as FEC will also improve the transmission efficiency and system performance.

Appendix A

Scattering Parameters

The scattering matrix, or S-parameters, provide a complete description of the network as seen at its N ports. While the impedance and admittance matrices relate the total voltages and currents at the ports, the scattering matrix relates the voltage waves incident on the ports to those reflected from the ports. The S-parameters can be measured directly with a network analyser [9].

Consider a N-port network as shown in Figure A.1, where V_n^+ is the amplitude of the voltage wave incident on port n, and V_n^- is the amplitude of the voltage wave reflected from port n. The scattering matrix, is defined in relation to these incident and reflected voltage waves as:

$$\begin{pmatrix} V_1^- \\ V_2^- \\ \vdots \\ V_N^- \end{pmatrix} = \begin{pmatrix} S_{11} & S_{12} & \cdots & S_{1N} \\ S_{21} & & & \vdots \\ \vdots & & & \vdots \\ S_{N1} & \cdots & \cdots & S_{NN} \end{pmatrix} \begin{pmatrix} V_1^+ \\ V_2^+ \\ \vdots \\ V_N^+ \end{pmatrix} \tag{A.1}$$

or

$$[V^-] = [S][V^+]. \tag{A.2}$$

A specific element of the $[S]$ matrix can be determined as:

$$S_{ij} = \frac{V_i^-}{V_i^+}|_{V_k^+=0} \quad \text{for} \quad {}_{k \neq j}. \tag{A.3}$$

S_{ij} is found by driving port j with an incident wave of voltage V_j^+, and measuring the reflected wave amplitude, V_i^-, coming out of port i. The incident

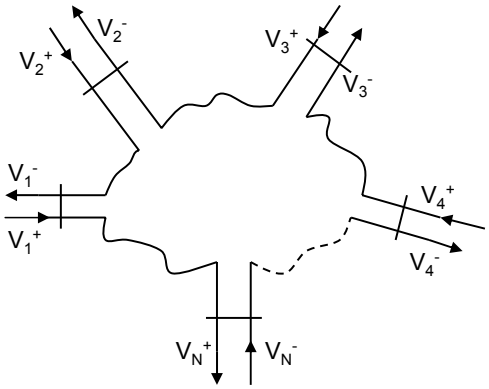

Figure A.1: An arbitrary N-port network (Reproduced from [9]).

waves on all other ports are set to zero, which means that all ports should be terminated in matched loads to avoid reflections. Thus, S_{ii} is the reflection coefficient seen looking into port i when all other ports are terminated in matched loads, and S_{ij} is the transmission coefficient from port j to i when all other ports are terminated with matched loads.

The powerline channel can be regarded as a two port network whose S-parameters can be measured using a network analyser.

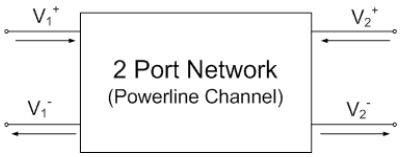

Figure A.2: Illustration of a two port network S-parameters.

From Figure A.2, S_{11} can be found as the reflection coefficient seen at port 1 when no signal is transmitted from port 2:

$$S_{11} = \frac{V_1^-}{V_1^+}\Big|_{V_2^+=0}. \tag{A.4}$$

While S_{21} can be found by applying an incident wave at port 1, V_1^+ and measuring the out-coming wave at port 2, V_2^-. This is equivalent to the transmission

coefficient from port 1 to port 2.

$$S_{21} = \frac{V_2^-}{V_1^+}\Big|_{V_2^+=0}. \tag{A.5}$$

S parameters magnitudes are presented in one of two ways, linear magnitude or decibels (dB). Because S-parameters are a voltage ratio, the formula for decibels in this case is:

$$S_{ij}(dB) = 20 \times log[S_{ij}(\text{magnitude})]. \tag{A.6}$$

Appendix B

Powerline Test Bed Attenuation

B.1 Mathematical Background for Statistical Analysis of Powerline Characteristics

- Average Attenuation

  Assume the attenuation between two outlet pairs is a vector data, i.e. $A_1, A_2, \cdots, A_N$, where $A_i = |H(\omega)|^2$ at frequencies $f_1, f_2, \cdots, f_N$, the average attenuation is defined as [95, 128]:

$$A_{ave} = \frac{1}{N} \sum_{i=1}^{N} A_i. \tag{B.1}$$

  Where A_{ave} and A_i are real value data. The average attenuation in dB is:

$$A_{ave}(dB) = 20 * log_{10}(A_{ave}). \tag{B.2}$$

- The standard deviation is defined as:

$$\sigma = \sqrt{\frac{1}{N-1} \sum_{i=1}^{N} [A_i(dB) - A_{ave}(dB)]^2} \tag{B.3}$$

B.2 Measured Attenuation Between Outlet Pairs in Ring 1 - Same Ring Transmission (50MHz - 1GHz)

Outlet Pairs		Attenuation in dB			
Name	Length (m)	Max	Min	Average	Std Dev
1A-1B	0	30.63	6.46	12.64	6.16
1A-2A	5	56.81	12.26	26.85	10.90
1A-2B	5	72.17	12.30	26.91	11.42
1A-3A	10	92.32	13.43	32.86	13.32
1A-3B	10	72.70	13.39	32.65	12.27
1A-4A	15	82.77	15.95	37.19	12.97
1A-4B	15	96.70	15.90	36.80	12.46
1A-5A	15	83.53	15.81	38.70	12.60
1A-5B	15	87.32	15.53	38.65	13.66
1A-6A	10	80.02	15.83	35.45	12.76
1A-6B	10	93.61	15.75	35.44	14.45
1B-1A	0	28.93	6.60	12.88	6.26
1B-2A	5	61.77	12.39	26.95	10.77
1B-2B	5	53.22	12.34	26.54	9.05
1B-3A	10	80.87	13.83	32.69	12.28
1B-3B	10	74.53	13.38	32.62	12.07
1B-4A	15	82.30	16.50	37.14	12.47
1B-4B	15	86.23	16.29	37.04	13.46
1B-5A	15	79.63	15.99	38.54	12.34
1B-5B	15	80.23	15.72	38.13	11.96
1B-6A	10	82.74	16.03	35.39	13.49
1B-6B	10	79.90	15.83	35.20	13.79
2A-1A	5	60.72	12.01	26.72	11.10
2A-1B	5	63.15	11.81	26.51	9.95
2A-2B	0	26.40	6.65	12.45	4.98
2A-3A	5	72.25	11.12	24.55	9.69
2A-3B	5	54.18	11.55	24.97	9.60
2A-4A	10	72.02	13.81	31.62	12.57
2A-4B	10	86.06	13.55	31.56	13.11
2A-5A	15	75.79	14.85	37.02	12.16
2A-5B	15	72.18	14.70	36.59	12.09
2A-6A	15	84.12	17.18	38.32	12.37
2A-6B	15	86.63	16.95	38.22	12.39

Table B.1: Attenuation of outlet pairs in the same circuit ring: Ring 1(1A-1B represents the location of Tx/Rx in a circuit ring in Figure 5.1).

Outlet Pairs		Attenuation in dB			
Name	Length (m)	Max	Min	Average	Std Dev
2B-1A	5	73.79	11.90	26.79	11.61
2B-1B	5	62.10	11.67	26.29	9.69
2B-2A	0	29.23	7.10	12.77	5.80
2B-3A	5	69.65	11.86	24.70	9.81
2B-3B	5	74.67	11.63	25.60	10.55
2B-4A	10	81.36	14.36	31.80	13.29
2B-4B	10	77.89	14.11	31.67	13.19
2B-5A	15	82.90	14.94	36.96	12.30
2B-5B	15	78.07	14.75	36.02	11.18
2B-6A	15	75.26	17.29	38.10	12.29
2B-6B	15	89.36	17.16	37.97	11.97
3A-1A	10	76.43	14.02	32.55	11.58
3A-1B	10	72.91	13.75	32.44	13.15
3A-2A	5	53.52	10.94	24.32	9.67
3A-2B	5	45.70	11.06	24.21	8.13
3A-3B	0	26.36	6.67	12.76	5.64
3A-4A	5	88.78	10.89	25.52	12.91
3A-4B	5	55.13	10.93	25.42	10.55
3A-5A	10	84.86	13.47	32.46	12.33
3A-5B	10	74.33	12.90	32.36	12.73
3A-6A	15	85.52	15.16	36.23	13.86
3A-6B	15	83.05	15.01	36.21	13.42
3B-1A	10	82.93	13.96	32.75	12.27
3B-1B	10	71.68	13.66	32.26	12.04
3B-2A	5	59.08	11.17	24.96	10.90
3B-2B	5	61.80	11.28	25.03	9.65
3B-3A	0	28.73	7.07	12.99	6.14
3B-4A	5	54.00	11.16	25.47	11.07
3B-4B	5	65.11	11.16	25.14	10.84
3B-5A	10	85.32	13.34	32.54	12.66
3B-5B	10	79.82	12.80	32.27	12.64
3B-6A	15	80.78	15.24	36.39	13.86
3B-6B	15	78.15	15.02	36.04	13.15

Table B.2: Attenuation of outlet pairs in the same circuit ring: Ring 1 (continue).

Outlet Pairs		Attenuation in dB			
Name	Length (m)	Max	Min	Average	Std Dev
4A-1A	15	84.09	15.07	36.71	11.51
4A-1B	15	78.28	14.74	36.13	11.62
4A-2A	10	83.22	13.29	31.19	12.57
4A-2B	10	72.13	13.26	31.31	11.81
4A-3A	5	74.88	10.77	25.54	13.32
4A-3B	5	63.95	11.17	25.07	10.48
4A-4B	0	23.35	6.20	12.08	4.70
4A-5A	5	67.09	11.49	25.70	9.66
4A-5B	5	53.58	11.17	25.67	9.05
4A-6A	10	68.17	12.69	32.25	11.77
4A-6B	10	78.25	12.44	32.29	12.30
4B-1A	15	91.46	15.27	37.21	13.58
4B-1B	15	93.60	15.06	36.63	13.14
4B-2A	10	76.16	13.42	31.40	12.97
4B-2B	10	90.40	13.40	31.36	12.53
4B-3A	5	53.12	10.90	25.57	11.05
4B-3B	5	58.48	11.31	24.95	9.51
4B-4A	0	29.97	6.83	12.39	5.01
4B-5A	5	78.51	11.53	25.67	9.50
4B-5B	5	89.08	11.16	26.10	10.33
4B-6A	10	75.55	12.79	32.03	12.08
4B-6B	10	78.03	12.40	31.88	12.04
5A-1A	15	82.13	14.94	38.17	12.81
5A-1B	15	81.98	15.00	38.00	12.62
5A-2A	15	82.42	14.84	36.79	12.98
5A-2B	15	89.77	14.85	36.64	12.78
5A-3A	10	74.26	13.88	32.37	12.26
5A-3B	10	78.21	13.52	32.16	12.45
5A-4A	5	74.66	11.68	25.50	9.78
5A-4B	5	67.67	11.78	25.33	9.59
5A-5B	0	29.03	6.14	11.91	5.76
5A-6A	5	70.31	11.38	24.82	10.02
5A-6B	5	72.28	11.59	25.06	9.69

Table B.3: Attenuation of outlet pairs in the same circuit ring: Ring 1 (continue).

Outlet Pairs		Attenuation in dB			
Name	Length (m)	Max	Min	Average	Std Dev
5B-1A	15	90.76	15.07	38.43	13.81
5B-1B	15	96.93	14.96	37.94	12.86
5B-2A	15	101.41	14.76	36.76	13.96
5B-2B	15	91.11	14.64	36.64	13.83
5B-3A	10	82.57	13.72	32.80	13.75
5B-3B	10	90.21	13.53	32.13	13.59
5B-4A	5	56.39	12.32	25.47	9.10
5B-4B	5	59.82	12.39	25.89	10.29
5B-5A	0	33.97	6.39	12.14	6.35
5B-6A	5	65.24	11.51	24.59	8.59
5B-6B	5	75.29	11.62	24.89	9.01
6A-1A	10	113.79	14.90	35.19	14.34
6A-1B	10	85.54	14.84	35.00	13.94
6A-2A	15	86.76	16.55	38.48	12.41
6A-2B	15	80.39	16.33	38.39	12.60
6A-3A	15	87.67	15.00	36.64	13.26
6A-3B	15	79.88	14.72	36.20	12.34
6A-4A	10	72.27	13.79	32.46	12.56
6A-4B	10	77.71	13.62	32.02	12.17
6A-5A	5	79.20	12.21	25.10	10.60
6A-5B	5	52.76	12.18	24.84	8.88
6A-6B	0	25.83	5.83	11.90	5.25
6B-1A	10	92.46	15.05	35.27	14.97
6B-1B	10	89.90	14.89	34.96	14.89
6B-2A	15	79.00	16.58	38.61	12.25
6B-2B	15	88.16	16.31	38.00	11.38
6B-3A	15	85.61	14.71	36.52	13.61
6B-3B	15	90.99	14.45	36.13	13.58
6B-4A	10	72.45	13.82	32.43	11.98
6B-4B	10	74.53	13.55	31.99	12.15
6B-5A	5	57.66	12.39	24.99	9.30
6B-5B	5	65.94	12.39	25.08	9.41
6B-6A	0	23.47	6.27	12.28	4.69

Table B.4: Attenuation of outlet pairs in the same circuit ring: Ring 1 (continue).

B.3 Measured Attenuation Between Outlet Pairs in Ring 1 and 2 - Cross Ring Transmission (50MHz - 1GHz)

B.3 Measured Attenuation Between Outlet Pairs in Ring 1 and 2 - Cross Ring Transmission (50MHz - 1GHz)

Outlet Pairs		Attenuation in dB			
Name	Length (m)	Max	Min	Average	Std Dev
R1.1A - R2. 1A	10.00	84.61	25.75	45.80	9.28
R1.1A - R2. 1B	10.00	87.89	26.25	46.28	8.85
R1.1A - R2. 2A	15.00	90.95	30.73	51.08	9.18
R1.1A - R2. 2B	15.00	89.98	29.91	51.13	9.51
R1.1A - R2. 3A	20.00	95.17	29.31	52.89	9.25
R1.1A - R2. 3B	20.00	84.89	28.69	53.36	8.24
R1.1A - R2. 4A	20.00	92.73	28.36	54.49	9.63
R1.1A - R2. 4B	20.00	99.96	27.77	53.93	9.39
R1.1A - R2. 5A	15.00	97.22	28.80	52.28	11.31
R1.1A - R2. 5B	15.00	94.68	28.46	51.70	9.41
R1.1A - R2. 6A	10.00	85.68	25.95	47.18	11.51
R1.1A - R2. 6B	10.00	91.29	25.29	47.32	12.11
R1.1B - R2. 1A	10.00	85.62	25.66	46.98	10.65
R1.1B - R2. 1B	10.00	82.81	25.41	46.96	9.84
R1.1B - R2. 2A	15.00	94.91	29.47	51.33	8.99
R1.1B - R2. 2B	15.00	92.17	29.11	52.06	9.88
R1.1B - R2. 3A	20.00	91.97	29.75	53.94	9.29
R1.1B - R2. 3B	20.00	84.24	28.40	53.93	8.70
R1.1B - R2. 4A	20.00	91.60	28.19	54.32	10.17
R1.1B - R2. 4B	20.00	91.28	28.15	54.24	10.01
R1.1B - R2. 5A	15.00	98.66	29.00	52.57	10.47
R1.1B - R2. 5B	15.00	98.14	28.89	51.75	10.10
R1.1B - R2. 6A	10.00	84.91	25.62	47.27	11.21
R1.1B - R2. 6B	10.00	90.58	24.94	47.52	11.95
R1.2A - R2. 1A	15.00	84.79	29.49	50.76	8.55
R1.2A - R2. 1B	15.00	91.71	29.09	50.48	9.22
R1.2A - R2. 2A	20.00	95.90	30.38	54.16	9.35
R1.2A - R2. 2B	20.00	91.49	30.31	54.82	9.05
R1.2A - R2. 3A	25.00	92.30	29.91	56.57	9.58
R1.2A - R2. 3B	25.00	100.39	28.82	56.48	9.21
R1.2A - R2. 4A	25.00	97.20	29.32	55.43	10.24
R1.2A - R2. 4B	25.00	96.88	28.46	55.94	9.24
R1.2A - R2. 5A	20.00	92.08	29.39	55.96	9.62
R1.2A - R2. 5B	20.00	95.03	28.71	54.61	9.04
R1.2A - R2. 6A	15.00	99.29	28.59	52.31	10.78
R1.2A - R2. 6B	15.00	94.96	28.08	52.11	10.95

Table B.5: Attenuation of outlet pairs in the same circuit ring: Cross Ring (R1.1A-R2.1B represents the location of Tx/Rx in circuit ring 1 and 2 in Figure 5.1).

B.3 Measured Attenuation Between Outlet Pairs in Ring 1 and 2 - Cross Ring Transmission (50MHz - 1GHz)

Outlet Pairs		Attenuation in dB			
Name	Length (m)	Max	Min	Average	Std Dev
R1.2B - R2. 1A	15.00	95.01	29.49	51.02	8.90
R1.2B - R2. 1B	15.00	86.77	29.10	50.67	8.63
R1.2B - R2. 2A	20.00	91.43	30.09	54.29	8.76
R1.2B - R2. 2B	20.00	90.59	29.84	54.14	8.08
R1.2B - R2. 3A	25.00	103.36	30.29	55.74	8.95
R1.2B - R2. 3B	25.00	101.74	28.94	55.83	9.07
R1.2B - R2. 4A	25.00	100.35	29.21	55.19	9.02
R1.2B - R2. 4B	25.00	98.96	28.70	55.27	8.87
R1.2B - R2. 5A	20.00	96.37	30.00	55.38	8.99
R1.2B - R2. 5B	20.00	101.65	29.21	55.16	9.62
R1.2B - R2. 6A	15.00	88.41	29.26	52.59	9.92
R1.2B - R2. 6B	15.00	97.05	28.62	52.60	11.02
R1.3A - R2. 1A	20.00	91.56	30.97	52.11	8.83
R1.3A - R2. 1B	20.00	88.98	29.90	51.89	8.02
R1.3A - R2. 2A	25.00	99.82	31.78	54.05	9.48
R1.3A - R2. 2B	25.00	98.59	31.00	54.50	8.04
R1.3A - R2. 3A	30.00	89.06	31.51	55.58	8.40
R1.3A - R2. 3B	30.00	90.22	30.63	56.52	8.61
R1.3A - R2. 4A	30.00	101.02	31.54	56.20	9.19
R1.3A - R2. 4B	30.00	93.27	30.98	56.13	8.72
R1.3A - R2. 5A	25.00	113.15	31.58	55.97	10.24
R1.3A - R2. 5B	25.00	98.32	30.69	55.72	9.58
R1.3A - R2. 6A	20.00	94.24	30.56	54.75	9.79
R1.3A - R2. 6B	20.00	97.53	30.02	54.16	9.86
R1.3B - R2. 1A	20.00	84.73	30.42	51.95	8.01
R1.3B - R2. 1B	20.00	83.12	29.80	50.71	8.50
R1.3B - R2. 2A	25.00	85.97	31.97	53.28	8.14
R1.3B - R2. 2B	25.00	102.85	31.32	55.06	9.39
R1.3B - R2. 3A	30.00	96.12	31.53	55.25	9.16
R1.3B - R2. 3B	30.00	90.84	30.51	55.57	8.11
R1.3B - R2. 4A	30.00	94.96	30.86	55.80	9.36
R1.3B - R2. 4B	30.00	102.42	30.72	56.46	8.80
R1.3B - R2. 5A	25.00	104.58	31.18	55.44	9.09
R1.3B - R2. 5B	25.00	98.01	30.81	55.42	9.01
R1.3B - R2. 6A	20.00	103.38	30.38	54.73	9.91
R1.3B - R2. 6B	20.00	93.91	30.24	54.70	9.60

Table B.6: Attenuation of outlet pairs in the same circuit ring: Cross Ring (continue).

B.3 Measured Attenuation Between Outlet Pairs in Ring 1 and 2 - Cross Ring Transmission (50MHz - 1GHz)

Outlet Pairs		Attenuation in dB			
Name	Length (m)	Max	Min	Average	Std Dev
R1.4A - R2. 1A	20.00	78.18	31.83	51.35	7.34
R1.4A - R2. 1B	20.00	98.54	31.01	50.88	7.88
R1.4A - R2. 2A	25.00	89.92	33.99	52.82	8.40
R1.4A - R2. 2B	25.00	86.64	32.73	52.97	7.37
R1.4A - R2. 3A	30.00	106.33	31.27	52.34	8.48
R1.4A - R2. 3B	30.00	90.55	30.13	53.34	7.13
R1.4A - R2. 4A	30.00	91.97	32.06	55.54	8.39
R1.4A - R2. 4B	30.00	92.90	31.85	55.39	7.76
R1.4A - R2. 5A	25.00	93.16	32.12	55.53	8.85
R1.4A - R2. 5B	25.00	108.48	31.34	55.67	8.57
R1.4A - R2. 6A	20.00	97.66	32.02	54.38	9.00
R1.4A - R2. 6B	20.00	86.57	30.99	54.14	8.31
R1.4B - R2. 1A	20.00	83.52	31.13	50.91	7.61
R1.4B - R2. 1B	20.00	92.89	31.12	50.96	7.98
R1.4B - R2. 2A	25.00	85.97	33.03	52.42	7.68
R1.4B - R2. 2B	25.00	90.07	32.01	52.45	7.58
R1.4B - R2. 3A	30.00	90.31	31.11	54.29	8.59
R1.4B - R2. 3B	30.00	87.62	30.49	54.08	7.54
R1.4B - R2. 4A	30.00	98.42	31.72	55.28	8.02
R1.4B - R2. 4B	30.00	88.08	31.19	54.98	7.44
R1.4B - R2. 5A	25.00	97.09	31.84	55.10	8.33
R1.4B - R2. 5B	25.00	94.19	31.17	55.37	8.87
R1.4B - R2. 6A	20.00	93.03	31.16	54.74	8.44
R1.4B - R2. 6B	20.00	98.50	30.06	54.18	8.43
R1.5A - R2. 1A	15.00	83.45	29.10	45.95	6.92
R1.5A - R2. 1B	15.00	74.65	28.19	45.85	6.46
R1.5A - R2. 2A	20.00	86.98	28.58	49.93	8.18
R1.5A - R2. 2B	20.00	82.60	27.62	49.80	7.20
R1.5A - R2. 3A	25.00	101.98	30.07	49.38	7.32
R1.5A - R2. 3B	25.00	88.72	29.36	50.56	6.68
R1.5A - R2. 4A	25.00	89.78	27.35	52.48	8.77
R1.5A - R2. 4B	25.00	85.57	27.05	52.77	7.86
R1.5A - R2. 5A	20.00	85.65	29.80	53.53	8.46
R1.5A - R2. 5B	20.00	91.28	28.42	53.13	8.00
R1.5A - R2. 6A	15.00	91.10	28.38	51.84	9.34
R1.5A - R2. 6B	15.00	97.16	28.33	51.76	9.59

Table B.7: Attenuation of outlet pairs in the same circuit ring: Cross Ring (continue).

B.3 Measured Attenuation Between Outlet Pairs in Ring 1 and 2 - Cross Ring Transmission (50MHz - 1GHz)

Outlet Pairs		Attenuation in dB			
Name	Length (m)	Max	Min	Average	Std Dev
R1.5B - R2. 1A	15.00	76.29	29.26	45.99	6.07
R1.5B - R2. 1B	15.00	85.04	28.34	46.86	8.50
R1.5B - R2. 2A	20.00	88.68	28.46	49.59	8.22
R1.5B - R2. 2B	20.00	90.81	27.75	48.84	7.33
R1.5B - R2. 3A	25.00	93.96	30.36	50.02	6.97
R1.5B - R2. 3B	25.00	94.70	29.72	51.31	7.45
R1.5B - R2. 4A	25.00	90.43	28.76	53.23	7.97
R1.5B - R2. 4B	25.00	83.43	28.39	51.15	7.44
R1.5B - R2. 5A	20.00	97.51	29.64	52.29	8.89
R1.5B - R2. 5B	20.00	84.65	28.76	52.53	8.86
R1.5B - R2. 6A	15.00	87.77	28.65	51.39	8.17
R1.5B - R2. 6B	15.00	93.20	28.60	50.92	9.01
R1.6A - R2. 1A	10.00	84.09	24.82	40.23	7.00
R1.6A - R2. 1B	10.00	66.20	23.89	40.27	5.63
R1.6A - R2. 2A	15.00	76.80	24.31	43.86	7.08
R1.6A - R2. 2B	15.00	69.52	23.79	44.08	6.03
R1.6A - R2. 3A	20.00	73.08	26.41	44.96	6.16
R1.6A - R2. 3B	20.00	83.71	25.48	46.78	7.60
R1.6A - R2. 4A	20.00	96.33	24.72	46.68	9.03
R1.6A - R2. 4B	20.00	87.35	24.72	47.08	7.54
R1.6A - R2. 5A	15.00	78.19	25.03	47.61	7.94
R1.6A - R2. 5B	15.00	86.46	24.92	48.28	7.79
R1.6A - R2. 6A	10.00	85.92	23.69	47.28	9.05
R1.6A - R2. 6B	10.00	88.51	23.31	47.23	10.06
R1.6B - R2. 1A	10.00	74.12	24.17	39.86	6.86
R1.6B - R2. 1B	10.00	73.01	23.63	41.10	6.14
R1.6B - R2. 2A	15.00	87.63	24.71	45.18	8.04
R1.6B - R2. 2B	15.00	78.86	24.16	44.81	6.09
R1.6B - R2. 3A	20.00	78.74	26.00	47.13	7.16
R1.6B - R2. 3B	20.00	98.81	25.07	46.54	7.20
R1.6B - R2. 4A	20.00	78.33	24.85	48.49	7.64
R1.6B - R2. 4B	20.00	83.02	24.54	48.36	8.24
R1.6B - R2. 5A	15.00	77.78	25.24	48.16	7.01
R1.6B - R2. 5B	15.00	80.80	24.76	48.24	7.51
R1.6B - R2. 6A	10.00	90.74	23.98	46.55	8.62
R1.6B - R2. 6B	10.00	82.91	23.50	45.77	9.05

Table B.8: Attenuation of outlet pairs in the same circuit ring: Cross Ring (continue).

Appendix C

Multiband - OFDM UWB Physical Layer

The PHY specification of MB-OFDM UWB model proposed for IEEE 802.15.3a standard group is described as below. The proposed system supports mandatory data rates of 55, 110 and 200Mbps for WPAN. The transmission front end of the PHY model consists of a number of steps including channel coding, bit interleaving, constellation mapping, OFDM symbol formation and frequency hopping.

C.1 Channel Coding and Bit Interleaving

As shown in Figure 6.7, the source data is firstly encoded using convolutional encoder, the encoder rate R is selected corresponding to the desired data rate. The convolutional encoder uses 1/3 code rate with the constrain length of 7, the generator polynomials are $g_0 = 133_8$, $g_1 = 145_8$, $g_2 = 175_8$, as illustrated in Figure C.1. The bit denoted as "A" shall be the first bit generated by the encoder, followed by bits denoted as "B" and finally "C". The various coding rates are derived from the rate $R = 1/3$ convolutional code by "puncturing" - a procedure for omitting some of the encoded bits in the Tx and adding zeros at the Rx in place of the omitted bits. The puncturing patterns for 5/8 and 3/4 code rate are illustrated in Figure C.2 and C.3, in which the puncture vectors are [1 0 1 0 0 1 1 0 1 1 0 0 1 0 1] and [1 0 0 1 0 1 0 0 1] respectively [119].

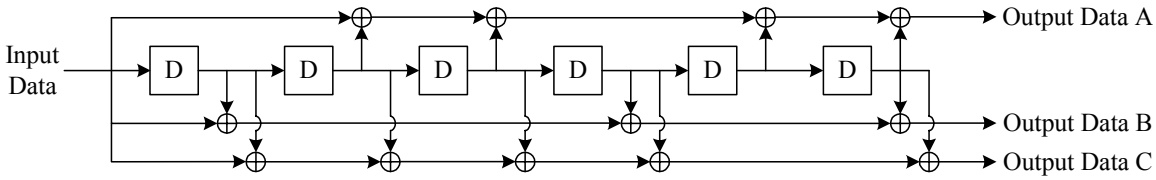

Figure C.1: Convolutional encoder: code rate 1/3, constraint length 7.

Figure C.2: Bit-stealing and bit-insertion procedure (R=5/8).

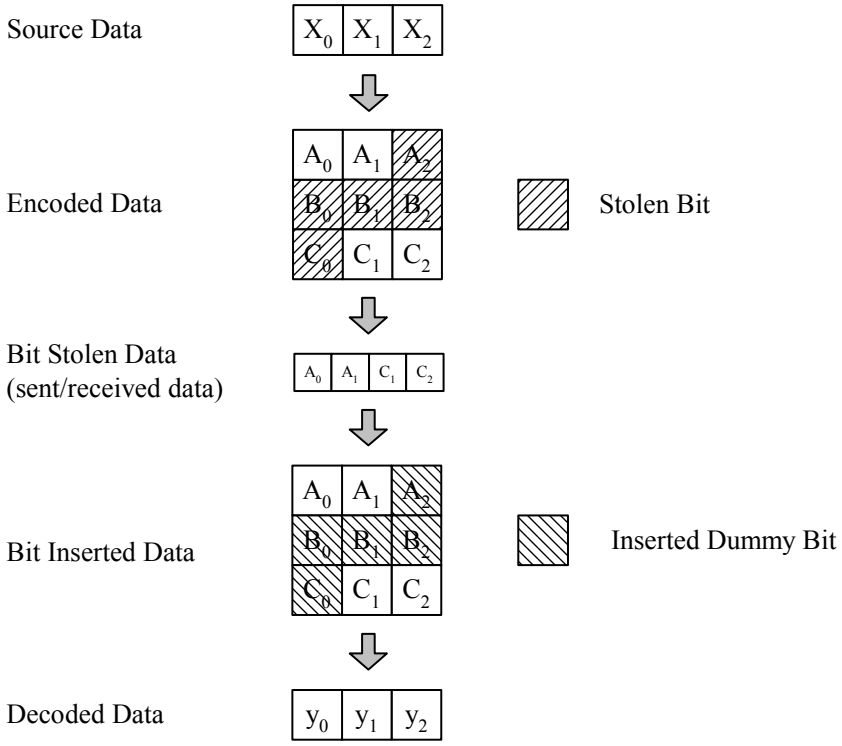

Figure C.3: Bit-stealing and bit-insertion procedure (R=3/4).

The coded bit stream is interleaved prior to modulation. Bit interleaving provides robustness against burst errors by writing data bits into a matrix row-by-row and reading them out column-by-column. In this model it is performed at two distinct stages: interleaving across OFDM frames and interleaving within OFDM frames. The former stage interleaves the bits over the 3 sub-bands within Band Group 1, thus exploits frequency diversity across different sub-bands; the latter stage permutes the bits across the 100 data sub-carriers within an OFDM symbol and exploits frequency diversity across sub-carriers to provide immunity to narrow-band interferences.

C.2 Sub-carrier Constellation Mapping

The OFDM sub-carriers are modulated using QPSK modulation. The coded and interleaved binary serial input data are divided into groups of 2 bits and

converted into complex numbers representing QPSK constellation points. The conversion shall be performed according to the Gray-coded constellation mapping, illustrated in Figure C.4, where b_0 determines the I value and b_1 determines the Q value (Table C.1). The output values, d, are formed by multiplying the resulting $(I + jQ)$ value by a normalisation factor k_{mode}:

$$d = (I + jQ) \times k_{mod}. \tag{C.1}$$

For QPSK modulation, k_{mod} equals to $1/\sqrt{2}$.

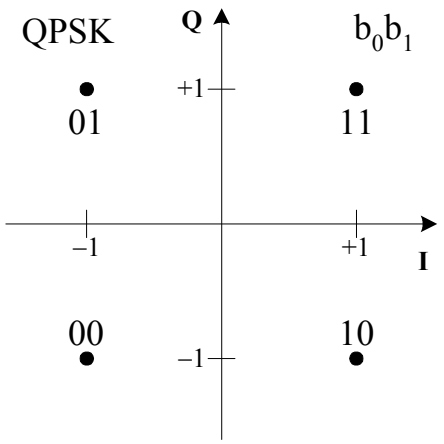

Figure C.4: QPSK constellation bit mapping.

Input bit (b_0b_1)	I-out	Q-out
00	-1	-1
01	-1	1
10	1	-1
11	1	1

Table C.1: QPSK encoding table.

C.3 OFDM Modulation

For data rates of 200Mbit/s, the stream of complex numbers is divided into groups of 100 complex numbers, corresponding to the 100 data sub-carriers of

OFDM symbol. Each complex data is transmitted over the sub-carrier, which is orthogonal to each other in the frequency domain. The sub-carriers are in the form:

$$\phi_k(t) = e^{j2\pi f_k t}, 0 \leq k \leq N-1, \tag{C.2}$$

where f_k is the frequency of the kth sub-carrier. Assuming the complex input data is $X_k = a_k + jb_k$, it multiplexes the N sub-carriers as:

$$s(t) = \frac{1}{N} \sum_{k=0}^{N-1} X_k \phi_k(t), 0 < t < T_{sym}, \tag{C.3}$$

where T_{sym} is the length of the OFDM symbol and the subcarrier frequencies are equally spaced at:

$$f_k = k\Delta f = \frac{k}{T_{sym}}. \tag{C.4}$$

Where Δf is the bandwidth of sub-carriers, $\Delta f = 1/T_{sym}$. Figure C.5 illustrates the modulated OFDM symbol in frequency domain, each complex data are separated by overlapping sub-carriers, thus increasing the spectral efficiency.

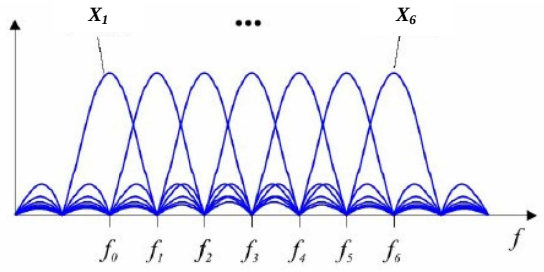

Figure C.5: Frequency overlapping of OFDM orthogonal sub-carriers.

C.3.1 The Use of Fourier Transform in OFDM

The wide use of OFDM technique is because of its simple implementation. IFFT and its counter part, FFT are used to convert the frequency domain signal to time domain signal, and vice versa. This is equivalent to mapping the input data

onto the sinusoidal sub-carriers [52]. If we apply IFFT to the complex input data $X_k = a_k + jb_k$, the transformed signal $x[n]$ will be:

$$x[n] = \frac{1}{N}\sum_{k=0}^{N-1} X[k]e^{j(2\pi/N)kn}. \tag{C.5}$$

Equation (C.5) can be written as:

$$x[n] = \frac{1}{N}\sum_{k=0}^{N-1} X[k]e^{j2\pi\frac{k}{N\Delta t}n\Delta t}, \tag{C.6}$$

where Δt is the system sampling time, $N\Delta t = T_{sym}$. Substitute (C.4) into (C.6) yields:

$$x[n] = \frac{1}{N}\sum_{k=0}^{N-1} X[k]e^{j2\pi f_k t_n}, \tag{C.7}$$

where t_n equals to the time samples, $t_n = n\Delta t$. Substitute the complex value of X_k to (C.7) and take the real part of the data as the signal, we will get:

$$s[n] = Re(x[n]) = \frac{1}{N}\sum_{k=0}^{N-1}\{a_k cos(2\pi f_k t_n) - b_k sin(2\pi f_k t_n)\} \tag{C.8}$$

If these components are applied to a low-pass filter at time intervals of Δt, a signal is obtained that closely approximates the frequency division multiplexed signal:

$$s(t) = \frac{1}{N}\sum_{k=0}^{N-1}\{a_k cos(2\pi f_k t) - b_k sin(2\pi f_k t)\}, 0 \leq t \leq N\Delta t. \tag{C.9}$$

$s(t)$ contains a bank of modulated sub-carriers, which are mutually orthogonal. If we compare (C.9) to the modulated QPSK signals in (C.3), it can be seen that the IFFT transform actually modulates the QPSK signal onto different sub-carriers [129].

C.3.2 Forming OFDM Signals in MB-OFDM

In the MB-OFDM model, OFDM signals are formed using 128 IFFT, among which only 100 sub-carriers are used for information data, 12 pilots and 10 guard sub-carriers, numbered [-61, ..., -1, 1, ..., 61], as illustrated in C.6. The 10 guard

sub-carriers are located on the edges of the OFDM symbol, at logical sub-carriers $\pm 61, \pm 60, ..., \pm 57$. The pilots are located at sub-carriers $\pm 55, \pm 45, \pm 35, \pm 25, \pm 15$ and ± 5, they are used for coherent signal detection and to provide robustness against frequency offset and phase noise. The information data are transmitted on the 100 remaining sub-carriers. The DC band (numbered 0) and the 5 unused bands are set to zero [119].

After IFFT, the coefficients 1 to 61 are mapped to the same numbered IFFT inputs, while the coefficients -61 to -1 are copied into IFFT inputs 67 to 127, the rest of the inputs are set to zero. After IFFT operation, a zero-padded prefix of length 32 is pre-appended to the IFFT output and a guard interval is added at the end of the IFFT to generate an output with 165 samples.

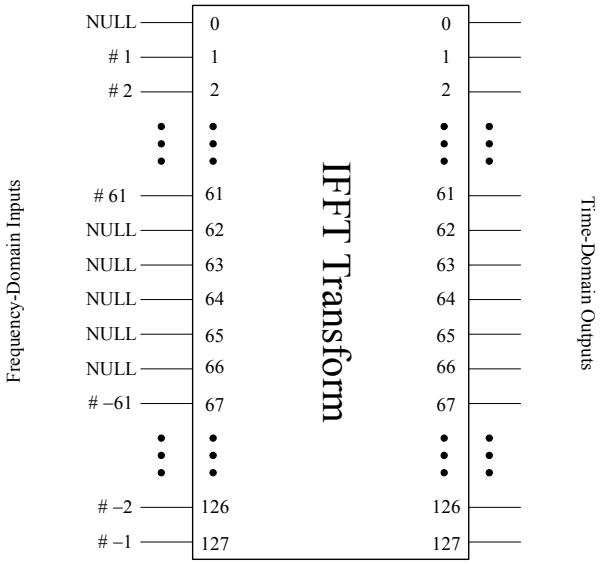

Figure C.6: Input and outputs of IFFT Transform.

C.3.3 Frequency Hopping and Spreading

For data rates below 200Mbps, a time-domain spreading operation is performed with a spreading factor of 2. That is, the same information is transmitted over two OFDM symbols, and these two OFDM symbols are transmitted over different

sub-bands to obtain frequency diversity. Figure C.7 illustrates the structure of an OFDM symbol and how it is hopping in Band Group 1 (3168MHz - 4752MHz).

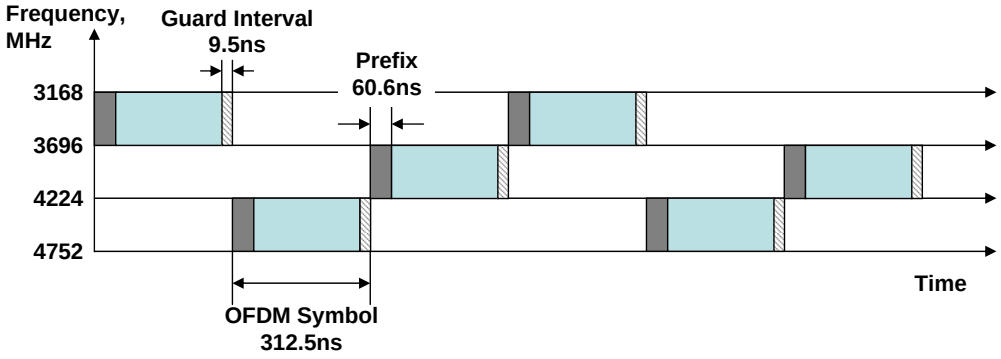

Figure C.7: Example of frequency hopping of MB-OFDM Symbol (Reproduced from [10]).

Appendix D

Radiated Emission Measurement

The layout of the EMC test site in Open University, Milton Keynes is shown in Figure D.1.

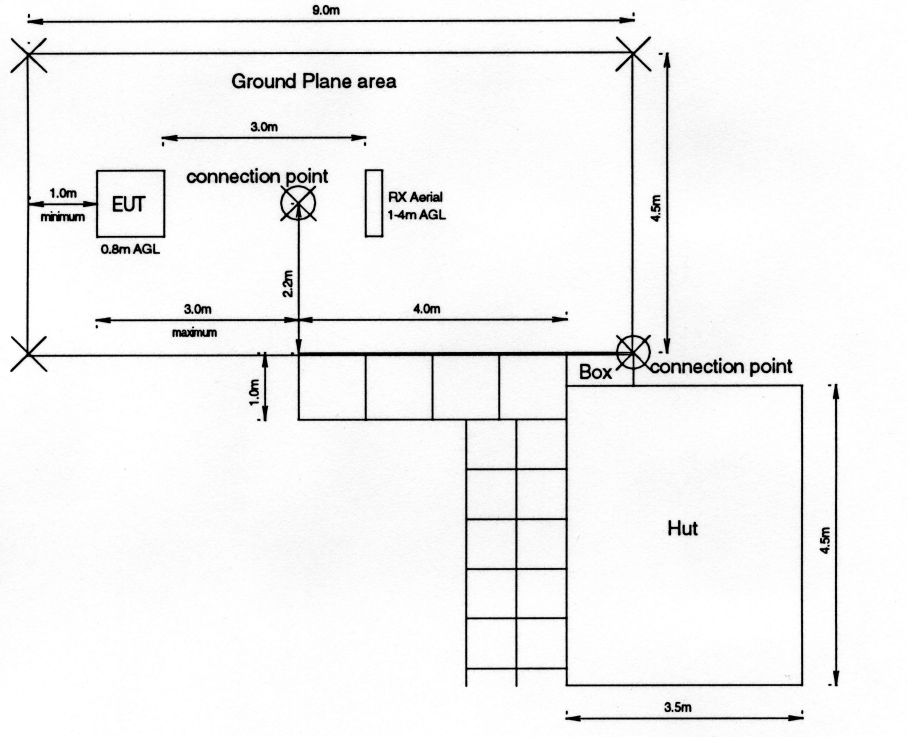

Figure D.1: Illustration of the EMC radiated emission test site in Open University.

Illustration of the single powerline ring circuit for radiated emission testing and the receiving antennas.

Figure D.2: Photograph of the single powerline ring circuit under test and the pulse generator.

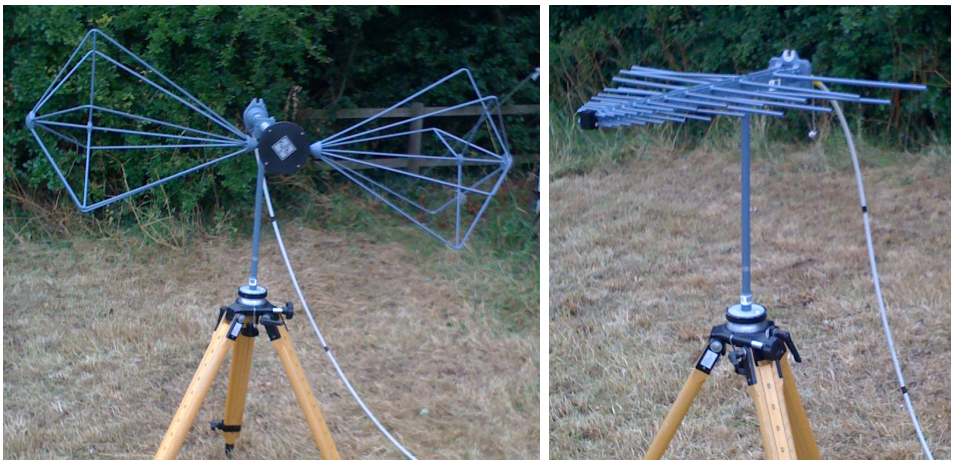

Figure D.3: Photograph of the receiving antennas: Bi-Conical (left) and Log-Perodic (right).

References

[1] A. Majumder and J. Caffery, "Power Line Communications: A Overview," *IEEE Potentials*, pp. 4–8, November 2004. 12, 24, 25, 32

[2] M. Gotz, M. Rapp, and K. Dostert, "Power Line Channel Characteristics and Their Effects on Communication System Design," *IEEE Communications Magazine*, pp. 78–86, April 2004. 12, 32, 33

[3] North Atlantic Treaty Organisation - Research and Technology Organisation, "HF Interference, Procedures and Tools - Final Report of NATO RTO Information Systems Technology, Panel Research Task Group IST - 050/RTG-022," NATO RTO, Tech. Rep., June 2007. 12, 34, 39, 41, 128

[4] M. Ghavami, L. Michael, and R. Kohno, *Ultra Wideband Signals and Systems in Communication Engineering.* Wiley, May 2004. 12, 44

[5] R. Kolic, "Ultra Wideband - the Next Generation Wireless Connection," Intel Technology Group, Tech. Rep., Feb 2004. 12, 45

[6] P. A. J. V. Rensburg and H. C. Ferreira, "Coupling Circuitry: Understanding the Functions of Different Components," in *7th International Symposium on Powerline Communications and Its Applications*, March 2003, pp. 204–209. 14, 79, 81

[7] "How RF Transformers Work," Mini-circuits, Tech. Rep. 14, 81

[8] "Data Sheet: Model Detailed Technical Information: ADT15-122+," Mini-circuits, Tech. Rep. 14, 82

[9] D. M. Pozar, *Microwave Engineering*, 2nd ed. Wiley, 1998. 17, 61, 71, 164, 165

[10] M. P. Wylie-Green, P. A. Ranta, and J. Salokannel, "Multi-band OFDM UWB Solution for IEEE 802.15.3a WPANs," in *IEEE/Sarnoff Symposium on Advances in Wired and Wireless Communication*, April 2005, pp. 102–105. 17, 185

[11] P. Brown, "Power Line Communications - Past Present and Future," in *IEEE International Conference on Powerline Communications and Its Applications*, Lancaster, 1999. 24

[12] K. Dostert, "Telecommunicaitons over the Power Distribution Grid - Possibilities and Limitations," in *IEEE International Conference on Powerline Communications and Its Applications*, Germany, 1997. 24

[13] ——, *Powerline Communications*. Prentice Hall PTR, 2001. 24, 68, 69

[14] D. Clark, "Powerline Communications: Finally Ready for Prime Time?" *IEEE Internet Computing*, January 1998. 24

[15] D. Hansen, "Megabits per Second on 50Hz Power Lines?" *IEEE EMC Society Newsletter*, 2001. 25

[16] M. E. Hazen, "The Technology Behind HomePlug AV Powerline Communications," *IEEE Computer Magazine*, vol. 41, pp. 90 – 92, Jine 2008. 26, 37, 156

[17] A. Skrzypczak, P. Siohan, and J.-P. Javaudin, "Application of the OFDM/OQAM Modulation to Powerline Communications," in *Proceedings of the IEEE International Conference on Power Line Communications and Its Applications, ISPLC 07*, March 2007, pp. 71–76. 26

[18] "HomePlug 1.0: Technology White Paper," HomePlug Powerline Alliance, Tech. Rep., November 2009. [Online]. Available: http://www.homeplug.org/products/whitepapers/ 26, 36

[19] I. Oppermann, M. Hamalainen, and J. Iinatti, *UWB: Theory and Applications*. Wiley, Septermber 2004. 26, 43

[20] D. Geer, "UWB Standardization Effort Ends in COntroversy," *IEEE Computer Magazine*, vol. 39, no. 7, pp. 13 – 16, July 2006. 26

[21] F. Bhesania and B. Hosler, "UWB: A High-Speed Wireless PAN Technology," September 2009. [Online]. Available: www.3g4g.co.uk/Other/Uwb/Wp/UWB_WirelessPAN.pdf 26, 46

[22] J. Newbury, "A Communicaiton Infrastructure for South Western Electricity," *IEEE Transactions on Power Delivery*, vol. 11, no. 3, pp. 1201 – 1208, July 1996. 30

[23] Q. Liu, B. Zhao, Y. Wang, and J. Hu, "Experience of AMR Systems Based on BPL in China," in *2009 IEEE International Symposium on Power Line Communications and its Applications*, Dresden, Germany, March 2009, pp. 280 – 284. 30

[24] K. McCabe, "IEEE Unifies Power, Communications and IT with Launch of Smart Grid Interoperability Standards Project P2030." 30

[25] G. S. Prasanna, A. lakshmi, S. S, V. Simha, and G. Koomullil, "Data Communication over the Smart Grid," in *2009 IEEE International Symposium on Power Line Communications and its Applications*, Dresden, Germany, March 2009, pp. 273 – 279. 30

[26] N. Weling and M. Koch, "Research and Customized Solutions on Any-Wire IP-Networks for Multiple Infrastructures," in *IEEE International Conference on Powerline Communications and Its Applications*. Dresden, Germany: Devolo, March 2009. 31

[27] Y. Yang and C. Arteaga, "Broadband over Powerline Field Trial For Commercial In-Building application in a Multi-Dwelling-Unit Environment," in *International Symposium of Powerline Communications and its Applications*, Dresden, Germany, March 2009, pp. 342 – 346. 31

[28] J. Nishioka, S. Tsuzuki, Y. Yamada, M. Yoshida, H. Kawasaki, and T. Shinpou, "Characteristics of 440V Power-Line Channels in Container Ships," in *International Symposium of Powerline Communications and its Applications*, Dresden, Germany, March 2009, pp. 217 – 222. 31

[29] M. Mohammadi, "Measurement Study and Transmission for In-Vehicle Power Line Communication," in *IEEE International Conference on Powerline Communications and Its Applications*, Dresden, Germany, March 2009, pp. 73 – 78. 31

[30] "BT Selects Comtrend's Power Line Communication Technology for a Second Year Running to Aid Delivery of Its Digital Content and Home-Entertainment Service, BT Vision," October 2008. [Online]. Available: http://www.sourcewire.com/releases/rel_display.php?relid=42008 31

[31] B. Beutler, "Opportunities abound in China's home networking marker," September 2009. [Online]. Available: http://www.edn.com/article/CA6385658.html 31

[32] G. T. Andreou, P. Labridis, and G. Papagiannis, "Modeling of Low Voltage Distribution Cables for Powerline Communications," *IEEE Bologna PowerTech Conference Proceedings*, vol. 2, pp. 6–11, June 23-26 2003. 31

[33] M. Tanaka, "High frequency noise power spectrum, impedance and transmission loss of power line in Japan on intra-building power line communications," *IEEE Transactions on Consumer Electronics*, pp. 321–326, 1988. 31

[34] T. Banwell and S. Galli, "A New Approach to the Modelling of the Transfer Function of the Power Line Channel," in *Proceedings of the IEEE International Conference on Power Line Communications and Its Applications, ISPLC 01*, April 2001. 31

[35] D. Fenton, "An Experimental Investigation into the Electromagnetic Compatibility aspects of High Frequency Power Line Communications," Ph.D. dissertation, Open University, August 2006. 31, 79

[36] J.R.Nicholson and J.A.Maalack, "RF impedance of power lines and line impedance stabilization networks in conducted interference measurements," *IEEE Transactions on Electromagnetic Compatibility*, pp. 84–86, May 1973. 31, 76, 96

[37] N. Pavlidou, A. H. Vinck, J. Yazdani, and B. Honary, "Power Line Communications: State of the Art and Future Trends," *IEEE Communications Magazine*, pp. 34–40, April 2003. 32

[38] E. Biglieri and P. di Torino, "Coding and modulation for a horrible channel," *IEEE Communications Magazine*, pp. 92–98, May 2003. 32, 35

[39] M. Tlich, H. Chaouche, A. Zeddam, and P. Pagani, "Novel Approach for PLC Impulsive Noise Modelling," in *IEEE International Conference on Powerline Communications and Its Applications, ISPLC'07*, March 2009, pp. 20 – 25. 32, 124

[40] J. A. C. Arrabal, L. Diez, and F. Canete, "Analysis of the Periodic Impulsive Noise Asynchronous with the Mians in Indoor PLC Channels," in *IEEE International Conference on Powerline Communications and Its Applications*, Dresden, Germany, March 2009, pp. 26 – 20. 32

[41] A. Mengi and H. Vick, "Impulsive Noise Error Correction in 16 OFDM for Narrowband Power Line," in *IEEE International Conference on Powerline Communications and Its Applications*, March 2009, pp. 31 – 35. 32

[42] P. Holger, "Modeling of the powerline communication channels," in *IEEE International Conference on Powerline Communications and Its Applications, ISPLC'99*, March 1999. 32

[43] M. Zimmermann and K. Dostert, "A Multipath Model for the Powerline Channel," *IEEE Transactions on communications*, vol. 50, no. 4, pp. 553–559, April 2002. 32, 66

[44] M. Babic, M. Hagenau, K. Dostert, and J. Bausch, "Theoretical postulation of PLC channel model," *OPERA-IST Integrated Project No. 507767*, 2005. 33, 121

[45] S. Galli and T. C. Banwell, "A Novel Approach to the Modeling of the Indoor Power Line Channel Part 1: Circuit Analysis and Companion Mode," *IEEE Transactions on Power Delivery*, vol. 20, no. 2, p. 2005, April 2005. 33, 66, 72

[46] S. Galli and T. Banwell, "A Novel Approach to the Modelling of the Indoor Power Line Channel , Part 2: Transfer Function and Channel Properties," *IEEE Transactions on Power Delivery*, vol. 30, no. 3, pp. 1869–1878, July 2005. 33

[47] M. Zhang and W. Lauber, "Evaluation of the Interference Potential of In-Home Power Line Communication Systems," in *IEEE International Conference on Powerline Communications and Its Applications*, 2008, pp. 263 – 268. 34

[48] Moh, R. Razafferson, G. Avril, and A.Zeddam, "Outline about the EMC properties and throughputs of the PLC systems up to 100 MHz," in *IEEE International Conference on Powerline Communications and Its Applications*, 2008, pp. 259 – 262. 34

[49] H. Hrasnica, A. Haidine, and R. Lehnert, *Broadband Powerline Communication Netwroks*. Wiley, 2004. 34, 51, 55

[50] J. Newbury, "Communication Services using the Low Voltage Distribution Network," in *IEEE Transmission and Distribution Conference and Exposition*, vol. 2, Atlanta, GA, USA, 2001, pp. 638 – 640. 34, 96, 127

[51] T.Sartenaer, "Multiuser Communications over Frequency Selective Wired Channels and Applications to The Powerline Access Network," PhD Thesis, University catholique de Louvain, 2004. 35

[52] L. Litwin and M. Pugel, "The Principles of OFDM," *RF Signal Processing*, pp. 30–48, January 2001. 35, 36, 183

[53] S. Galli, "PHY Layer and Standardisation," in *IEEE International Conference on Powerline Communications and Its Applications*, March 2009. 36, 37

[54] (2009, September) Home Grid Forum. [Online]. Available: http://www.homegridforum.org/home 36, 37

[55] L. E. Frenzel, "Powerline Communication Standards Continue To Struggle," September 2009. [Online]. Available: www.electronicdesign.com 36

[56] "HomePlug AV White Paper," HomePlug Alliance, Tech. Rep., 2005. 37

[57] (2009, September) High Definition Powerline Communication. [Online]. Available: http://www.hd-plc.org/ 37

[58] (2009, September) IEEE P1901 Working Group. [Online]. Available: http://grouper.ieee.org/groups/1901/ 37

[59] "Top Ten Things You Need to Know About the New G.hn Standard," *DS2 Blog*, September 2009. [Online]. Available: http://blog.ds2.es/ds2blog/2009/05/top-ten-things-about-ghn-standard.html 37

[60] L. Gould, "Next Generation Home Networks: ITU-T G.hn and The HomeGrid Form," in *IEEE International Conference on Powerline Communications and Its Applications*, Dresden, Germany, March 2009. 37

[61] D. Tomimura and V. Neto, "A Regulatory Framework for Broadband PLC," in *International Symposium of Powerline Communications and its Applications*, Dresden, Germany, March 2009, pp. 319 – 324. 38, 127

[62] C. Hensen and S. Schwarze, "CISPR 22 Compliance Test of Power-Line Transmission Systems," in *IEEE International Symposium of Powerline Communications and Its Applications*, March 2002. 38

[63] ECC and CEPT, "PLT, DSL, Cable Communications (including cable TV), LANS and their effect on Radio Services ," ECC and CEPT, Tech. Rep., May 2003. 38

[64] CEPT ECC/REC/(05)04, "Criteria for the Assessment of Radio Interference Caused By Radiated Disturbances from Wire-line Telecommunication Networks," 2005. 39

[65] FCC, "In the Matter of Carrier Current Systems, including Broadband over Power Line Systems - Amendment of Part 15 regarding new requirements and measurement guidelines for Access Broadband pver Power Line Systems," February 2004. 40

[66] "FCC Part 15 Report," pp. 698–699, September 2009. [Online]. Available: http://www.access.gpo.gov/nara/cfr/waisidx_00/47cfr15_00.html. 40, 146

[67] A. M. Tonello, "Wideband Impulse Modulation and Receiver Algorithms for Multiuser Power Line Communications," *EURASIP Journal on Advances in Signal Processing*, vol. 2007, 2007. 42, 47

[68] J. H. Reed, Ed., *An Introduction to Ultra Wideband Communication Systems.* Prentice Hall, 2005. 43, 137

[69] A. Batra, J. Balakrishnan, and A. Dabak, "Multiband OFDM: Why it Wins for UWB," *CommsDesign*, September 2009. [Online]. Available: http://www.commsdesign.com/design_corner/showArticle.jhtml?articleID=16501259 44, 45

[70] S. Shetty and R. Aiello, in *The IET Seminar on Ultra Wideband Systems, Technologies and Applications*, April 2006, pp. 23–29. 45

[71] J. G. Proakis, *Digital Communications.* New York: McGraw-Hill, 2001. 45

[72] C. E. Shannon, "A Mathematical Theory of Communication," *Bell Syst. Tech. J.*, vol. 27, pp. 379 – 423, July 1948. 45

[73] W. Carney, "IEEE 802.11g New Draft Standard Clarifies Future of Wireless LAN," Texas Instrument, Tech. Rep., 2002. 46

[74] W. Alliance, "UWB - Best Choice to Enable WPANs," WiMedia Alliance White Paper, Tech. Rep., January 2008. 46

[75] (2009, June) Pulse Link. [Online]. Available: http://www.pulselink.net/wire_current.html 46

[76] G. Mekuria and H. Hirsch, "UWB Pulse Transmission over Powerline Channel," in *IEEE International Conference on Powerline Communications and Its Applications, ISPLC'07*, April 2007. 46

[77] A. M. Tonello, "A Wide Band Modem Based on Impulse Modulation and Frequency Domain Signal Processing for Powerline Communications," in *IEEE Globecom 2006*, 2006. 47

[78] G. Mathisen and A. M. Tonello, "WireNet: An experimental system for in-house power line communications," in *10th International Symposium on Powerline Communications and Its Applications*, March 2007, pp. 137–142. 47

[79] Pulse∼Link, "Pulse∼link demonstrates whole-home HD networking at the cable show'07," June 2007. [Online]. Available: www.pulselink.net/press 47

[80] (2007, June) Artimi news. [Online]. Available: http://artimi.com/news/archive/press_releases/06_jan_05.html 47

[81] X. Chen, "Gigabit Powerline Communications-Case for Support," October 2005. [Online]. Available: http://www.epsrc.ac.uk 47

[82] E. Liu, Y. Gao, O. Bilal, and T. Korhonen, "Broadband Characterisation of Indoor Powerline Channel," in *IEEE International Symposium of Powerline Communications and Its Applications*, 2004. 51, 139

[83] CST Microwave Studio, 2006. 52, 56

[84] "Understanding Common Mode Signals," Dallas Maxim Press Release, Tech. Rep., September 2009. [Online]. Available: www.maxim-ic.com/an2045 53

[85] C. R. Paul, *Analysis of Multi-conductor Transmission Lines.* John Wiley & Sons, 1994. 54

[86] H. W. Johnson and L. Gioia, *High-speed Signal Propagation: Advanced Black Magic.* Pearson Professional Education, 2003. 54

[87] W. Kim, S. H. Lee, M. Swaminathan, and R. R. Tummala, "Robust Extraction of the Frequency Dependent Characteristics Impedance of Transmission Lines using One-port TDR Measurements," in *Electrical Performance of Electronic Packaging*, October 2001, pp. 113 – 116. 56

[88] "TDR Impedance Measurements: A Foundation for Signal Integrity," Tektronix, Tech. Rep. 56

[89] R. Brannon, T. Haq, J. Newbury, K. Morris, and F. Robertson, "Evaluation of Key Parameters for Determining the Efficiency of Signal Propagation in Broadband PLC Systems," in *Proceedings of the IEEE International Conference on Power Line Communications and Its Applications, ISPLC 05*, April 2005, pp. 228 – 232. 59, 134

[90] S. Tsuzuke, T. Takamatsu, H. Nishio, and Y. Yamada, "An Estimation Method of the Transfer Function of Indoor Power-line Channels for Japanese Houses," in *The 6th International Symposium on Power-Line Communications and Its Applications*, 2002. 64

[91] H. Meng, S. Chen, Y. Guan, C. Law, P.L.So, E.Gunawan, and T.T.Lie, "A Transmission Line Model for High-Frequency Power Line Communication Channel," in *Power System Technology, 2002. Proceedings. PowerCon 2002*, vol. 2, Oct 2002, pp. 1290–1295. 66

[92] S. Ramo and J. R. Whinnery, *Fields and Waves in Communication Electronics*. John Wiley & Sons, 1984. 71

[93] O. Bilal, E. Liu, Y. Gao, and T. O. Korhonen, "Design of Broadband Coupling Circuits for Powerline Communication," in *Proceedings of the IEEE International Conference on Power Line Communications and Its Applications, ISPLC 04*, 2004. 76, 79

[94] F. J. Canete, J. A. Cartes, L. Diez, and J. T. Entrambasaguas, "Modeling and evaluation of the indoor powerline transmission medium," *IEEE Communications Magazine*, pp. 41–47, April 2003. 76

[95] D. Liu, E. Flint, B. Gaucher, and Y. Kwark, "Research Report-High Speed Communication System Performance Using the Home AC Powerline," IBM Resaerch Division, Tech. Rep., 1999. 79, 116, 167

[96] W. H. Choi and C. Y. Park, "A Simple Line Coupler with Adaptive Impedance Matching for Powerline Communication," in *11th International Symposium on Powerline Communications and Its Applications*, 2007, pp. 187–191. 79

[97] H. K. Podszeck, *Carrier Communication over Power Lines*. Springer-Verlag, 1972. 80

[98] "IEEE Guide for Power-Line Carrier Applications," IEEE Standard 643, Tech. Rep., 1980. 80

[99] P. A. J. V. Rensburg and H. C. Ferreira, "Practical Aspects of Component Selection and Circuit Layout for Modem and Coupling Circuit," in *7th International Symposium on Powerline Communications and Its Applications*, March 2003, pp. 197–203. 80

[100] A. C93.1-1972, "Requirements for Powerline Coupling capacitors," Tech. Rep. 80

[101] L. SIMOES and J. GERALD, "A Communication System for Power Lines," in *5th Conference on Telecommunications*, Tomar, Portugal, April 2005. 80

[102] "BS: 7671 (IEE Wiring Regulations, 17th Edition)," The IEE, Tech. Rep., January 2008. 93

[103] M. Mullins, "The Origin of the BS 1363 Plug and Socket Oulet System," *IEE Wiring Matters*, pp. 6–8, 2006. 93

[104] M. White, "The Advantages of the 32A Ring Final Circuit," in *The IEE Wiring Regulations - Ring Circuits*, October 2007. 93

[105] F. J. Canete, J. Cortes, J. Entrambasaguas, and J. Carmona, "Fundamentals of the Cyclic Short-Time Variation of Indoor Powerline Channels," in

IEEE International Symposium of Powerline Communications and Its Applications, 2005, pp. 157 – 161. 115

[106] O. G. Hooijen, "A Channel Model for the Residential Power Circuit Used as A Digital Communications Medium," *IEEE Transactions of Electromagnetic Compatibility*, vol. 40, no. 4, pp. 331–336, November 1998. 116

[107] M. Zimmermann and K. Dostert, "Analysis and Modeling of Impulsive Noise in Broad-Band Powerline Communications," *IEEE Transactions on Electromagnetic Compatibility*, vol. 44, no. 1, pp. 249–258, Feb 2002. 116, 119, 124

[108] ——, "An Anlysis of the Broadband Noise Scenario in Powerline Network," in *International Symposium of Powerline Communications and its Applications*, 2000, pp. 131–138. 116, 118

[109] *User Manual FSP 40*, Rohde & Schwarz. 117

[110] Y. Ma, P.L.So, E. Gunawan, and Y. Guan, "Analysis of Impulsive Noise and Multipath Effects on Broadband Power Line Communications," in *International Conference on Power System Technology - POWERCON*, November 2004, pp. 1404 – 1409. 121

[111] A. Alomainy, "Antennas and radio propagation for body-centric wireless networks," Ph.D. dissertation, Queen Mary University of London, June 2007. 122

[112] J. E. Newbury, "Broadband Powerline Communications for the Electricity Supply Industry," in *IEEE Transmission and Distribution Conference and Exposition*, April 2008, pp. 1 – 8. 127

[113] J. Zyren and A. Petrick, "Tutorial on Basic Link Budget Analysis," Intersil Corporation," Application Note, 1998. 137

[114] H. Liu, J. Song, B. Zhao, and X. Li, "Channel Study for Medium Voltage Power Network," in *IEEE ISPLC 2006*, 2006, pp. 245–250. 139

[115] R. G. Gallager, *Information Theory and Reliable Communication.* John Wiley & Sons, 1968. 139

[116] E. Liu, Y. Gao, O. Bilal, and T. Korhonen, "Broadband Characterisation of Indoor Powerline Channel and its Capacity Consideration," in *Proceedings of ICC 2005*, May 2005. 140

[117] (2009, June) MultiBand OFDM Alliance. [Online]. Available: www.multibandofdm.org 146

[118] G. R. Hiertz, Y. Zang, J. Habetha, and H. Sirin, "Multiband OFDM Alliance - The Next Generation of Wireless Personal Area Networks," in *2005 IEEE/Sarnoff Symposium on Advances in Wired and Wireless Communication*, April 2005, pp. 208 – 214. 147

[119] A. Batra, "Multi-band OFDM Physical Layer Proposal for IEEE 802.15 Task Group 3a," Texas Instruments, Tech. Rep., November 2003. 148, 178, 184

[120] R. S. Sherratt, "Design Considerations for the Multiband OFDM Physical Layer in Consumer Electronic Products," in *IEEE Tenth International Symposium on Consumer Electronics, ISCE'06*, September 2006, pp. 1 – 5. 148

[121] M. Clark, M. Mulligan, D. Jackson, and D. Linebarger, "Fixed-point modelling in an Ultra Wideband (UWB) Wireless Communication System," *Matlab Digest*, May 2004. [Online]. Available: http://www.mathworks.co.uk/company/newsletters/digest/may04/uwb.html 148

[122] A. V. Oppenheim and A. S. Willsky, *Signals and Systems.* Prentice Hall, 1996. 150

[123] E. Guerrini, G. Dell'Amico, P. Bisaglia, and L. Guerrier, "Bit-loading Algorithms and SNR estimate for HomePlug AV," in *IEEE International Conference on Powerline Communications and Its Applications*, 2007, pp. 77 – 82. 153

[124] S. Morosi, D. Marabissi, E. D. Re, R. Fantacci, and N. D. Santo, "A Rate Adaptive Bit-Loading Algorithm for Building Powerline Communications Based On DMT-Modulated Systems," *IEEE Transcations on Power Delivery*, vol. 21, no. 4, pp. 1892–1897, October 2006. 153

[125] N. Andreadou, C. Assimakopoulo, and F. Pavlidou, "Performance Evaluation of LDPC Codes on PLC Channel Compared to Other Coding Schemes," in *International Symposium of Powerline Communications and its Applications*, March 2007, pp. 296 – 301. 153

[126] N. Andreadou and F. Pavlidou, "QC-LDPC Codes and their Performance on Powerline Communication Channelodes and their Performance on Powerline Communication Channel," in *International Symposium of Powerline Communications and its Applications*, Dresden, Germany, March 2009, pp. 244 – 249. 153

[127] L. Guerrier, P. Bisaglia, D. Amico, and E. Guerrini, "Performanace of the turbo coded HomePlug AV system over powerline channels," in *International Symposium of Powerline Communications and its Applications*, 2007, pp. 138 – 143. 153

[128] D.Liu, E.Flint, B.Gaucher, and Y.Kwark, "Wideband AC Powerline Characterization," *IEEE Transations on Consumer Electronics*, vol. 45, pp. 1087–1097, November 1999. 167

[129] D. Matiae, "OFDM as a possible modulation technique for multimedia applications in the range of mm waves," *Introduction to OFDM*, pp. 1 – 18. 183